CENTRO DE INVESTIGACIÓN Y DE ESTUDIOS
AVANZADOS DEL INSTITUTO POLITÉCNICO
NACIONAL

UNIDAD ZACATENCO

PROGRAMA DE DOCTORADO NANOCIENCIAS Y
NANOTECNOLOGÍAS

Efecto sobre las propiedades electrónicas y termoeléctricas de sistemas 2D de los compuestos laminares III-VI debido al confinamiento cuántico

TESIS

que presenta

HANNAN ELSAYED SADEK ABDELGELIL

Para obtener el grado de

DOCTORA EN CIENCIAS
EN NANOCIENCIAS Y NANOTECNOLOGÍA

DIRECTORES DE LA TESIS:

DR. RITO DANIEL OLGUÍN MELO

PROF. ANDRÉS CANTARERO SÁEZ

Ciudad de México Febrero, 2022

CENTER FOR RESEARCH AND ADVANCED STUDIES OF THE NATIONAL POLYTECHNIC INSTITUTE

ZACATENCO CAMPUS

NANOSCIENCE AND NANOTECHNOLOGY PHD PROGRAM

The effect of quantum confinement on the Electronic and thermoelectric properties of 2D structures of III–VI layered materials

Thesis

Presented by

HANNAN ELSAYED SADEK ABDELGELIL

To obtain the degree of

DOCTOR IN SCIENCE
IN NANOSCIENCES AND NANOTECHNOLOGY

SUPERVISED BY:

DR. RITO DANIEL OLGUÍN MELO

PROF. ANDRÉS CANTARERO SÁEZ

Mexico City February, 2022

To the only one who has been always there for me,
Sadek

Acknowledgements

I want to thank all the people who helped me to accomplish my PhD thesis,

At first I'd like to express my gratitude and love to my lovely family.

I would like to express my deepest gratitude to my thesis supervisors, Dr. Daniel Olguin and Prof. Andres cantarero For their persistent helpful suggestions, encouragement and reading throughout the manuscript which have rendered the realization in Mexico.

I want to express my sincere gratitude to all the members in the in the department of Nano-science and Nano-technology in CINVESTAV especially the previous and new director of the department Dr. Jose Gerardo Cabañas, and Dr. Arturo Isaias Martinez Enriquez for their continuous help and cooperation. Also I want to thank the staff in CINVESTAV for their collaborations, especially Yasmina De Lorenz and Ivan Buendia.

Also, I would like to thank the family of Dr. Daniel, especially his wife Maria and their kids for helping me in all the hard situation and being my family in Mexico.

I gratefully acknowledge the financial support from CONACYT Mexico. Also, I am grateful for the computational facilities presented to us from CINVESTAV-IPN and the group of Alberto Rubio. In particular, the abacus and xiuhcoatl. I want to express my acknowledgements to the SEP-Cinvestav grant FIDSC2018/211 for the partial financial support.

Contents

Abstract

To find a new effective, mechanically and thermally stable, and non-toxic thermoelectric material that can be used in future in thermoelectric devices for power generation. In this thesis we present a comprehensive study on the effect of the quantum confinement and the pressure on the electronic band structure and thermoelectric coefficients of the $\varepsilon-$polytype of GaSe, InSe and $\mathrm{InGaSe_2}$. Three structures have been studied in each case; the bulk, nanoplates (7 quadruple layer), and monolayer (one quadruple layer). The calculations have been done within the framework of the density functional theory since the electronic properties were calculated using the full potential linearized augmented plane wave method as implemented in the Wien2k package. Based on the calculations of the band structure, the evolution of the transport coefficient as a function of the chemical potential are evaluated with the use of the Boltzmann transport theory as implemented in the BoltzTraP code. The transformation occurred in the shape of the band structure of each material and the cross over from direct to indirect gap transitions that occurred in the pristine materials, GaSe and InSe as a result of decreasing the thickness to the nanometric range has been elucidated. A great enhancement is found in the values of the Seebeck coefficient in the monolayer case of all the studied materials. The origin of this enhancement was analyzed based on the aspect the electronic structure of each material. To predict how would be the figure of merit of the studied cases was calculated by making an assuming that the electronic and lattice thermal conductivity are identical. It is found also that the pressure has a positive effect on the Seebeck coefficient till a certain pressure that was different in each material; 20 GPa in InSe and 10 GPa in both GaSe and $\mathrm{InGaSe_2}$. The contributions achieved in this thesis can be considered as part of the extensive research that made daily to look for new thermoelectric materials. Our results assert that the pressure and quantum confinement could be effective ways to enhance the thermoelectric properties even of the existing thermoelectric material. A future experimental research on the synthesis and measuring the electronic and thermoelectric properties of all the structures studied in this thesis will complement our study and will be the only way to evaluate the validity of our results.

Resumen

Con el fin de encontrar un nuevo material termoeléctrico efectivo, mecánica y térmicamente estable y no tóxico que pueda usarse en el futuro en dispositivos termoeléctricos para la generación de energía, en esta tesis presentamos un estudio exhaustivo sobre el efecto del confinamiento cuántico y la presión sobre la estructura de bandas electrónicas y coeficientes termoeléctricos del politipo ε de GaSe, InSe e $\mathrm{InGaSe_2}$. En cada caso se han estudiado tres estructuras; el bulk, nanoplacas (7 capas cuádruples) y monocapa (una capa cuádruple). Los cálculos se han realizado en el marco de la teoría del funcional de la densidad (DFT), ya que las propiedades electrónicas se calcularon utilizando el método de ondas planas aumentadas linealizadas de potencial completo implementado en el código Wien2k. Usando los cálculos de la estructura de la banda se evalúa la evolución del coeficiente de transporte en función del potencial químico con el uso de la ecuación de transporte de Boltzmann (BTE) implementado en el código BoltzTraP. La transformación ocurrió en la forma de la estructura de la banda de cada material como resultado de la disminución del espesor a rango nanométrico ha sido dilucidado. Se encuentra una gran mejora en los valores del coeficiente de Seebeck en el caso de monocapa de todos los materiales estudiados. El origen de esta mejora se analizó en función del aspecto de la estructura electrónica de cada material. Para predecir cómo sería la figura de mérito de los casos estudiados, se calculó asumiendo que la conductividad térmica de las vibraciones de la red (fonones) y de los electrones libres son idénticas. También se encuentra que la presión tiene un efecto positivo en el coeficiente de Seebeck hasta una cierta presión, 20 GPa en InSe y 10 GPa tanto en GaSe como en $\mathrm{InGaSe_2}$. Las contribuciones alcanzadas en esta tesis pueden considerarse como parte de la extensa investigación que se realiza diariamente para buscar nuevos materiales termoeléctricos. Nuestros resultados afirman que la presión y el confinamiento cuántico podrían ser formas efectivas de mejorar las propiedades termoeléctricas incluso del material termoeléctrico existente. Una futura investigación experimental sobre la síntesis y medición de las propiedades electrónica y termoeléctrica de todas las estructuras estudiadas en esta tesis complementarán nuestro estudio y serán la única forma de evaluar la validez de nuestros resultados.

Motivation

The world is facing two real problems, the first one is the energy crisis due to the vast consumption of non-renewable energy resources, fossil fuels, and to the continuous growth of the world economy and industrial development. In a previous review [1] on the renewable energy they mentioned that the global reserve/production ratio for oil estimated in 2012 is 54.2 years. The second problem is the Global warming and the climate change produced by the increase of the carbon dioxide level in the environment in the last decade due to the burning of fossil fuels. Consequently, looking for an alternative effective, clean, low cost, and sustainable energy resources for power generation, such as photovoltaics, wind, bio fuels and thermoelectric energy conversion devices, is a must. This demand has stimulated interest in different research fields to find energy conversion techniques that satisfy the world's increasing demand for energy. It is found that that more than half the energy that flows through our economy is ultimately wasted and the main part of this energy is dissipated as rejected heat [2]. This thermal energy could be exploited to create an electrical energy via thermoelectric generators [3, 4]. Over the past decades, there has been a growing interest in discovering efficient thermoelectric materials [5–8] for power generation due to their potential applications as a clean energy source with many attractive features as they work silently and without having any moving parts or environmentally harmful fluids. In addition to the recovery of the wasted heat, the thermoelectric devices have been also investigated for their use in thermoelectric-solar hybrid systems [9, 10] and thermoelectric refrigeration [11].

The efficiency of the thermoelectric device depends on the properties of the used thermoelectric material. The thermoelectric performance of a given material is characterized by the dimensionless figure of merit:

$$ZT = \frac{S^2\sigma}{k}T, \tag{1}$$

where S, σ, T are the Seebeck coefficient, the electrical conductivity and the absolute temperature, respectively. k is the total thermal conductivity which is composed of the electronic contribution k_e and phononic (or lattice) contributions k_l. A high value of ZT means high value of the powerfactor, $S^2\sigma$ and low thermal conductivity k. However, we cannot increase $S^2\sigma$ infinitely and decrease k due to the interdependence between those parameters. Since the electronic thermal conductivity is linked to the electrical conductivity by the Wiedemann–Franz law [12, 13]:

$$k_e = L\sigma T, \tag{2}$$

where $L = 2.45 \times 10^{-8} W\Omega K^{-2}$. Also, σ and S have opposite proportional relationship with the carrier concentration [3, 14]. It means that any attempts to maximize one parameters will probably minimize the other one and the simultaneous optimization of all the parameters is very difficult. Hence the design of good thermoelectric materials depends on the ability to reach a subtle balance between those three parameters. The challenge to face is to find materials that show electronic properties typical of heavily doped semiconductors combined with a poor ability to conduct heat since heavily doped semiconductors provide a balance between the large S of lightly doped semiconductors and the high σ of metals. Several strategies have been adopted to overcome this obstacle. Since the Seebeck coefficient and electrical conductivity are strongly dependent on the geometry of the band structure, band engineering is regarded as one of the most efficient approach to develop high performance thermoelectric materials. Therefore, Electronic transport can be improved by manipulating the density of states and band structures of a material by involving complex dopants, interfaces [15], nano-structuring [16] and unusual electronic structures [17, 18]. The reduction of the thermal conductivity can be achieved by the scattering of phonons on atomic length scales through rattling atoms [19], vacancies, impurities, interstitials, or substitutional atoms, the concept of phonon-glass electron crystal (PGEC [20]), and dimensional reduction nanostructured materials [21, 22] .

One of the most influential concepts in thermodynamics is the dimensional reduction as it can simultaneously improve the power factor and reduce the lattice thermal conductivity. This started with the approach, proposed by Hicks and Dresselhaus [16], of the possibility to increase Z of certain materials by preparing them in quantum-well superlattice structures. They found that the ZT of a single layer thick Bi_2Te_3 increased by a factor of 13 over the bulk value also the grain boundaries and interfaces within the single layers could facilitate the scattering of mid/long-wavelength phonon, contributing to a reduction in the thermal conductivity. Their calculations showed that layering has the potential to increase significantly the figure of merit of a highly anisotropic material such as Bi_2Te_3 that has ascertained their early assumption. This stimulated subsequent work on nanostructured thermoelectrics to increase the figure of merit [23, 24] especially, in the layered compounds [25, 26] as it is found that the electronic band structure of the bulk case of this compound changes qualitatively as the thickness is reduced down to a few monolayers [27–31]. For example, the indirect to direct gap transition that occurs at monolayer thicknesses of the Mo and W transition metal dichalcogenides (TMDCs) [32].

GaSe and InSe are $III - VI$ semiconducting layered compounds [33–35] that have been characterized by theeir strong structural anisotropy and nonlinear optical properties [36–45]. A lot of studies have been realized on them from the basic aspects, as their photovoltaic, photo electronic [46–48] and thermoelectric properties. Concretely, indium-selenium-based compounds have received much attention as thermoelectric materials since a high thermoelectric figure of merit of 1.48 at 705 K was observed in $In_4Se_{2.35}$ [49]. Also Wang et al. [50] investigated theoretically the structural, electronic, and thermoelectric properties of several nanotubes strcuctures

of InSe at room temperature and they found that the power factor with respect to relaxation time of one of the studied nanotube is nearly 10 times larger than that of BiSb nanotubes due to the appearance of light and heavily bands around the Fermi level that boosted them to be high-performance thermoelectric materials.

Additionally, one of the great advantages of the layered materials is the presence of strong chemical bonds only between atoms in a single layer and the absence of strong interfacial bonds between the layers. This can be exploited to grow heterojuctions and superlattices, in the direction of the weak bond by using the van der Waals epitaxy[51, 52], even between two materials with different physical properties, different crystalline parameters and with various types of crystal symmetry. Several studies[53–59] have proved that several layered materials can be grown experimentally on other layered materials in spite of the large differences in the lattice constant and the crystal structure between them. Various techniques have been used to grow those $III - VI$ materials like the molecular beam epitaxy, chemical vapor deposition, chemical bath deposition, evaporation technique, and electrochemical atomic layer epitaxy[60–64]. All of these have motivated us to theoretically study the electronic and thermoelectric properties of each of GaSe, InSe, the new supper lattice $\mathrm{InGaSe_2}$ in three different structures; the bulk and one layer (monolayer) and 7 layer (nanoplates).

Objectives and structure of the thesis

The main purpose of this work is to look for new thermoelectric materials with good transport properties that could be implemented in thermoelectric devices. Hence, in this thesis a comprehensive study of the electrical and thermoelectric properties of the bulk, nanoplates and monolayer of each of GaSe InSe and the superlattice $\mathrm{InGaSe_2}$ have been presented. The thesis have been organized as follows:

- In Chapter 1 a general introduction about thermoelectrics is presented.
- In Chapter 2 a brief description of the theories and the codes used in the calculations is exhibited.
- In Chapters 3, 4, 5 a comparison between the calculated band structure, density of states and the transport coefficients of each of the bulk, nanoplates, and monolayer structures in GaSe, InSe, and $\mathrm{InGaSe_2}$ is discussed, respectively.
- In Chapter 6 the effect of hydrostatic pressure on the transport on the bulk case of in three studied materials is elucidated.
- Finally the conclusion of this work is presented.

Chapter 1

General Introduction

The foundation of technology is based on the understanding of the material system. Specific material properties are required depending on the application. For example, the electrical conductivity of copper is exploited to build circuits, and the compressive strength of concrete is needed to create skyscrapers. Therefore the progress in the technology can be measured by how much we know about the properties of the materials, that are based mainly on its constitution. Such as, the metallic bonds that hold the atoms in the metals together leaves the electrons free to drift through the material when an electric field is applied. However, there is another factor that can affect the behaviour of the materials: its size. The electrical conductivity, chemical reactivity, mechanical properties, and even how a material interacts with light can all change at the nanoscale of some materials. Consequently the properties of a material reckon on its size then the understanding the properties of the materials on microscopic and macroscopic level is important. One of these properties is the thermoelectric property. The ability of the material to convert the heat to electricity was discovered in 1821 by the physicist Thomas Seebeck, called Seebeck effect, and then was explored in more detail by French physicist Jean Peltier and two other thermoelectric effects have been found.

1.1 Thermoelectric effects

1.1.1 Seebeck Effect

Thomas Johanson Seebeck noticed the deflection of a compass magnet close to a circuit made of two different materials that were joined in two places with a temperature difference between the junctions. At first, Seebeck thought that the deflection could be due to magnetism induced by the temperature difference. Then it was realized the generation of an electric current due to the potential difference induced between the two junctions and the current deflects the magnet by Ampere's law. This phenomenon is know as the Seebeck effect. Figure 1.1 shows a schematic diagram of this effect where a voltage difference is created across the terminal of an

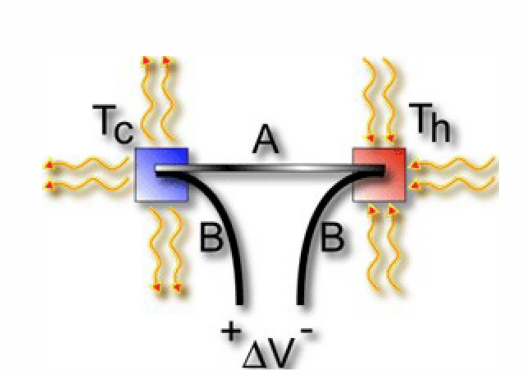

FIGURE 1.1: The Voltage difference, ΔV, produced across the terminals of an open circuit made from a pair of dissimilar metals, A and B, whose junctions are kept at different temperatures, is directly proportional to the temperature difference $\Delta T = T_h - T_c$ between the hot and cold junction temperatures

open circuit made from a pair of dissimilar metals, A and B, whose two junctions are kept at different temperatures.

At a microscopic level, this could be explained by the higher thermal velocities of the charge carriers in the hot side of the materials with respect to the cold side. Then they will diffuse from the hot to the cold side more quickly than in the opposite direction [4, 65]. If a thermal gradient is maintained across the material, a continuous flow of charge carriers give rise to a voltage difference between the two sides. This is due to the fact that in the warmer side there is an excess of carriers as compared to the coldest part and the carriers diffuse in order to be homogeneous through the material. The voltage difference ΔV is proportional to the temperature difference ΔT between the hot and cold sides of the junction;

$$\Delta V = -S\Delta T. \tag{1.1}$$

The constant of proportionality S is termed as Seebeck coefficient or thermopower. Even though the term thermopower is a misnormer since it measures the voltage or electric field(actually the electromotive force) induced in response to a temperature difference, not the electric power. It has the units of V/K although in practice it is more common to use microvolts per Kelvin, $\mu V/K$. The Seebeck coefficient depends on the crystal structure of the materials and the conductive properties. It has low values in metals as both the electrons and holes contribute to the induced thermoelectric voltage, hence they cancel the contributions of each others to the voltage, whereas semiconductors can be doped with an excess amount of electrons or holes and thus can have large positive or negative values of the thermopower depending on the type of the charge carriers. Thus the sign of the thermopower can determine if the semiconductor is $n-$ or $p-$ type.

1.1.2 Peltier Effect

This is the reverse of the Seebeck effect and it bears the name of the physicists who has discovered it, Jean-Charles Peltier. He found that the flow of electric current through a junction between two dissimilar metals can produce heating or cooling. Thus, the heat is absorbed in one junction and rejected in the other junction. The Peltier coefficient Π is defined as the heat transfer per unit of the applied current and is described mathematically by the equation [4, 20]:

$$\Pi = \frac{Q}{I}, \tag{1.2}$$

where I is the electrical current and Q is the rate of heating or cooling.

1.1.3 Thomson Effect

In 1851, Lord Kelvin predicted the Thomson Effect that comprise both the Seebeck and Peltier effects. It describes the heating or cooling of a homogeneous conducting due to current passing through it as a result of a thermal gradient [66]. The proportionality constant, known as the Thomson Coefficient κ is related by thermodynamics to the Seebeck coefficient. The relations with the Seebeck and Peltier coefficients are [67]:

$$\kappa = \frac{ds}{d\ln T} = \frac{d\Pi}{dT} - s. \tag{1.3}$$

Chapter 2

Theory

2.1 Density functional theory

The fundamental tenet of the density functional theory is that any property of a system of many interacting particles can be viewed as a functional of the ground state density $n_0(r)$. That is, one scalar function of positions $n_0(r)$, in principle, determines all the information in the many-body wave functions for the ground state and all the excited states. The existence proofs for such functionals, given in the original work of Hohenberg and Kohn and of Mermin[68], are simple. However, they provide no guidance for constructing the functionals, and no exact functionals are known for any system of more than one electron.

Density functional theory (DFT) would remain a minor curiosity today if it were not for the ansatz made by Kohn and Sham [69], which has provided a way to make useful, approximate ground state functionals for real systems of many electrons. The remarkable successes of the approximate local density(LDA) [70] and generalized-gradient approximation(GGA) functionals within the Kohn-Sham approach have led to widespread interest in density functional theory as the most promising approach for accurate, practical methods in the theory of materials. The attraction of density functional theory is evident by the fact that one equation for the density is remarkably simpler than the full many-body Schrödinger equation that involves 3N degrees of freedom for N electrons.

2.1.1 The quantum many body problem

A solid constitute of heavy, positively charged nuclei and lighter negatively charged electron. Understanding the properties of this interacting electrons and atomic nuclei is the base of material science. The exact many-particle Hamiltonian for a system of N nuclei and ZN electrons is:

$$\hat{H} = -\frac{\hbar^2}{2}\sum_i \frac{\nabla^2_{\vec{R}_i}}{M_i} - \frac{\hbar^2}{2}\sum_i \frac{\nabla^2_{\vec{r}_i}}{m_i} - \frac{1}{4\pi\epsilon_0}\sum_{i,j}\frac{e^2 Z_i}{|\vec{R}_i - \vec{r_j}|} + \frac{1}{4\pi\epsilon_0}\sum_{i\neq j}\frac{e^2}{|\vec{r_i} - \vec{r_j}|} + \frac{1}{4\pi\epsilon_0}\sum_{i\neq j}\frac{e^2 Z_i Z_j}{|\vec{R}_i - \vec{R}_j|}, \tag{2.1}$$

the first term represents the kinetic energy operator for the nuclei, the second for the electrons. The last three terms describe the Coulomb interaction between electrons and nuclei, between electrons and other electrons, and between nuclei and other nuclei. The direct solution of Schrodinger's equation with this Hamiltonian is an extremely impractical proposition. Almost all the properties of materials can be known given suitable computational tools for solving this particular problem in quantum mechanics. Several simplifications has applied to this Hamiltonian to solve the Schrodinger's equation and find acceptable approximate eigenstates. The first one is the Bohr-Oppenheimer approximation [71]; in this approximation the nuclei are assumed to be frozen at fixed positions and the electrons are in instantaneous equilibrium with them as a result of the fact that the nuclei are much heavier than the electrons. Now the problem is much more simplified to be a problem of a collection of NZ interacting negative particles moving in the external potential of the nuclei. It means that the nuclei do not move any more hence their kinetic energy turned to be zero and the Coulomb interaction between nuclei and other nuclei reduced to a constant. Then Hamiltonian is reduced to be:

$$\hat{H} = \frac{\hbar^2}{2m_e}\sum_i \nabla^2_i + \sum_i V_{ext}(r_i) + \frac{1}{2}\sum_{i\neq j}\frac{e^2}{|r_i - r_j|} + E_{II}. \tag{2.2}$$

2.1.2 The Hohenberg and Kohn theorems

After using the Bohr-Oppenheimer approximation, the problem is much simpler than before but still too difficult to be solved. The use of density functional theory could simplify the problem and reduce equation 2.2 to an approximate but tractable form. The formulation of the Density functional theory as an exact theory of many-body systems is based upon two theorems, proved by Hohenberg and Kohn:

Theorem I : For any system of interacting particles in an external potential $V_{ext}(r)$, there is one to one correspondence between the ground state particle density $n(r)$ and the external potential $V_{ext}(r)$. It means that the potential is determined uniquely by the ground state density $n(r)$. Consequently, the Hamiltonian is fully determined and hence the many body wavefunctions for all states (ground and excited) are determined. Therefore all the properties of the system are completely determined given only the ground state density $n(r)$ hence the ground state expectation value of any observable $\hat{O}$ is a unique function of the ground-state electron density.

$$\langle\Psi|\hat{O}|\Psi\rangle = O[n]. \tag{2.3}$$

Theorem II: For $\hat{O}$ being the Hamiltonian $\hat{H}$ hence universal functional for the energy $E[n]$ in terms of the density $n(r)$ can be defined, valid for any external potential $V_{ext}(r)$. For any particular $V_{ext}(r)$, the exact ground state energy of the system is the global minimum value of this functional, and the density that minimizes the functional is the exact ground state density $n(r)$. As mentioned before that all the properties can be viewed as a functional of $n(r)$, including the total energy functional:

$$\begin{aligned} E_{v_{ext}}[n] &= \langle\Psi|\hat{T}+\hat{V}|\Psi\rangle + \langle\Psi|\hat{V}_{ext}|\Psi\rangle + E_{II}, \\ &= F_{HK}[n] + \int d^3r V_{ext}(r)n(r) + E_{II}, \end{aligned} \tag{2.4}$$

where E_{II} is the interaction energy of the nuclei. The Hohenberg-Kohn density functional F_{HK} represents all internal energies, kinetic and potential, of the interacting electrons system which must be universal by construction since the kinetic energy and interaction energy of the particles are functionals only of the density. Unfortunately, The Hohenberg-Kohn doesn't provide the form of the energy functional $E_{v_{ext}}[n]$. Hence, to solve the equation using the DFT sufficiently accurate approximations are needed.

2.1.3 The Kohn-Sham ansatz

The approach proposed by Kohn and Sham is a practical procedure to obtain the ground state density by replacing the original difficult many body problem by an auxiliary independent particle problem that can be solved more easily. Hence, the many-body system, obeying the Hamiltonian(2.2), is replaced with a different auxiliary non-interacting system that has the same ground state density of the original interacting system. This leads to independent-particle equations for the non-interacting system that can be considered soluble with all the difficult many-body terms incorporated into an exchange-correlation functional of the density. By solving the equations one finds the ground state density and energy of the original interacting system with the accuracy limited only by the approximations in the exchange-correlation functional.

Therefore this approach is based upon two important assumptions:

1. The ground state density of the original many body system can be replaced by the ground state density of an auxiliary system of non –interacting particles. This is called "non-interacting-V-representability".

2. The auxiliary hamiltonian is chosen to have the usual kinetic operator and an effective local potential $V^{\sigma}_{eff}(r)$ acting on an electron of spin σ at point r. The local form isn't essential, but it is an extremely useful simplification that is often taken as the defining characteristics of the Kohn-Sham approach.

The actual calculations are performed on the auxiliary independent-particle system defined by the auxiliary Hamiltonian (using Hartree atomic units $\hbar = m_e = e = 4\pi/\epsilon_0 = 1$):

$$\hat{H}^{\sigma}_{aux} = -\frac{1}{2}\nabla^2 + V^{\sigma}(r). \tag{2.5}$$

The Kohn-Sham approach to the full interacting many-body problem is to rewrite the Hohenberg-Kohn expression for the ground state energy functional in the form:

$$E_{KS} = T_s[n] + \int dr V_{ext}(r)n(r) + E_{Hartree}[n] + E_{II} + E_{xc}[n], \tag{2.6}$$

here $V_{ext}(r)$ is the external potential due to the nuclei and any other external fields and E_{II} is the interaction between the nuclei. The independent particle kinetic energy T_s is given by:

$$T_s = -\frac{1}{2}\sum_{\sigma}\sum_{i=1}^{N^{\sigma}}(\psi_i^{\sigma}|\nabla^2|\psi_i^{\sigma})\frac{1}{2}\sum_{\sigma}\sum_{i=1}^{N^{\sigma}}|\nabla\psi_i^{\sigma}|^2. \tag{2.7}$$

$E_{Hartree}[n]$ the Hartree energy, the classical coulomb interaction energy of the electron density $n(r)$ interacting with itself, is given by:

$$E_{Hartree}[n] = \frac{1}{2}\int d^3r d^3r' \frac{n(r)n(r')}{|r-r'|}. \tag{2.8}$$

It means that all the many-body effects of exchange and correlation are grouped into the exchange correlation energy E_{xc} . Comparing the Hohenberg-Kohn (2.4) and Kohn-Sham (2.6) expressions for the total energy shows that E_{xc} can be written in terms of the Hohenberg-Kohn functional as:

$$\begin{aligned} E_{xc}[n] &= F_{HK}[n] - (T_s[n] + E_{Hartree}[n]) \\ &=< \hat{T} > -T_s[n] + < \hat{V}_{int} > -E_{Hartree}[n]. \end{aligned} \tag{2.9}$$

Thus E_{xc} is just the difference of the kinetic and internal interaction energies of the true interacting many-body system from those of the fictional independent-particle system with electron-electron interactions replaced by the Hartree energy. If the universal functional $E_{xc}[n]$ was known then the Kohn-Sham equations for independent particles could be solved and then the exact ground state energy and density of the many-body electron problem could be found since the density of the auxiliary system is given by the sum of squares of the orbitals $\psi_i^{\sigma}(r)$ for each spin σ:

$$n(r) = \sum_{\sigma} n(r,\sigma) = \sum_{\sigma}\sum_{i=1}^{N^{\sigma}}|\psi_i^{\sigma}(r)|^2. \tag{2.10}$$

The Kohn-Sham method provides a feasible approach to calculating the ground state of many-body electron system when a good approach can be found to describe the true exchange-correlation energy.

2.1.4 The local density approximation

The only approximation that was made till now is the Born-Oppenheimer approximation after that no approximation were made. To define the exchange-correlation functional an approximation should be made. In the Kohn-Sham work they stated that the solids can often be considered as close to the limit of the homogeneous electron gas. In that limit, it is known that the effects of exchange and correlation are local in character, and they proposed making the local density approximation, in which the exchange correlation energy is has this form:

$$E_{xc}^{LDA} = \int n(r)\epsilon_{xc}^{hom}(n(r))d^3r, \tag{2.11}$$

where ϵ_{xc} is the exchange correlation eneergy of the homogeneous electron gas. It means that the exchange correlation energy due to a particular density could be found by dividing the materials into very small volumes with a constant density. Each such volume contributes to the total exchange correlation energy by an amount equal to the exchange correlation energy of an identical volume filled with a homogeneous electron gas, that has the same total density as the original material has in this volume. Hence, LDA is expected to perform well for systems with a slowly varying density. Surprisingly it was very accurate in many other (realistic) cases too, this could be reasonable due to the fact that for typical densities found in solids, the range of the effects of exchange and correlation is rather short.

2.1.5 Generalized-gradient approximations (GGAs)

The success of LDA and then the discovering of its shortcoming has led to the development of various Generalized-gradient approximations (GGAs) with marked improvement over LDA for many cases. In this approximation the exchange-correlation contribution of every tiny volume not only depends on the local density in that volume, as in LDA, but also on the density in the neighboring volumes. Thus, in GGA there is a functional of the magnitude of the gradient of the density $|\nabla n|$ as well as the value n at each point and the functional could be defined as a generalized form of eq. 2.11:

$$E_{xc}^{GGA} = \int n(r)\epsilon_{xc}^{hom}(n, \nabla n)d^3r, \tag{2.12}$$

where $\epsilon_{xc}^{hom}(n, \nabla n) = F_{xc}(n, \nabla n)\epsilon_x^{hom}$, F_{xc} is dimensionless, and ϵ_x^{hom} is the exchange energy of the unpolarized gas. Widely used GGAs can now provide the accuracy required for density functional theory to be widely adopted by the chemistry community. Even though the performance of GGA is slightly better than LDA, there are a few drawbacks. Since in LDA approximation there is only one exchange correlation functional, because there is a unique definition for ϵ_{xc} but in the GGA approximation there is some freedom to incorporate the density gradient, and therefore several versions of GGA exist. Moreover, in practice one often fits a candidate GGA-functional with free parameters to a large set of experimental data on atoms and molecules. The best values for these parameters are fixed then, and the functional is ready to be used in solids. Therefore such a GGA-calculation is strictly spoken not an ab initio calculation, as some experimental information is used. Nevertheless, the one used in our calculations is parameter free.

2.1.6 Solving the equations

After using the approach of Kohn-Sham, an infinite set of one-electron equations has been obtained:

$$\left(-\frac{\hbar^2}{2m_e}\hat{\nabla}_m^2 + \frac{e^2}{4\pi\epsilon_0}\int\frac{\rho(\vec{r}')}{|\vec{r}-\vec{r}'|}d\vec{r}' + V_{xc} + V_{ext}\right)\phi_m(\vec{r}) = \epsilon_m\phi_m(\vec{r}), \tag{2.13}$$

the ϕ_m are mathematical single particle orbitals. Solving in most methods means that we want to find the coefficients C_p^m needed to express ϕ_m in a given basis set ϕ_p^b:

$$\phi_m = \sum_{p=1}^{P} C_p^m \phi_p^b. \tag{2.14}$$

The wave functions ϕ_m belong to a function space which has an infinite dimension, P is therefore in principle infinite. Practically, one works with a limited set of basis functions. Such a limited basis will never be able to describe ϕ_m exactly but one could try to find a basis that can generate a function that is close to the true wave function ϕ_m.

Having chosen a basis (and hence a finite value for P we realize that we can deal with the equations 2.13 as eigenvalue problem) for a given m, substitute eq. 2.14 in eq. 2.13 and left-multiplied with $< \phi_i^b | (i = 1, \ldots, P) >$, this leads to:

$$\begin{bmatrix} \ldots & \ldots & \ldots \\ \vdots & < \phi_i^b|\vec{H}_{sp}|\phi_i^b) > -\epsilon_m < \phi_i^b|\phi_i^b) > & \vdots \\ \ldots & \ldots & \ldots \end{bmatrix} = \begin{bmatrix} C_1^m \\ \vdots \\ C_p^m \end{bmatrix} = \begin{bmatrix} 0 \\ \vdots \\ 0 \end{bmatrix}. \tag{2.15}$$

Diagonalization of the Hamiltonian matrix will lead to P eigenvalues and P sets

of coefficients that express each of the P eigenfunctions in the given basis. The larger P leads to better approximated eigenfunction, but there is time-consuming the diagonalization of the matrix in equation eq. 2.15. The basis set that we have used in this work is the linearized augmented plane wave.

2.1.7 The Linearized Augmented plane wave (LAPW) method

The LAPW method is a procedure for solving the Kohn-Sham equations for the ground state density, total energy, and eigenvalues (energy bands) of a many-electron system by introducing a basis set which is especially adapted to the problem. This adaptation is achieved by dividing the unit cell into: (1) non-overlapping atomic spheres (centered at the atomic sites) called muffin tin spheres and (2) an interstitial region as shown in Figure 2.1. The method uses two different basis sets in the two regions:

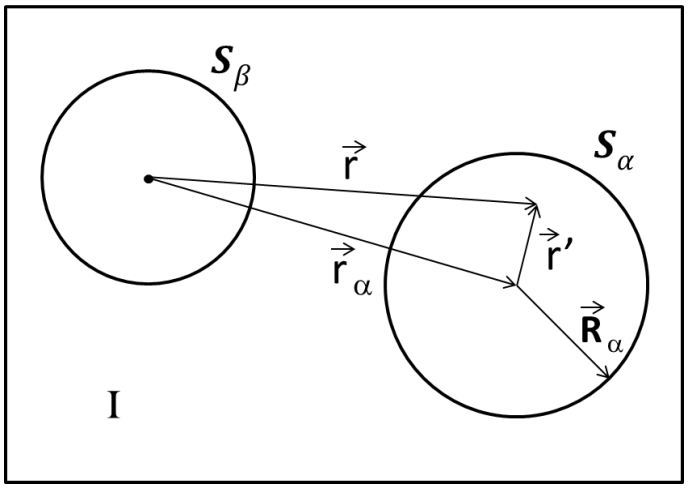

FIGURE 2.1: Division of a unit cell in muffin tin regions and the interstitial region, for a case with two atoms. The block dot is the region of the axis system (which may but not need to coincide with the nucleus of an atom)

1. Inside the atomic sphere (S_α) of radius (R_α) a linear combination of radial functions times spherical harmonics $Y_m^l(\hat{r'})$ is used:

$$\phi_{\vec{k}}^{\vec{K}}(\vec{r}) = \sum_{l,m}(A_{l,m}^{\alpha,\vec{k}+\vec{K}} u_l^\alpha(r', E_{1,l}^\alpha) + B_{l,m}^{\alpha,\vec{k}+\vec{K}} \dot{u}_l^\alpha(r', E_{1,l}^\alpha))Y_m^l(\hat{r'}), \tag{2.16}$$

where $\vec{K}$ is a reciprocal lattice vector, $\vec{k}$ is a vector in the first Brillouin zone, $\vec{r}$ is the vector position, α labels the different atoms in the unit cell,$A_{l,m}^{\alpha,\vec{k}+\vec{K}}$, $B_{l,m}^{\alpha,\vec{k}+\vec{K}}$ are undetermined parameters, $\vec{r'} = \vec{r} - \vec{r_\alpha}$ is the position inside the sphere given with respect to the center of each sphere, $\hat{r'}$ indicates the angles θ' and φ' which specifying the direction of $\vec{r'}$ in spherical coordinates, $u_l^\alpha(r', E_{1,l}^\alpha)$ is the solution to the radial part of the Schrödinger equation for a free atom α with energy $E_{1,l}^\alpha$ (chosen normally at the center of the corresponding band), and $\dot{u}_l^\alpha(r', E_{1,l}^\alpha)$ is the energy derivative of $u_l^\alpha(r', E_{1,l}^\alpha)$ evaluated at the same energy $E_{1,l}^\alpha$.

2. In the interstitial region, a plane wave expansion is used:

$$\phi_{\vec{k}}^{\vec{K}} = \frac{1}{\sqrt{V}} e^{i(\vec{k}+\vec{K})\vec{r}}, \tag{2.17}$$

where V is the volume of the unit cell.

The coefficients $A_{l,m}^{\alpha,\vec{k}+\vec{K}}$, $B_{l,m}^{\alpha,\vec{k}+\vec{K}}$ which appeared in Eq. 2.16 are determined by requiring that the function in the sphere matches the plane wave both in value and in slope (derivative) at the sphere boundary (following basis quantum mechanics). But to do that, it is easier first to expand the plane wave in spherical harmonics around the origin of the sphere of the atom α .$u_l^\alpha(r', E_{1,l}^\alpha)$,$\dot{u}_l^\alpha(r', E_{1,l}^\alpha)$ are obtained by numerical integration of the radial part of the Schrödinger equation on a mesh inside the sphere. The solutions to the Kohn-Sham equations are expanded in this combined basis set of LAPW's according to the linear variational method.

$$\phi_{\vec{k}}^n(\vec{r}) = \sum_{\vec{K}} C_{\vec{K}}^{n,\vec{k}} \phi_{\vec{k}}^{\vec{k}}(\vec{r}), \tag{2.18}$$

where n is the band index. The coefficients $C_{\vec{K}}^{n,\vec{k}}$ are determined by the Rayleigh-Ritz variational principle. Note that this basis set is $\vec{k}$ dependent: all eigenstates $\phi_{\vec{k}}^n(\vec{r})$ that have the same $\vec{k}$ but a different n will be expressed in the basis set this particular value of $\vec{k}$. For eigenstates with another $\vec{k}$, a new basis set using a different $\vec{k}$ has to be used. In practice we cannot work with an infinite basis set, and we have to limit it somehow. For the LAPW basis set a good quantity to judge the accuracy of the result is the product $R_\alpha^{min} K_{max}$ between the smallest muffin tin radius and K_{max} (which is the radius of a sphere centered at the origin in the reciprocal space where all the reciprocal lattice vectors that are inside this sphere are taken into the basis set). In the following sections, we will write it RK_{max} for abbreviation.

2.1.8 LAPW with local orbitals (LAPW+LO)

The orbital that contain electron which is extremely well bound to the nucleus and behave almost exactly as if it were in a free atom is called core state. The core state does not participate directly in the chemical bonding with other atoms. Therefore, it must be located entirely in the muffin tin sphere. valence states leaks out of the muffin tin sphere as they participate in chemical bonds. While the valence states in the LAPW are represented by plane waves, the core states are treated as in free atoms, but subjects to the potential due to the valence states. The low-lying valence states (which lay near the Fermi level) are called semi-core states. It frequently happens that states with the same l but a different principal quantum number n are both valence states. To choose the energy $E^{\alpha}_{1,l}$ in this case, we need to add another type of basis set, called a local orbital (LO). A local orbital is defined as:

$$\phi^{lm}_{\alpha,LO}(\vec{r}) = \begin{cases} 0 & \vec{r} \notin S_{\alpha}. \\ (A^{\alpha,LO}_{lm} u^{\alpha}_{l}(r', E^{\alpha}_{1,l}) + B^{\alpha,LO}_{lm} \dot{u}^{\alpha}_{l}(r', E^{\alpha}_{1,l}) + C^{\alpha,LO}_{lm} u^{\alpha}_{l}(r', E^{\alpha}_{2,l}))Y^{l}_{m}(\hat{r'}) & \vec{r} \in S_{\alpha}. \end{cases} \tag{2.19}$$

A local orbital is defined for a particular l and m and for a particular atom α. A local orbital is zero in the interstitial region and in the muffin tin spheres of other atoms, hence its name local orbital. In the muffin tin sphere of atom α, the same $u^{\alpha}_{l}(r', E^{\alpha}_{1,l})$ and $\dot{u}^{\alpha}_{l}(r', E^{\alpha}_{1,l})$ as in the LAPW basis set are used, with the linearization energy $E^{\alpha}_{1,l}$ as suitable value for the highest of the two valence states. The lower valence state (that is much more free-atom-like) is sharply peaked at an energy $E^{\alpha}_{2,l}$). A single radial function $u^{\alpha}_{l}(r', E^{\alpha}_{2,l}))$ at that same energy will be sufficient to describe it. Local orbitals are not connected to plane waves in the interstitial region; they have hence neither $\vec{k}$ nor $\vec{K}$-dependence. The three coefficients $A^{\alpha,LO}_{lm}$, $B^{\alpha,LO}_{lm}$ and $C^{\alpha,LO}_{lm}$ are determined by requiring that the LO is normalized, and has zero value and zero derivative at the boundary of the muffin tin sphere.

2.1.9 General considerations

In its general form, the LAPW method expands the potential in the following form [ref]:

$$V(r) = \begin{cases} \sum_{lm} V_{lm}(r) Y_{lm}(\hat{r}) & \text{inside the sphere,} \\ \sum_{G} V_{G} e^{iGr} & \text{outside the sphere,} \end{cases} \tag{2.20}$$

and the charge densities analogously. Thus no shape approximations are made, a procedure frequently called a full potential method.

2.1.10 WIEN2k Package

The code that we have used in this work is called WIEN2K. It consists of several independent programs which are linked via C-SHELL SCRIPTS. The flow and usage of the different program is illustrated in Figure 2.2. After creating the structure file which contains information about the geometry of the compound, the calculations are initialized. The initialization consists of running a series of auxiliary programs, which generates the inputs for the main programs. Those programs are:

1. SETRMT a program which helps to select the proper RMT values.
2. NN using this program a list of the nearest neighbor distances up to a specified limit (defined by a distance factor) is created and thus helps to determine the atomic sphere radii. In addition it is a very useful additional check of the structure file (equivalency of atoms). At the same time check that the muffin tin spheres do not overlap.
3. SGROUP determines the space group of the structure defined in the structure file.
4. SYMMETRY generates from the structure file, the initial file), the space group symmetry operations, determines the point group of the individual atomic sites, generates the lm expansion for the lattice harmonics expansion and determines the local rotational matrices.
5. LSTART generates the free atomic densities and determines how the different orbitals are treated in the band structure calculations (i.e. as core or band states, with or without local orbitals). By inspection (from the output of the file), we can decide if it is necessary to include a set of orbitals as local orbitals.
6. KGEN generates a k-mesh in the irreducible part of the BZ.
7. DSTART generates a starting density for the self-consistency cycle (SCF) by a superposition of atomic densities generated in LSTART.

Then a self-consistency cycle is initiated and repeated until the convergence criteria (energy convergence, charge convergence or force convergence) are reached. This cycle consists of the following steps:

1. LAPW0 (potential) generates potential from density.
2. LAPW1 (BANDS) calculates the valence bands (eigenvalues and eigenvectors).
3. LAPW2 (RHO) computes valence charge densities from eigenvectors (wave functions).

4. LCORE computes core states and densities.
5. MIXER mixes input and output densities to guarantee convergence.

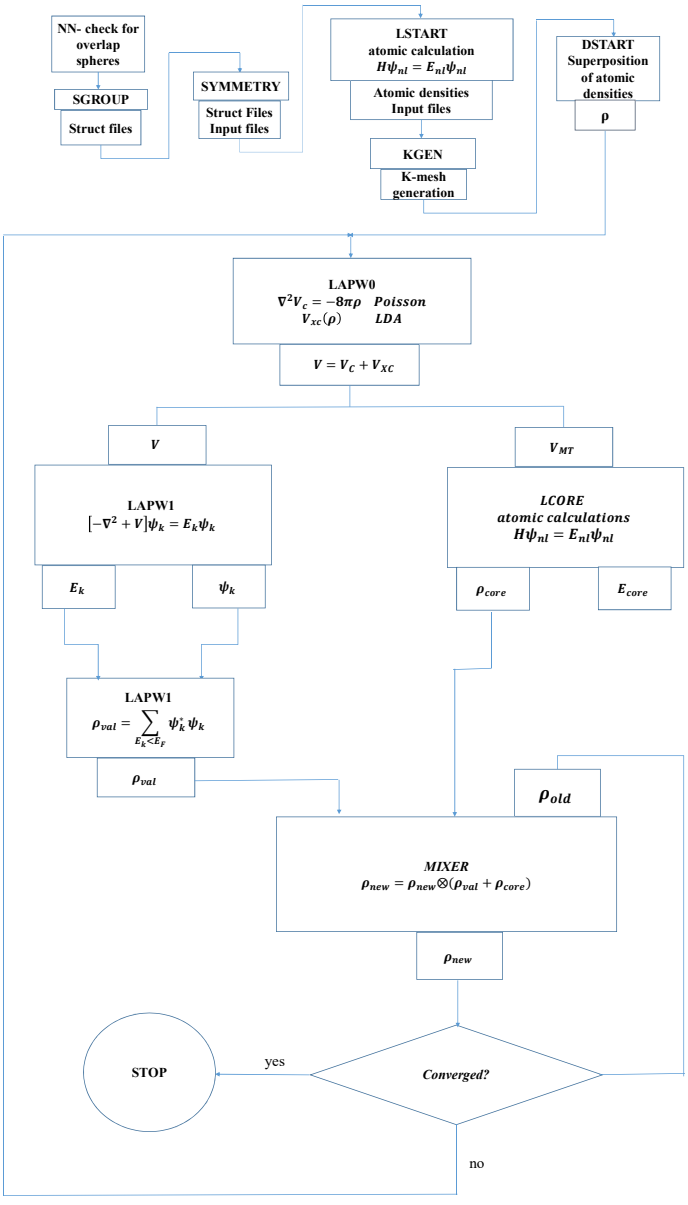

FIGURE 2.2: Program flow in WIEN2k.

2.2 Boltzmann theory: The semi-classic equations

The efficiency of the thermoelectric devices is limited by the electronic and thermal transport properties of the available thermoelectric materials, represented in the figure of merit:

$$ZT = \frac{\sigma S^2}{\kappa} T \quad , \tag{2.21}$$

where S is the Seebeck coefficient, also known as the thermopower, σ and k are the electronic and thermal conductivities, respectively. A modeling of this parameters is important in the search for a good thermoelectric materials. The most common procedure for modeling them is semi empirical by using a combination of a parametrized band structure fitted to experimental results. This approach works reasonably well in the study of the regions that is not too far from the conditions of the experiment used to fit the model as found in previous studies [72–74]. So it will be of limited when applied for the discovery of a new thermoelectric materials. The other approach proposed by Madsen et. al.[75] that will be adopted in this study is based on obtaining as much information as possible from first-principles calculations of the electronic structure to reduce the empirical information required to a minimum.

The parameters in eq. 2.21 can be deduced using the Boltzmann theory [76–79]. While the Seebeck coefficient, the electrical conductivity, and the electronic thermal conductivity can be obtained from the Boltzmann transport equation (BTE) for electrons, the BTE for phonons gives the lattice or phonon thermal conductivity. In general in a microscopic model of transport process, the electric current j, produced due to applying an electric and magnetic field and a thermal gradient, can be written in terms of the conductivity tensors as follows:

$$j_i = \sigma_{ij} E_j + \sigma_{ijk} E_j B_k + v_{ij} \nabla_j T + ... \tag{2.22}$$

This conductivity tensors can be expressed in terms of the group velocity:

$$\sigma_{\alpha\beta}(i,k) = e^2 \tau_{i,k} v_\alpha(i,k) v_\beta(i,k), \tag{2.23}$$

, where the group velocity is defined as the gradient in reciprocal space of the dispersion relation (band structure) of the electrons in the crystal, and equal:

$$v_\alpha(i,k) = \frac{1}{\hbar} \frac{\partial \varepsilon_{i,k}}{\partial k_\alpha}. \tag{2.24}$$

From the solution of the Boltzmann equation, in the constant relaxation time approximation, the transport coefficients can be written as[75]:

$$\sigma_{\alpha\beta}(T;\mu) = \frac{1}{\Omega} \int \sigma_{\alpha\beta}(\varepsilon)[-\frac{\partial f_\mu(T;\varepsilon)}{\partial \varepsilon}] d\varepsilon. \tag{2.25}$$

$$v_{\alpha\beta}(T;\mu) = \frac{1}{eT\Omega}\int \sigma_{\alpha\beta}(\varepsilon)(\varepsilon-\mu)[-\frac{\partial f_\mu(T;\varepsilon)}{\partial\varepsilon}]d\varepsilon. \tag{2.26}$$

$$k^0_{\alpha\beta}(T;\mu) = \frac{1}{e^2T\Omega}\int \sigma_{\alpha\beta}(\varepsilon)(\varepsilon-\mu)^2[-\frac{\partial f_\mu(T;\varepsilon)}{\partial\varepsilon}]d\varepsilon. \tag{2.27}$$

$$S_{ij} = E_i(\nabla_j T)^{-1} = (\sigma^{-1})_{\alpha i}v_{\alpha j}. \tag{2.28}$$

k^0 is the electronic part of the thermal conductivity. $\sigma_{\alpha\beta}(\epsilon)$ is the energy projected conductivity tensor can be defined using the conductivity tensor as :

$$\sigma_{\alpha\beta}(\epsilon) = \frac{1}{N}\sum_{i,k}\sigma_{\alpha\beta}(i,k)\frac{\delta(\varepsilon-\varepsilon_{i,k}}{d\varepsilon}), \tag{2.29}$$

where N is the number of the sampled k-points. All the parameters depends on the relaxation time τ. Hence, for calculation of the semi-classic transport coefficients, we need to calculate first the group velocity. Calculating the group velocity using the definition in equation 2.24 is numerically difficult to implement. Therefore, electronic structure codes is used to calculate it, one of them is the BoltzTraP code.

2.2.1 BoltzTraP code

Electronic structure codes usually evaluate the band energies in a numerical mesh for the Brillouin zone sampling, therefore the group velocity must be evaluated as a numerical derivative. This differentiation requires the use of a computationally costly very fine grid. In order to reduce the computational cost, the BoltzTraP program [75] is used as it employs a Fourier expansion of the band energies where the space group is maintained by using star functions:

$$\tilde{\varepsilon}(k) = \sum_R C_{Ri}S_R(k), \quad S_R(k) = \frac{1}{n}\sum_{[\Lambda]} e^{(ik.\Lambda R)}, \tag{2.30}$$

R is a direct lattice vector, $[\Lambda]$ are the n point group rotations. The idea is based on using more star functions than the band energies, and constraining the fit so $\tilde{\varepsilon}_i$ are exactly equal to the band-energies ε_i. Therefore, after obtaining the analytical representation of the band-structure it is then a reasonable procedure to calculate band structure dependent quantities.

Chapter 3

The electronic, and thermoelectric properties of GaSe

3.1 The Crystal structure

GaSe and InSe crystallize in a layered structure. The basic structure and symmetry of an isolated layer is the same in all the layered materials (D_{3h} point group) since each layer has a hexagonal symmetry and is composed of two planes of metal atoms sandwiched between two chalcogen planes and stacked along the c-axis. These layered compounds are characterized by highly anisotropic bonding forces; the bonds inside such a tetralayer are of covalent type with some ionic contributions since the cations are tetrahedrally coordinated (three anions and one cation), while the anions are bounded to three cations. Covalent cation-cation bonds are oriented perpendicular to the layers. This bonds saturate the bonding in the crystal and are responsible for the semiconducting behavior. The layers are stacked together with predominantly van der Waals forces the distance between the layers is called the van der Waals gap.

Due to the weakness of interlayer bonding various polytypes exist with different stacking sequences of the layers. The stacking geometry determines the polytype of macroscopic crystal. Most of the structures crystallize in the hexagonal or rhombohedral lattice showing four possible stacking arrangements of the complex layers, leading to four polytypes, named β, ε, γ, and δ. ε, β and δ have hexagonal structure with different number of atoms in the unit cell while γ has rhombohedral lattice. A strong covalent bonding within the layer and the weak van der Waals bond between them lead to a strong anisotropy in all the polytypes. Hence the optical and electrical properties, and the thermal conductivity, etc. remarkably differ in the directions along the c-axis (perpendicular to the layer planes) and in the plane of the layers.

In the case of GaSe , the most common polytype is the hexagonal [80] $\varepsilon-$ GaSe with the space group $P\bar{6}m2$ (D_{3h} point group) and is characterized by two lattice parameters a and c. There are two layers per hexagonal unit cell and two formula units (four atoms) per layer. While for InSe , the most common polytype is $\gamma-$InSe

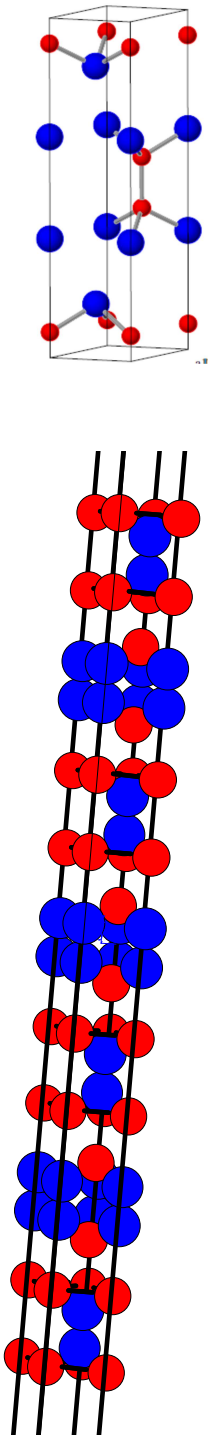

FIGURE 3.1: The upper panel display the unit cell of the hexagonal $\varepsilon-$ polytype of GaSe or InSe. The largest spheres (blue) represents the anions (Se) atoms and the smaller ones (red) represents the cations (Ga or In) atoms. Only the bonding between the interlayer atoms is showed to illustrate the layered character of the compounds. The lower Panel shows nanoplates of 7 layers of GaSe or InSe

with a space group $R\bar{3}m$ (C_{3v} point group) with a sequence of three layer in the rhombohedral unit cell [81]. In this work, only the ε-polytype of both GaSe and InSe has been studied to compare their structural, electrical and thermoelectric properties with the ε-polytype of new superlattice $\mathrm{InGaSe_2}$. A fragment of the crystal lattice of $\varepsilon-$Polytype of GaSe or InSe is shown in the upper panel of figure 3.1, where the layered atomic arrangement is clearly visible. In the lower panel of the figure The structure of a supercell constructed of 7 layers in the z direction and called it nanoplates is presented.

3.2 Computational details

The electronic structure calculations of the bulk, nanoplates, and monolayers cases of all the studied compounds have been performed within the framework of the density functional theory by using the full potential linearized augmented plane wave(FP-LAPW) method as implemented in the Wien2k code [82]. Core states are treated within a multi-configuration relativistic Dirac-Fock approach, while valence states are treated in scalar relativistic approach. The generalized gradient approximation(GGA) with the formalism of Perdew et al.[83] has been used to calculate the exchange correlation energy.

The convergence of the calculations in terms of the size of the plane-wave basis set and the k-points sampling within the irreducible part of the Brillouin zone have been guaranteed, by varying the value of the cutoff parameter $R_{MT}\ K_{max}$ (where K_{max} is the largest reciprocal lattice vector used in the plane wave expansion and made the expansion up to $l_{max} = 6$ in the muffin tins, where l_{max} is the maximum value of the angular momentum and R_{MT} is the smallest of the Muffin tins sphere radii.), G_{max} (where G_{max} is the magnitude of the largest vector G in the Fourier expansion of the product of two orbitals and the generated potential in the interstitial region (Eqs. (13) and (14) in the paper[84]) and $k - \mathrm{mesh}$ (the number of $k-$points in the irreducible wedge of the Brillouin zone), and calculate the total energy as a function of these parameters.

From these calculations the value of RK_{max}, G_{max} and $k - mesh$ at which the total energy is a minimum has been determined. The value of RK_{max} was 12 Ry for the case of GaSe and 13 Ry for InSe. The value of the atomic sphere radius R_{MT} has chosen to be $2.25, 2.35\ a.u.$ for In and Se atom respectively in InSe while for the case of GaSe , it has chosen to be $2.15\ a.u.$ for both Ga and Se atom. The value of G_{max} was 13 and 14 Ry for GaSe and InSe, respectively. A set of $48\ k-$points, equivalent to a $14 \times 14 \times 2$ Monkhorst-Pack grid in the unit cell has been chosen for GaSe and InSe The steps of the structure optimization procedure were :

- firstly, the lattice parameters were taken from experimental studies[85]; for GaSe , the experimental lattice parameters were $a = 3.759$Å and $c = 15.968$Å, while for InSe $a = 3.999$Å and $c = 16.7$Å have been used.

- Then the volume was relaxed towards the minimum of the total energy. From the curves of total energies calculated with the GGA as a function of the volume, the optimized value of the lattice parameter is taken by using the Birch–Murnagham equation of state[86].

The nanoplates structure has been created by using the unit cell of the optimized structure of the bulk and then the supercell program, inside the wien2k code, has been executed to obtain only 7 atomic layers in the $z-axis$ and no changes have been made in both the $y-$ and $x-$ axis.

For the case of monolayer, a vacuum region of 20Å was added so that the interactions between the monolayer and its period image can be neglected.

The electronic band structures of the bulk case for all the studied materials have been calculated within the GGA at the theoretical equilibrium lattice constants, the optimized ones that we have obtained, without and with the modified Beck-Johnson correction [87] which allows the calculations of the band gaps with an accuracy similar to very expensive GW calculations [88, 89]. For the 2D structures, nanoplates and monolayer, the modified Beck-Johnson correction was not used as it is known that the correction doesn't work well for the case of the few layers calculation, and the band structure has been calculated using the lattice constant of the optimized bulk structure.[82]

According to the Boltzmann transport, the thermoelectric transport coefficients can be expressed as a function of the transport distribution function [90, 91], which can be determined by the electronic structure and the electron scattering mechanisms of the materials. Hence the electronic transport coefficients are derived from the calculated electronic structure of all the studied cases based on the semiclassical Boltzmann transport theory and rigid-band model, as implemented in the BoltzTraP code. Within this method, the Seebeck coefficient S can be calculated independent of the relaxation time τ, however, the electrical conductivity σ is calculated with τ inserted as a parameter, that is, what we obtain is σ/τ . We plot the calculated electronic transport coefficients as a function of the chemical potential μ. The transport coefficients have been calculated using a dense mesh of 364 $k-$ points in the irreducible wedge of the Brillouin zone that is equivalent to a $30 \times 30 \times 6$ Monkhorst-Pack grid in the unit cell.

3.3 Electronic properties

3.3.1 Electronic band structure

The investigation of the electronic band structure helps to understand the electronic, optical, and thermoelectric properties of the material. The electronic structure calculations have been done using the optimized lattice parameters obtained for $\varepsilon-GaSe$; $a, b = 3.8145$Å and $c = 16.2035$Å. This optimized lattice parameters are larger than the experimental ones [92, 93]. This could be explained based on the fact that the layered semiconductors have a complicated structural for a normal structure optimization procedure, since it includes the interlayer van der Waals interaction that is not taken into account within the DFT. And also it is known that the generalized gradient approximation(GGA) tends to overestimate the interatomic distances and hence the lattice parameters of the unit cell. In this section a comparison between the electronic band structure of the bulk, nanoplates, and monolayer of $\varepsilon-$GaSe will be presented and discussed. The band structure of three studied structures of $\varepsilon-$GaSe is shown in fig 3.2. The curves were plotted along the high symmetry directions of a 3D Brillouin zone, so the electronic structure of thin and bulk crystals could be compared. The blue dotted curves represent the band structure that has been calculated by including the modified Becke and Johnson correction (mBJ) [87] while the black curves represent the band structure that has been calculated by using only the generalized gradient approximation with the formalism of Perdew et. al. [83]. The high symmetry points (axes), labeled as Γ, M, K, Γ and A are used to describe the electronic band structure.

Fig. 3.2 shows that for the bulk case of the $\varepsilon-$ GaSe , both valence band maxima and conduction band minima occurs at the center of the Brillouin Zone, Γ. Indicating that the bulk GaSe is a direct band gap semiconductor, the same results have been obtained in a previous theoretical work [94]. At the same time we noticed that after applying the modified Becke and Johnson correction, the minimum of the conduction band has been shifted to higher values leading to an increase of the band gap value in comparison to the one calculated only with the GGA approximation. This coincide with the fact that DFT underestimates the conduction band energies[95–97] and leeds to a low estimate of the band gap value hence the value of the band gap calculated with the mBJ correction is supposed to be closer to the experimental value. It can be also noticed from the bands located between -7.0 eV and -3 eV that the mBJ correction displaces up the valence bands at the Γ point.

Then when we move to the middle and lower part of fig. 3.2 where the 2 dimensional cases are presented, nanoplates and monolayer, respectively. It was found that even though the minimum of the conduction band, in both cases, still occurs at Γ the same as in the bulk case, the evolution of the valence band has changed depending on the thickness of the material. It has been noticed that the maximum of the Valence band has moved to be in the $\Gamma - K$ direction. This changes in the location of the maximum of the valence band started slightly in the case of nanoplates

as there was a very small difference, 0.00196 eV, between the energy of the MVB and the valence band maximum at Γ. This difference has increased in the case of monolayer, 0.09967 eV, and creates a valley in the valence band which has been named in the literature by Mexican hat dispersion [98]. This results indicate that by moving from the three dimensional case to the two dimensional cases, $\varepsilon-$GaSe exhibited a crossover from a direct to an indirect gap semiconductor and this behaviour occurred not only in the case of one layer but also in the case of 7 layers which is the case of nanoplates in our study. In the nanoplates case the number of bands increased as a result of the increase of the number o atoms in the unit cell.

We should mention that there is another maximum between Γ and M the difference between this maximum and the maximum of the valence band is a bout 2.8×10^{-4} and 3×10^{-3} eV for nanoplates and monolayer, respectively. Hence, the valence band is less dispersed than the conduction band. Since, in the conduction band the minimum is located Γ while in the valence band the maximum is located between two symmetry points. It means the electrons can easily transfer between the two maximum of the valence band with a small amount of energy. The same behavior has been obtained in the previous theoretical study of monolayer $\varepsilon-$GaSe [99], as they expected the cross over from direct to indirect gap semiconductor in the 2D sheet limits. As the valence band has less dispersion in both the nanoplates and monolayer cases in comparison with the bulk case, it means that the effective mass of the holes in the 2D cases is larger than the effective mass of the holes of the bulk case. This behavior indicates that the p-type doping of the 2D $\varepsilon-$ GaSe may be more preferable for good thermoelectric properties than the n-type. A similar feature was previously found to exist in bulk InSe under pressure. [100]

TABLE 3.1: Calculated band gap in eV for the bulk, nanoplates, and monolayer GaSe

	GaSe		
	E^{GGA}_{direct}(eV)	$E^{GGA}_{indirect}$(eV)	E^{mBJ}_{direct}(eV)
Bulk	0.82689		1.85041
Nanoplates	0.85451	0.85255	
Monolayer	1.90071	1.80104	

The band gap value of the bulk, nanoplates, and monolayer $\varepsilon-$ GaSe without and with the using of the mBJ correction are shown in table 3.1. In the table, we can see the big difference between the band gap value of the bulk calculated with and without the mBJ correction that have been mentioned before. The moderate band gap of $\varepsilon-$ GaSe indicates the thermoelectric performance can be easily optimized within a reasonable doping level. For both the nanoplates and monolayer cases the calculation has been done using only using the GGA. By looking in the table 3.1, it is clear that in the nanoplates case there was a little increase in the value of the band gap in comparison with the bulk case while in the monolayer case this increase was larger and led to a wider band gap this increase could be attributed to the absence of the interlayer bond in the monolayer case.

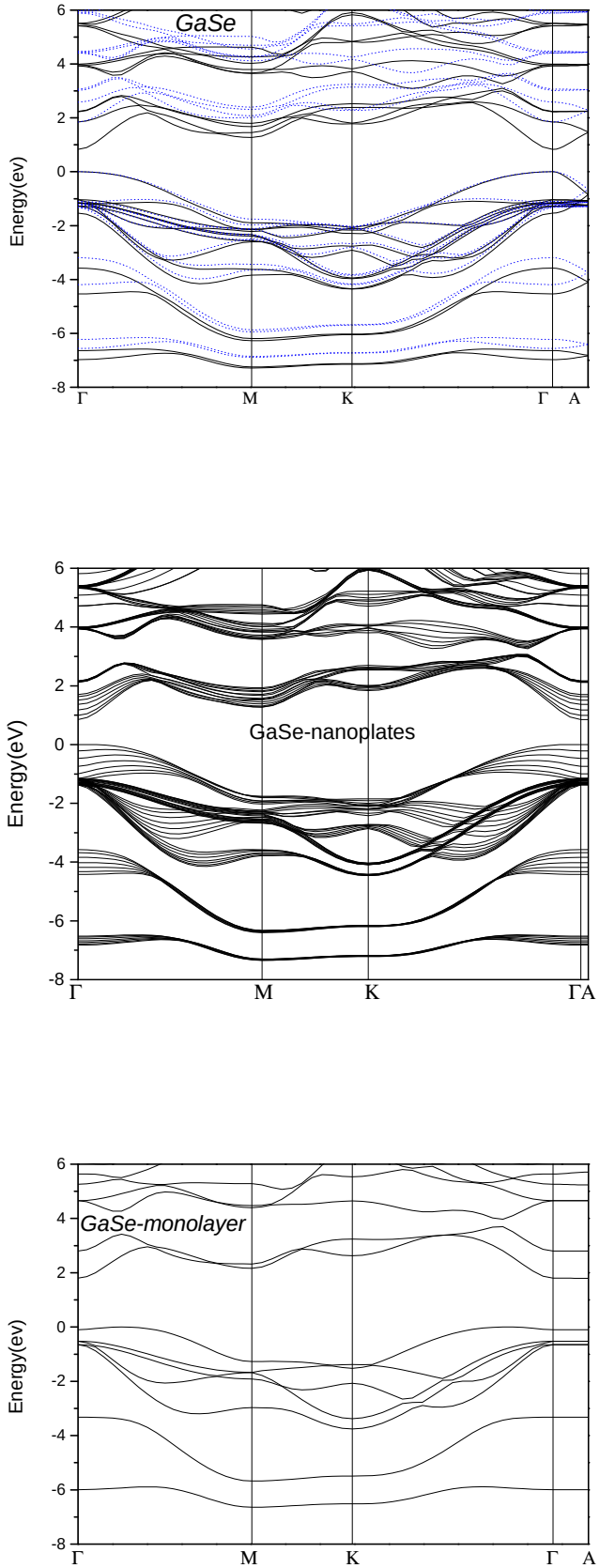

FIGURE 3.2: The calculated band structure for bulk $\varepsilon-$ GaSe in the bulk, nanoplates and monolayer structures. The dark solid line represents the calculation with GGA. The blue dotted line represents the calculation with GGA+mBJ

3.3.2 Total and partial density of states

The calculated total (DOS) and partial density of states (PDOS) of bulk, nanoplates, and monolayer $\varepsilon - GaSe$ and has been presented and discussed in this section to be able to investigate the difference between the two dimensional and three dimensional cases. Figures 3.3, 3.4 and 3.5 show the total density of states, the contribution of the Ga atoms to the DOS and the contribution of the Se atoms to the DOS, of the three studied cases, respectively. The partial DOS for each element is a sum of a partial DOS over all muffin-tin spheres of the same compound.

Our calculation showed the Ga-$3d$ states are about 15.2 eV below the top of the valence band and are considered as a core states. The lowest band contribution to the bound is around 7.0 eV below the maximum of the valence band. The way by which the orbitals of the cation and anion contributes to the valence and conduction band has not been affected qualitatively by the reduction of the dimensional of the GaSe compounds. All the states shown in figure 3.3 are $4s - 4p$ Ga states hybridized with the $4p$ Se states and a very small contribution from $4s$ Se states. The lower valence band is dominated by the main contribution that comes from Ga $4s$ states also there are little contributions from Se- $4s$, $4p_z$ and $4(p_x + p_y)$ states to that band. The valence band at Fermi level has the p characters as it is formed mainly from Se and Ga $4p_z$ and $4(p_x + p_y)$ orbitals, while there is a very small contribution comes from Ga $4s$ state. On the other hand, the lower conduction bands are mainly constituted of Ga $4s-$orbital hybridized with Ga and Se $4p_z$, $4(p_x + p_y)$ states as in previous study [94]. For the three studied cases of $\varepsilon-$ GaSe even though the contribution of the atomic orbitals is qualitatively similar, there was a noticeable difference between the values of the total density of states since the largest value has been found in the nanoplates case and the lower one was in the case of monolayer since in this case the number of atoms is smaller that coincide with the number of atoms involved in each case. Also, the most important change that was found between the three cases was at the maximum of the valence band since only in the monolayer case there was an abrupt increase in the total density of states at the Fermi level and this could improve the thermoelectric properties of the monolayer case in comparison with the bulk and nanoplates cases. At the same time, in the monolayer case the density of states tends to have more defined peaks while for the bulk and nanoplates the appearance of these peaks over the continues curve were less defined and this could be due to the absence of the interlayer interactions in this case.

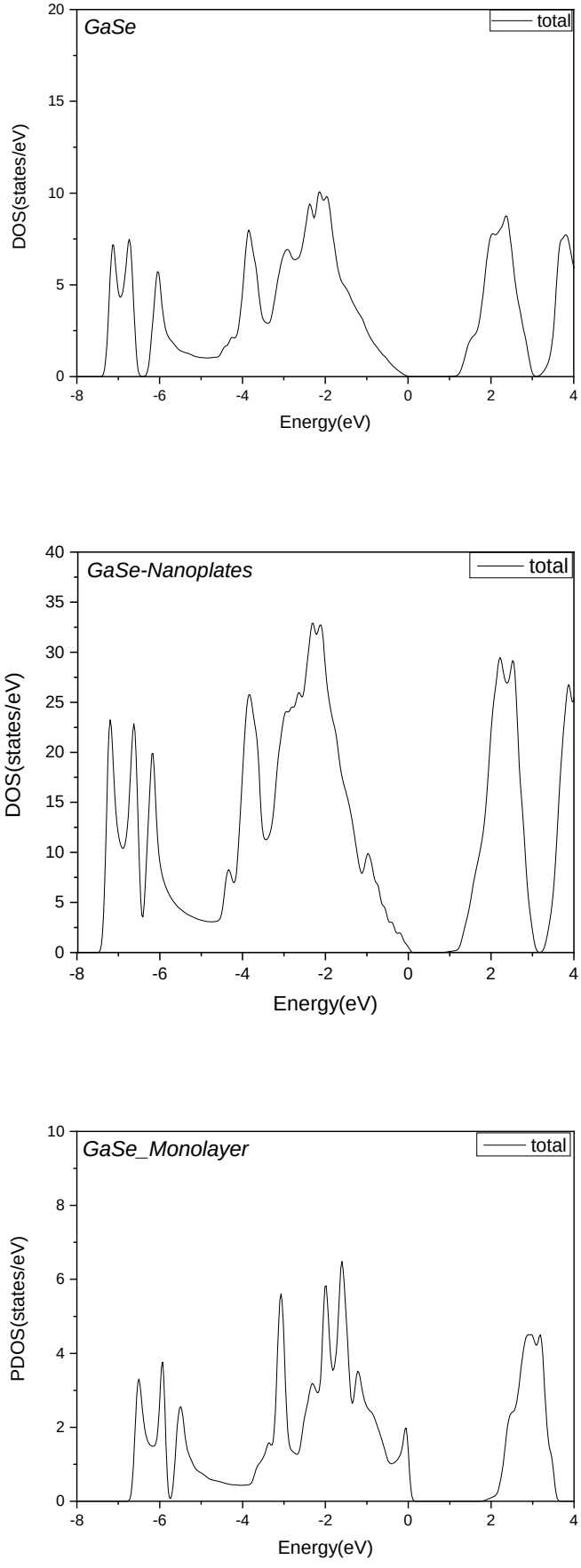

FIGURE 3.3: The calculated total density of states for bulk, nanoplates, and monolayer $\varepsilon - GaSe$

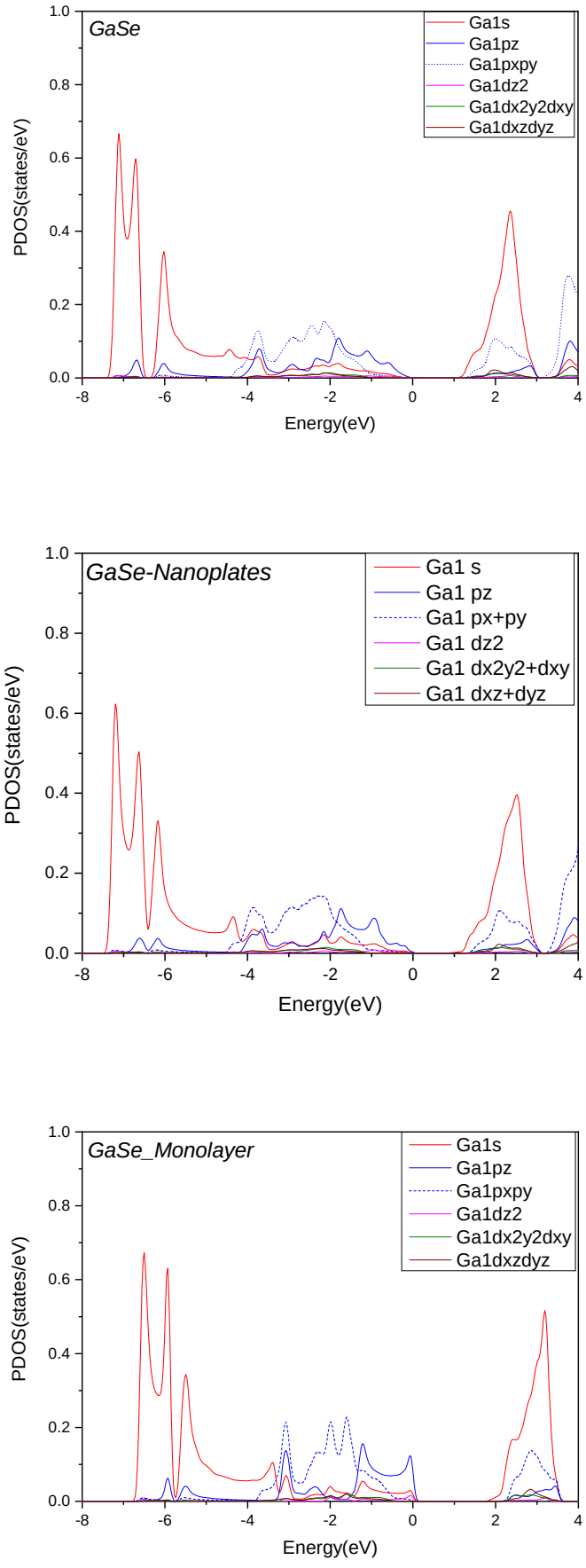

FIGURE 3.4: The partial contribution of Ga atoms to the total density of states in bulk, nanoplates, and monolayer $\varepsilon - GaSe$

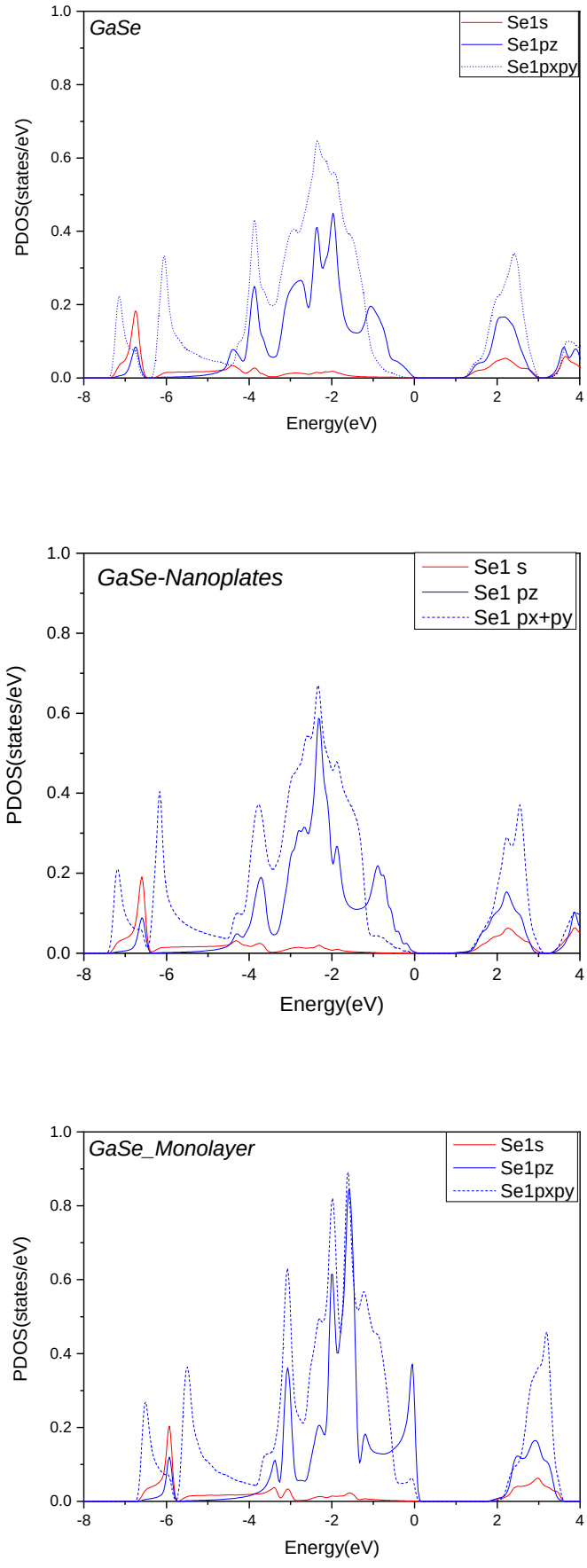

FIGURE 3.5: The partial contribution of Se atoms to the total density of states in bulk, nanoplates, and monolayer $\varepsilon - GaSe$

3.4 Transport Coefficients

3.4.1 Seebeck Coefficient

The conversion of heat into electricity at the junction of different types of wire is known by the Seebeck effect that has been discovered by Thomas Johann Seebeck in 1821 [101]. The ratio of the resulting voltage difference, produced between the two edges of a sample due to an applied temperature gradient between these two points when the electrical current is zero, and the temperature difference is defined as the Seebeck coefficients S and it is often referred to as thermopower even though it is more related to potential than power. Actually if we short circuit the two ends of the sample, a current (electromotive force) will flow through the sample.

The response of the materials to any applied temperature gradient can be understood by the behavior of the Seebeck coefficient of the materials as it is related to the its electronic structure. The sign of the Seebeck coefficient with reference to the chemical potential indicates the type of the dominant charge carrier, positive S represents the $p-$type materials whereas $n-$type materials have negative S. The chemical potential defines the doping level or carrier concentration in a material, which is very important for enhancing the thermoelectric nature of a material for practical realization. However, we should keep in mind that the magnitude of the charge carrier concentration corresponding to the chemical potential depends on the actual band structure, which are not claimed to be exactly predicted by the single particle DFT calculations. Since it is known that besides the advantage of DFT, it has its limitation [102, 103].

It is known that the electronic structure near the Fermi energy is significant for thermoelectric properties i.e. when the electronic states of the studied material around the Fermi level are extremely dense this would play a vital role for the thermoelectric nature of these materials. So we are going to explain the relation between the electronic structure near the band edges and the results of the Seebeck coefficient. Within the constant scattering time approximation the Seebeck coefficient is directly determined by the electronic band structure with no adjustable parameters. A comparison between the Seebeck coefficients of the bulk, nanoplates, and monolayer $\varepsilon-$ polytype of GaSe material vs chemical potential at 300 K are presented in the figure 3.6 in order to see the effect of the quantum confinement in this material on its Seebeck coefficient. It is assumed that μ=0 corresponds to the middle of the band gap. In the rigid band approximation [104, 105] the band structure is assumed unaffected by doping, which only leads to a shift of the chemical potential. For semiconductors, it is a good approximation for calculation of the transport properties, when the doping level is not too high [106, 107].

One can see in the vicinity of E_F that the Seebeck coefficients exhibit two pronounced peak for $n-/p-$type of all the studied case. The range where the materials exhibit good values for the Seebeck coefficient was similar in

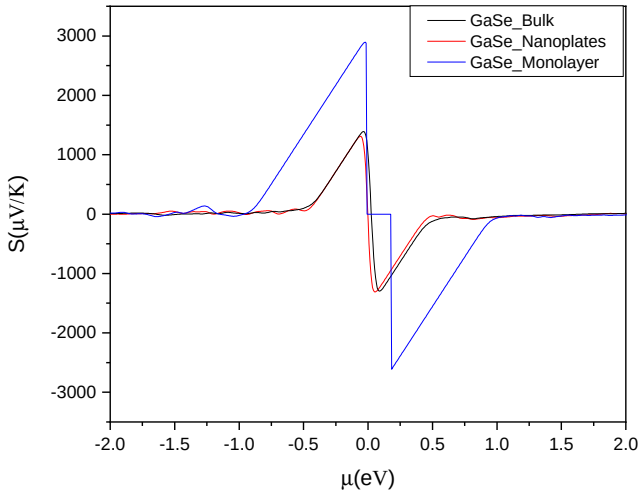

FIGURE 3.6: The Seebeck coefficients of the bulk, nanoplates and monolayer $\varepsilon-$ GaSe at 300 K

the bulk and nanoplates cases $[-0.55, 0.55]$ while it was wider in the case of monolayer$[-0.95, 0.95]$ which indicates that in the bulk and nanoplates cases the compounds favor low doping. Beyond those points the Seebeck coefficient decreases. The discontinuity in the behavior of the Seebeck coefficient in the monolayer case could be attributed to the precision of the calculations, in the study of the thermoelectric properties of the fully hydrogenated graphene similar behavior has been obtained for the calculated Seebeck coefficients at 300K [108].

We noticed that the Seebeck coefficient exhibits the same behaviour in both the bulk and nanoplates cases although there was a small difference between the maximum values obtained in the $p-$type and $n-$type in each case. Since the maximum value of the Seebeck coefficient in the $n-$type($p-$type) was 1294 (1388) $\mu V/K$ and 1310 (1311) $\mu V/K$ in the bulk and nanoplates, respectively. It is clear that the highest values of the Seebeck coefficients, obtained from all the studied case, were the one of monolayer GaSe since the maximum value of the Seebeck coefficient at $300K$ in the $p-$type region was $2893.8\mu V/K$ while it was $2611.59\mu V/K$ in the $n-$type region. Even though the values of the Seebeck coefficient obtained in both the nanoplates and bulk cases were smaller in comparison with the values obtained in the case of monolayer, their values were high in comparison with the typical values obtained in the semiconductors materials. Usually the values of the Seebeck coefficient should be larger than $200\mu V/K$ in the efficient thermoelectric materials [109, 110], no matter $p-$type or $n-$type for all the studied structures, the average of S is much larger than this value within a reasonable value of the carrier concentration level, which indicates higher values of S and there may be higher values of $S^2\sigma$ and ZT. We found that our calculated values for the Seebeck coefficient are larger than those found for the Bi_2Te_3 and Bi_2Se_3 systems, as well as for other alloys. For example, at ambient pressure, measured value for polycrystalline $Sb_{1.5}Bi_{0.5}Te_3$ is reported to be $212\mu V/K$ [111], while a value of $287\mu V/°C$ at 54 $°C$ was reported for a $9.8\mu m$ thick

Bi_2T_3 thin film[112]. Also from the DFT calculations, using the vand der waals correction, Luo et al.[113] report a value of $S = 300\mu V/K$ for Bi_2Te_3 while for Bi_2Si_3 they found a value of $S = 600\mu V/K$. Comparing the Seebeck coefficients in $n-$type and $p-$type region, it can be noticed that for all the cases studied in this chapter the maximum values of S was higher in the $p-$type region. This indicated the prominence of the $p-$type doping in these materials.

The great enhancement in the values of the Seebeck coefficient for monolayer case in comparison with the values obtained in the bulk and nanoplates cases could be attributed to the following reasons:

1. The strong quantum confinement effect which makes S^2 increases linearly with decreasing the thickness. This is based on the theoretical prediction of Hicks and Dreselhaus in 1993 [16] that the electronic properties could be enhanced by putting the thermoelectric materials in superlattice structures with insulating barrier layers and that the improvement is largest for the shortest period superlattices.

2. The enhancement in the Seebeck coefficient of the monolayer case also can be explained based on the Mahan-Sofo theory [91], which suggests that a local increase in the total density of states over a narrow energy range around the Fermi level can achieve a high S [114, 115]. The same explanation could be inferred from the definition of the Seebeck coefficient in the Mott equation [116]. Therefore, the increase of S could be attributed to the sharp slope near the Fermi level in the density of states (DOS) of the monolayer case that comes from the increase in the contribution of Ga and Se $4P_z$ states as can be seen from the figure of the total density of states of monolayer 3.3.

3. By referring to the band structure of the studied cases shown in figure 3.2. In the monolayer case, there is less dispersion in the valence band around its maximum value in comparison with the bulk and nanoplates. It means that the effective mass of the holes in the monolayer case is higher than its corresponding value in the bulk and nanoplates cases. If we refer to the relation between the Seebeck coefficient and the effective mass for the metal [117]:

$$S = \frac{8\pi k_0^2}{3eh^2} m^* T (\frac{\pi}{3n})^{2/3}, \tag{3.1}$$

where h,n,e and m^* are Planck's constant, carrier concentration, electronic charge and the effective mass of the carrier, respectively. Even though our materials are semiconductor, we can use this relation to understand our results in a qualitative way. From this relation we can see that there is a direct relation between the Seebeck coefficient and effective mass of the carrier. As we have stated that the holes effective mass value should be higher in the monolayer case than its value in the bulk and nanoplates cases so we can expect that the value of the Seebeck coefficient is larger for the monolayer case which agrees with the results that we have obtained for the Seebeck coefficient which is shown in figure 3.6

3.4.2 Electrical conductivity

The electrical conductivity in metals originates from the motion of the electrons in the conductors while in semiconductor both holes and electrons contribute to the electrical conductivity. The charge carriers in the semiconductors are formed by thermal activation. Hence their concentration is temperature dependent, in contrary to the case of metal, where the electron concentration is basically constant. According to the equation:

$$\sigma = ne\mu_n + pe\mu_p \tag{3.2}$$

The temperature dependence of the conductivity σ can be expressed as a function of the mobilities μ_n and μ_p of electrons and holes, respectively, and the charge carrier concentration, n for electrons and p for holes.

Based on the electronic structure we calculated the electrical conductivity relative to the relaxation time (σ/τ, called the transport function) as a function of the chemical potential. Within the framework of Boltzmann transport (BT) theory [75], the constant scattering relaxation time (τ) approximation is usually adopted and the relaxation time is taken to be direction independent and isotropic. The validity of this approach has been tested earlier [91, 118–121] and the approximation has succeeded even for systems with highly anisotropic crystal axes [121]. As a consequence, the electrical conductivity (σ) is expressed in the form of the ratio (σ/τ). It is impossible to calculate σ itself without the knowledge of the scattering rate τ. In order to calculate τ an electron phonon interaction mechanism, or electron-impurity, must be assumed. Till now and up to our knowledges there is no data on scattering rate τ for GaSe material. Figure 3.7 shows the evolution of the electrical conductivity of the bulk, nanoplates, and monolayer ε GaSe relative to the relaxation time as a function of the chemical potential at temperature $T = 300$ K. The chemical potential μ represents doping or the charge carrier concentration. σ/τ has been taken in units $10^{20}\ 1/\Omega ms$.

All the studied structure shown a typical semiconductor behavior since the lower values of the σ/τ has been obtained at the lower values of the chemical potential, then it starts to increase as the carrier concentration increase in both the $p-$type and $n-$type regions. Furthermore, σ/τ is high in highly doped region for both $p-$type and $n-$type region. In both the monolayer and nanoplates, the maximum value of σ/τ has been obtained in $n-$type region while in the bulk case it is achieved in the $n-$type region.

In the $n-$type region, at a certain value of the chemical potential σ/τ starts to increase linearly as the chemical potential increase till it reaches to the maximum value and then starts to decrease again. The value of the chemical potential at which σ/τ starts to increase or decrease was different in each case. In this region, the maximum value of σ/τ has been obtained in the bulk GaSe is $3.46 \times 10^{20}\ 1/\Omega ms$ followed by $2.495 \times 10^{20}\ 1/\Omega ms$ in the nanoplates and the lowest values obtained in the monolayer case $2.1 \times 10^{20}\ 1/\Omega ms$.

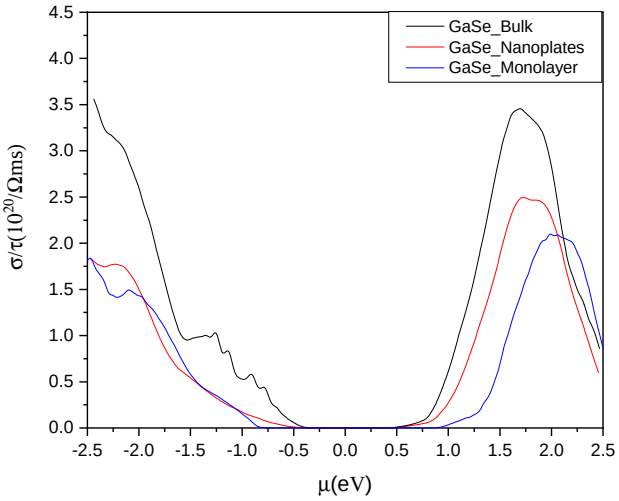

FIGURE 3.7: σ/τ of the bulk, nanoplates and monolayer $\varepsilon-$ GaSe at 300K

The behavior σ/τ in the $p-$type region was different from the $n-$type, there is a fluctuation in the increase of σ/τ as a function of the chemical potential whereas the overall behavior of σ/τ is that it increases as a function of the chemical potential until it reaches a maximum value at a certain value of the chemical potential, there was some points at which σ/τ decreases. In this region, the maximum value of σ/τ have been obtained also in the bulk case 3.56×10^{20} $1/\Omega ms$ followed by 1.82×10^{20} $1/\Omega ms$ in both the nanoplates and monolayer case. From the the results of σ/τ it was obvious that the confinement effect didn't improve the electrical conductivity of the GaSe this could be a result of the increase of the band gap values occurred in the 2 dimensional cases.

3.4.3 Power factors

It is known that the thermoelectric properties of the materials could be improved by enhancing the figure of merit (ZT). As the power factor comes as a numerator in the figure of merit relation $ZT = S^2\sigma T/k$, therefore, improving ZT can occur by maximizing the power factor $PF = S^2\sigma$ or minimizing k. Different approach have been adopted to increase ZT like doping or lowering the dimensionality of these materials to decrease the thermal conductivity [122, 123]. Also, there is a recent investigation that suggested that the output power, Q, is more important than ZT for the case of unlimited heat source such as solar or waste heat sources [124]. The maximum value of the output power, Q_{max}, includes the power factor ($PF = S^2\sigma$) as $Q_{max} = PF(T_h - T_c)/4L_1$, where T_h and T_c are the hot and cold side temperatures, respectively and L_1 is the length between the hot and cold sides. Hence, This parameter gives an indication of the thermoelectric properties since the higher PF is, the better is the efficiency of the TE device.

Using the existing information on the Seebeck coefficient (S) and the electrical conductivity relative to the relaxation time (σ/τ), one can obtain the power factor relative to the relaxation time ($PF/\tau = S^2\sigma/\tau$). It is clear that the power factor is directly proportional to Seebeck coefficient and electrical conductivity. The calculated power factor of bulk, nanoplates, and monolayer $\varepsilon-$ GaSe relative to the relaxation time at 300 K as a function of chemical potential between ∓ 2 eV as illustrated in Fig.3.8. PF/τ has been taken in units $10^{14}\mu W/cmK^2s$.

At the vicinity of the Fermi level, the power factor exhibits its minimum values. This is attributed to that σ/τ shows its minimum values in the vicinity of the Fermi level. beyond this region the values PF/τ started to increase.

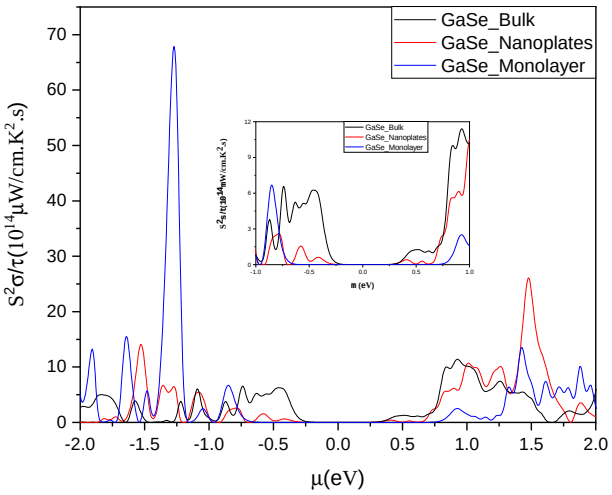

FIGURE 3.8: PF/τ of the bulk, nanoplates and monolayer $\varepsilon-$ GaSe at 300 K

In all the cases, the PF/τ as a function of the chemical potential consists of several peaks with different maximum value. The behavior of PF/τ was similar in both the $n-$type and $p-$type. The maximum value of PF/τ obtained in the $p-$type region was found in the monolayer case 67.86×10^{14} $\mu W/cmK^2s$ at -1.27 eV of the chemical potential while the maximum value in the $n-$type region was obtained in the nanoplates case 26.11×10^{14} $\mu W/cmK^2s$ at 1.48 eV. As we can see both values have been obtained at a high value of the chemical potential, and hence high doping value, which isn't favorable so we will have more interest in the higher good values obtained for PF/τ in the region with a smaller values of the chemical potential, and hence low doping concentration, as it is shown in the inset of fig. 3.8. In this interval of the chemical potential $[-1, 1]$ eV that is presented in the inset, it can be observed that in both $p-$type and $n-$type regions the better values of PF/τ has been found in the bulk case. In table 3.2 the highest values of the PF/τ obtained for each case inside this interval is written down. So even though the 2D cases have better values for PF/τ but obtaining this values at higher values of the chemical potential wouldn't be achieved easily in the experiment so the bulk cases would be recommended due to its good values obtained at smaller values of μ.

TABLE 3.2: The highest values of PF/τ obtained in the $n-/p-$ type region of bulk $\varepsilon-$polytype of bulk, nanoplates and monolayer GaSe at 300 K

	Bulk-GaSe		Nanoplates-GaSe		monolayer-GaSe	
	$p-$type	$n-$type	$p-$type	$n-$type	$p-$type	$n-$type
$PF/\tau(10^{14}\mu W/cmK^2s)$	6.56	11.40	2.60	10.54	6.69	2.51

3.4.4 Electronic thermal conductivity

The total thermal conductivity (k) is the sum of electronic thermal conductivity (k_e) and thermal conductivity of the phonons (k_l), i.e. $k = k_e + k_l$. since in metals and semiconductors, the responsible for their thermal conductivity are the electrons and phonon vibrations. Whereas the semiconductor's thermal conductivity is dominated by phonons, in metals this contribution is mainly due to electrons or free carriers [125, 126]. BoltzTraP calculates only the electronic part. For simplification k is used here to refer to the electronic part of the chemical potential instead of $k = k_e$.

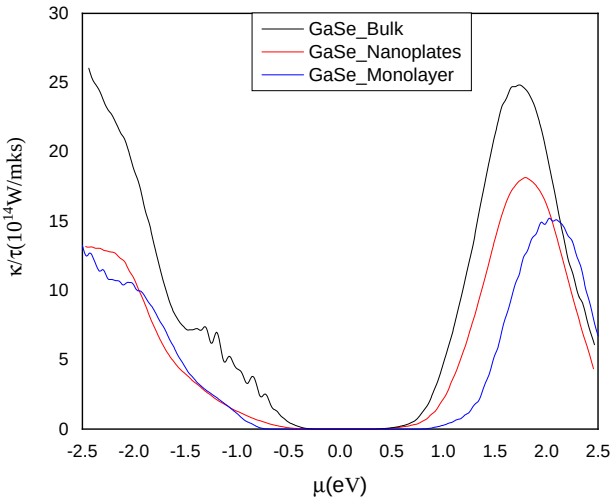

FIGURE 3.9: (k/τ) of the bulk, nanoplates, and monolayer $\varepsilon-$ GaSe at 300 K

The electronic thermal conductivity per relaxation time (k/τ) of the bulk, nanoplates, and monolayer $\varepsilon-$GaSe versus the chemical potential at the temperature of 300 K is depicted in Figure 3.9. When the value of the chemical potential is zero the thermal conductivity shows its minimum value and increases as the potential increases. The behavior of the thermal conductivity as was similar to the behavior obtained for the electrical conductivity 3.7 as they are linked by the Wiedemann–Franz law in the $p-$type region, the values of k/τ for all the investigated materials increases as the chemical potential increases. Its peak values were 26.035 (at -2.43 eV), 13.18(at -2.47 eV) and 13.13(at -2.49 eV) $\times 10^{14} W/mKs$ in bulk, nanoplates, and monolayer respectively.

In the $n-$type region the increase of k/τ as a function of the chemical potential was more pronounced than in the $p-$type region. At a certain point k/τ started to increase linearly as the chemical potential increase till it reaches to a maximum value and then starts to decrease again. In this region, the lowest value of k/τ has found for monolayer case the same as in $p-$type region. The maximum values of k/τ was 24.84 (at 1.74 eV), 18.15(at 1.8 eV) and 15.21(at 2.02 eV) $\times 10^{14} W/mKs$ in bulk, nanoplates, and monolayer, respectively. So in both the $n-$type and $p-$type region the lower values of thermal conductivity was obtained in the 2D cases.

As we mentioned before that the BoltzTraP code used in our calculations can only calculate the electronic part of k, we cannot provide a complete prediction of the figure of merit of the calculated systems without knowing the lattice thermal conductivity. However, in order to expect how would it be the figure of merit in the studied structure we assumed that the lattice and electronic thermal conductivities are quantitatively equivalent and calculate ZT as a function of the chemical potential. Our calculated value for the figure of merit was 0.5 for both the bulk and monolayer and 0.45 for the nanoplates. It means that GaSe could be preferable as a good thermoelectric materials in the bulk and monolayer case than in the nanoplates. However we claim that ZT in both the monolayer and nanoplates would be better than the obtained values since in the two dimensional case the lattice thermal conductivity is expected to be smaller in the nano-structuring as the scattering of the phonons increases in this structure.

Chapter 4

The electronic, and thermoelectric properties of InSe

4.1 Electronic properties

4.1.1 Electronic band structure

In this section a comparison between the calculated electronic band structure of the bulk, nanoplates and monolayer $\varepsilon - \mathrm{InSe}$ is presented. Our results are a good opportunity to study how the progressive enhancement of quantum size confinement can strongly tune the electronic properties of these atomically thick layer. As in the case of GaSe, the electronic structure calculations of $\varepsilon - \mathrm{InSe}$ have been done using the the generalized gradient approximation with the formalism of Perdew et. al. [83] for the correlation potential for all the studied cases, while for the bulk case the recently proposed modified beck and Johnson correction(mBJ) correction [87] has been added to improve the value of the band gap and get a value close to the experimental values and the results are presented in figure 4.1. The calculations of the electronic structure have been done using the optimized lattice parameters obtained for $\varepsilon - \mathrm{InSe}$, $a, b = 4.1593$Å and $c = 17.3649$Å after the relaxation process to the experimental lattice parameters. The optimized parameters were larger than the experimental values that are listed in the literature [85] as a consequence of the fact that the interlayer coupling is mostly driven by van der Waals interactions, which are not reproduced by the PBE energy functional. The high symmetry points (axes), labeled as Γ, M, K, Γ and A are used to describe the electron band structure of the bulk case while in the 2D case there was no need to plot the dispersion along the $\Gamma - A$ of the Brillouin zone as we mentioned before that it has no physical meaning and we already showed in the case of GaSe that the band structure is dispersionless along this line.

For the bulk case of $\varepsilon-$ InSe, both valence band maxima and conduction band minima occur at the center of the Brillouin Zone, Γ, indicating that they are direct band gap semiconductors. In a previous work on $\gamma-$ InSe [94] they found that the compound is a direct gap semiconductor but the minimum of the conduction band and

the maximum of the valence band both occur at $Z-$point of the brillouin zone. The use of the modified Beck and Johnson correction (mBJ) has displaced the minimum of the conduction level to higher values, like in the case of GaSe, leading to an increase in the value of the band gap as can be seen from the figure 4.1(a). It has also displaced up the valence bands located between -7.0 eV and -3 eV.

For the monolayer and nanoplates cases of $\varepsilon - \mathrm{InSe}$ the calculation has been done by using only the GGA. The central and lower panel of figure 4.1 displays their electronic band structure. We found that the quantum confinement effect on the electronic band structure of InSe was similar to the results obtained in GaSe. Since the minimum of the conduction band still occurs at Γ as in the bulk case and the real change was in the the maximum of the valence band. The maximum of the valence band was displaced from being at Γ point to be between K and Γ exhibiting a cross over from the direct to indirect gap semiconductor. The difference between the direct and indirect band gap was small in comparison with the band gap value since the difference between the two maximums of the valence band was .015 and 0.08 in the nanoplates and monolayer respectively. Another maximum has been found between Γ and M, the difference between this maximum and the maximum of the valence is almost 6.2×10^{-4} and 3.1×10^{-3} eV for nanoplates and monolayer, respectively. As the valence band in the monolayer case has less dispersion in comparison with the bulk case, it means that the effective mass of the holes in the monolayer case is larger than the effective mass of the holes of the bulk case. The low dispersion of the valence band in the two dimensional cases indicates that the p-type doping of this material may be more preferable for good thermoelectric properties than the n-type. A similar feature was previously found to exist in bulk InSe under pressure where they found that the valence band maximum turned to be ring shaped at 7 GPa. They explained that the pressure provokes a change in some parameters in the equation of the hole effective mass in the framework of the $k.p$ model which in turn leaded to different dispersion of the valence band maximum. [100]

TABLE 4.1: Calculated band gap in eV for the bulk, nanoplates, and monolayer InSe

	InSe		
	E^{GGA}_{direct}(eV)	$E^{GGA}_{indirect}$(eV)	E^{mBJ}_{direct}(eV)
Bulk	0.45096		1.31028
Nanoplates	0.3131	0.29784	
Monolayer	1.17843	1.098	

The values of the band gap obtained in the three studied cases are recorded in table 4.1. As the use of the modified Beck and Johnson correction has displaced the minimum of the conduction band to higher values, it implies that the band gap value of the bulk obtained by using this correction is larger than its value without it which is already demonstrated in the table. In the previous theoretical study [94] on $\gamma - \mathrm{InSe}$, they found that the band gap (0.44 eV) calculated using the GGA approach was lower than one half of the experimental value (1.23 eV) and the use of

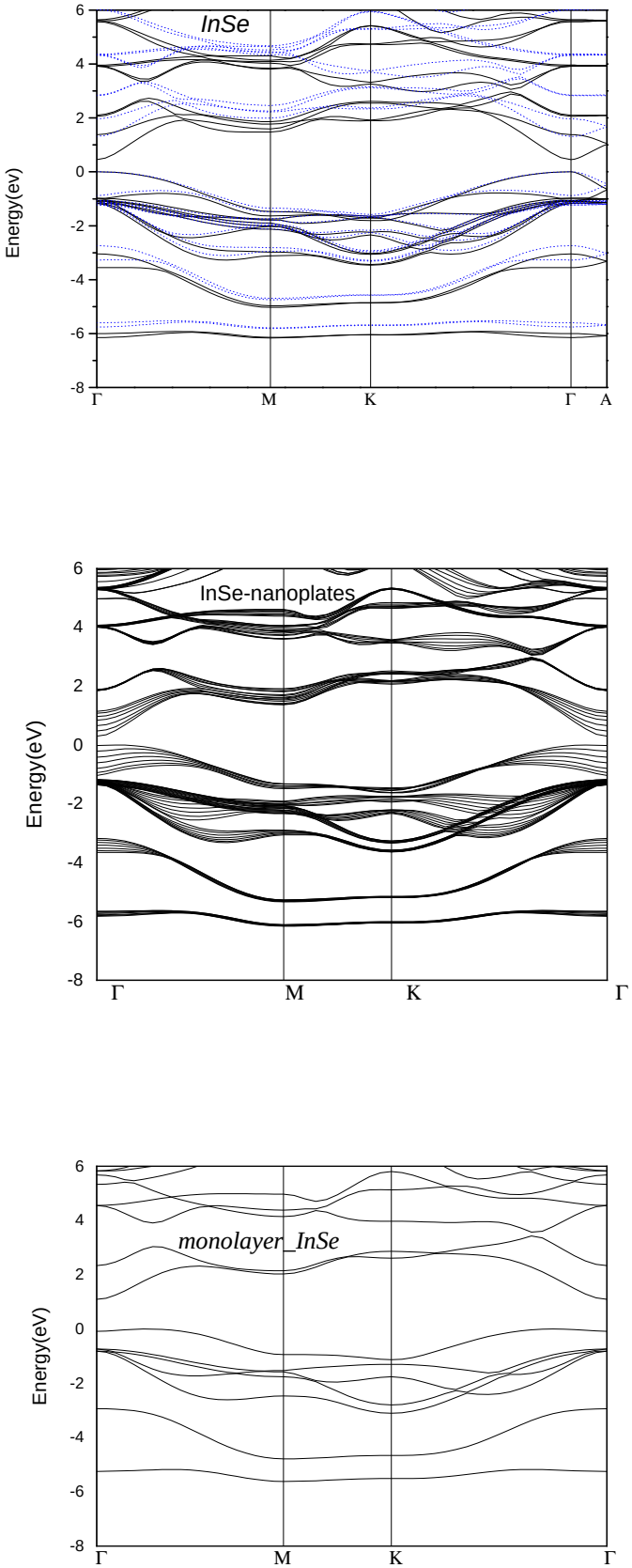

FIGURE 4.1: The calculated band structure of $\varepsilon-$ InSe in the bulk, nanoplates and monolayer structures. The dark solid line represents the calculation with GGA. The blue dotted line represents the calculation with GGA+mBJ

m-BJ correction improves the calculated band gap value to be 1.83 eV but this value is about 49% bigger than the experimental one. To the best of our knowledge, there are no experimental data for the energy band gap of the $\varepsilon-$ structure available in the literature to make a meaningful comparison. However, we can compare our calculated energy gaps using the m-BJ correction with the experimental band gap value of $\gamma - \mathrm{InSe}$ which shows a reasonable agreement. In the monolayer case there was a large increase in the value of the band gap in comparison with the bulk case, and that increase could be attributed to the absence of the interlayer bond in the monolayer case that is similar to the results obtained in the case of GaSe. The band gap of the nanoplates was smaller than the band gap of the bulk case in contrast to the results found for GaSe.

4.1.2 Total and partial density of states

In this section, we present the calculated total (DOS) and partial density of states (PDOS) of bulk, nanoplates, and monolayer $\varepsilon - \mathrm{InSe}$. Figures 4.2, 4.3 and 4.4 show their total density of states, the contribution of the In, and Se atoms to the total density of states, respectively. The partial DOS for each element is a sum of a partial DOS over all muffin-tin spheres of the same compound.

There was a prominent difference between the values of the total density of states of the three studied structures that was consistent with the number of atoms included in each case. In the total density of states we found that the lowest band contribution to the bond is around 6.0 eV below the maximum of the valence band in the Bulk and nanoplates and around 5.5 eV in the monolayer.

From the plots of the partial density of states it is obvious that the cation and anion orbitals contribute in a similar way to the valence and conduction band which was expected and has already been found before in the case of GaSe in the previous chapter. The upper valence band states have a band–width of about 5.11, 5.49 and 5.05 in the bulk, nanoplates, and monolayer respectively. The valence band maximum in this compound has predominant Se-$4p_z$ character while the following deeper valence bands have predominant Se-$4(p_x + p_y)$ character as discussed in the literature [127–129] and there is a very small contribution comes to the band from In $5s$ and $5p$ states. The lower valence band is dominated by the main contribution that comes from In $5s$ states, and lower contributions from Se $4(p_x+p_y)$, $4s$, and $4p_z$ states to that band has been found. On the other hand, the lower conduction bands are mainly constituted of In $5s-$orbital hybridized with Se $4p_z$, $4(p_x + p_y)$ states. An important change has been noticed at the maximum valence band of the monolayer case as there was an abrupt increase in the total density of states, from Se-$4p_z$ orbitals, at the Fermi level. This increase is predicted to enhance the Seebeck coefficient Values in the monolayer case.

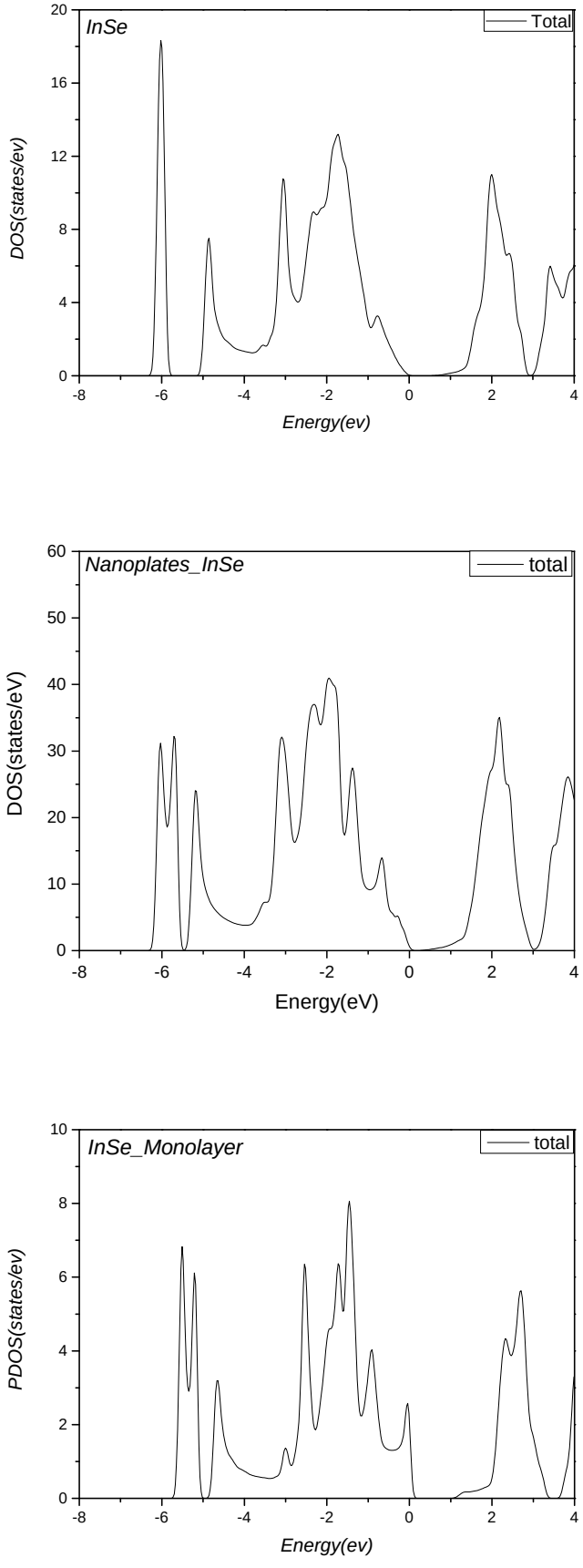

FIGURE 4.2: The calculated total density of states for bulk, nanoplates, and monolayer $\varepsilon - InSe$

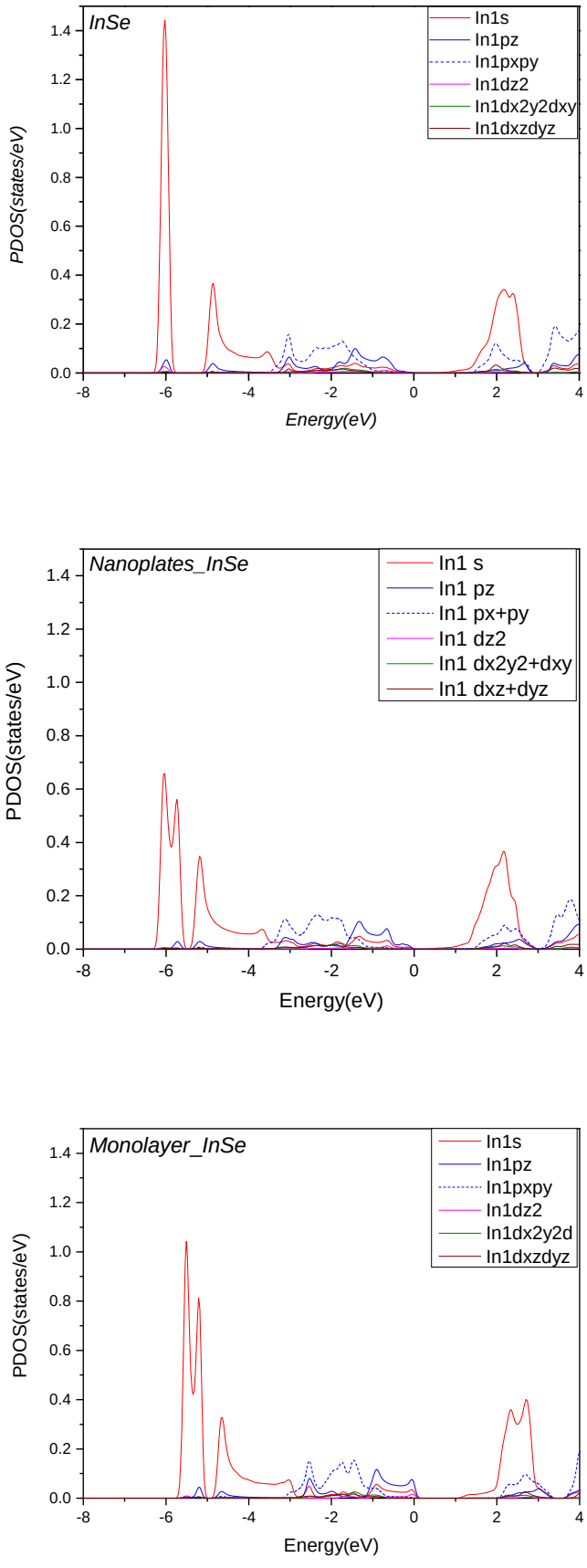

FIGURE 4.3: The partial contribution of In atoms to the total density of states in bulk, nanoplates, and monolayer $\varepsilon-$ InSe

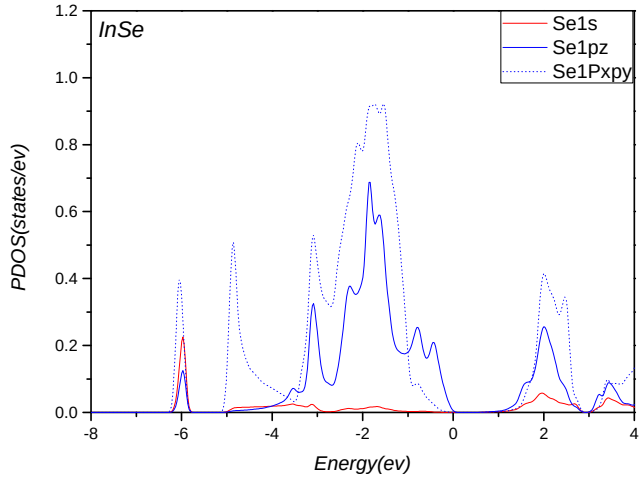

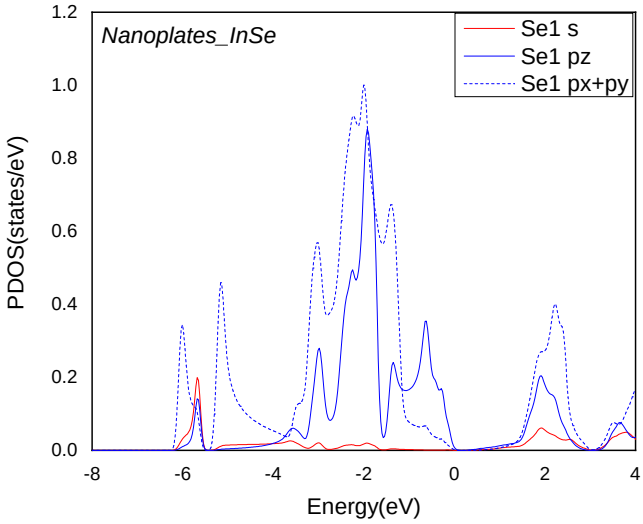

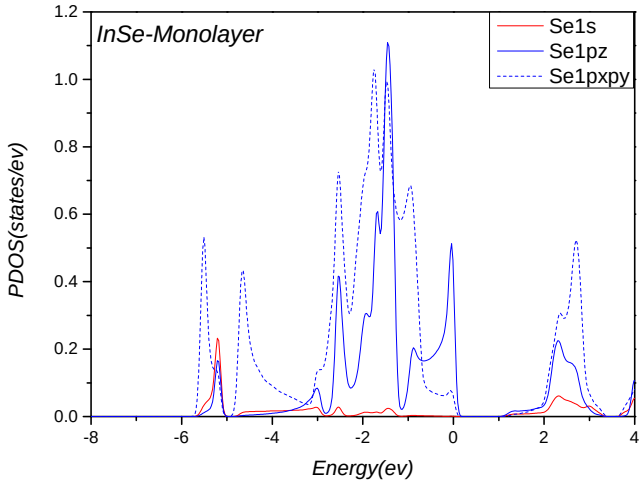

FIGURE 4.4: The partial contribution of Se atoms to the total density of states in bulk, nanoplates, and monolayer $\varepsilon-$ InSe

4.2 Seebeck Coefficient

The constant scattering time approximation, known as the constant relaxation time approximation, consists in taking the energy dependence of the band structure as the main factor in the energy dependence of the conductivity in the transport equation. Using this approximation the scattering time in the expression for the thermopower is cancelled, so that the thermopower is obtained as a function of temperature and doping level from the band structure without any additional input. In this section the relation between the electronic structure near the band edges and the values of the Seebeck coefficient in InSe will be discussed. The Seebeck coefficient of the bulk, nanoplates, and monolayer $\varepsilon-$ InSe vs. chemical potential at 300 K are presented in the figure 4.5.

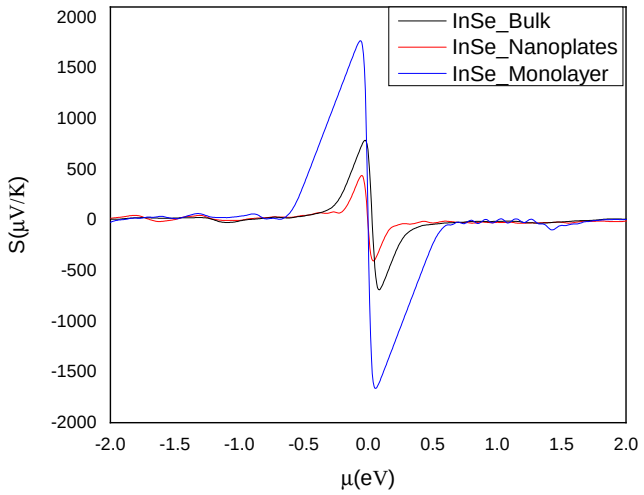

FIGURE 4.5: The Seebeck coefficients of the bulk, nanoplates and monolayer $\varepsilon-$ InSe at 300 K.

The Seebeck coefficients exhibit two pronounced peak for $n-/p-$type around the E_f in all the studied case. The highest value of the Seebeck coefficients has been obtained for the monolayer case since the maximum value of the Seebeck coefficient at $300K$ for the $p-$type region was $1765\mu V/K$ while it was $1662\mu V/K$ for $n-$type region. In the case of the bulk S exhibits lower values as it was $785\mu V/K$ in the $p-$type region $689\mu V/K$ in $n-$type region while the lowest value of the Seebeck coefficient has been found in the nanoplates, S was $437\mu V/K$ in the $p-$type region $405\mu V/K$ in $n-$type region. Comparing between the Seebeck coefficients values in $n-$type region and $p-$type region. It can be noticed that for all the studied materials to get good values for the Seebeck coefficient the $p-$type region will be more desirable that the $n-$type region. All the obtained values were good in comparison with the values obtained in a recent studied materials since for example in a computational study [130] of the transport properties of a single layer of Bi_2Se_3 the values reported for the Seebeck coefficient were between $-90\mu V/K$ at $300K$ and $-174\mu V/K$ at $900K$.

For all the studied cases in this chapter, no matter $p-$type or $n-$type, within a reasonable value of the carrier concentration level, the average of S is larger than the recommended values for efficient thermoelectric materials [109, 110]. The higher values of S could lead to higher values of $S^2\sigma$ and ZT.

The range where the materials exhibit good values for the Seebeck coefficient was different in the studied materials as it was wider in the case of monolayer than for both the bulk and nanoplates. The range was $[-0.64, 0.6]$ eV for Monolayer, $[-0.37, 0.4]$ eV for bulk, and $[-0.22, 0.24]$ eV nanoplates. Beyond these points the Seebeck coefficient decreases. It means that the range where the materials exhibits a good value for the Seebeck coefficient has been more extended in the monolayer case than in the bulk case which indicates that in the bulk case the compounds favor low doping.

As we commented before in the chapter of GaSe, the great enhancement in the values of the Seebeck coefficient for monolayer case in comparison with the bulk and nanoplates could be attributed to three reasons; the strong quantum confinement effect on the values of the Seebeck coefficient [16], the local increase in the total density of states over a narrow energy range around the Fermi level that has been found in the monolayer and was shown in fig. 4.2 that is supposed to lead to higher values of the S according to the Mahan-Sofo theory[16, 91, 114, 115], and the low dispersion of the valence band of the monolayer case shown in figure 4.1 indicate a high value of the hole effective mass and hence higher values of the Seebeck coefficient as a result of the direct relation between the Seebeck coefficient and effective mass of the carrier.

4.3 Electrical conductivity

Within the frame work of constant scattering time approximation (σ/τ) can be obtained directly from the electronic structure as a function of the carrier concentration and the temperature. To calculate σ itself, the knowledge of the scattering rate is a must at the same time up to our knowledges there is no data on the scattering rate τ for bulk or nanoplates or monolayer InSe. Figure 4.6 shows the electrical conductivity of the bulk, nanoplates, and monolayer InSe relative to the relaxation time as a function of the chemical potential μ at temperature $T = 300$ K. The chemical potential μ represents doping or the charge carrier concentration.

The behaviour of σ/τ as a function of the chemical potential in all the studied case of InSe was the typical expected behavior of semiconductor materials; since σ/τ increased as a function of the chemical potential, i.e. the number of carriers, in both the $p-$type and $n-$type regions. Furthermore, while in both the monolayer and nanoplates of InSe the maximum value of σ/τ has been obtained in $n-$type region, the opposite have been found in the case of bulk since the maximum value of σ/τ is in the $p-$type region. Meanwhile, the overall behavior of σ/τ was similar in the three cases in both $p-$type and $n-$type region.

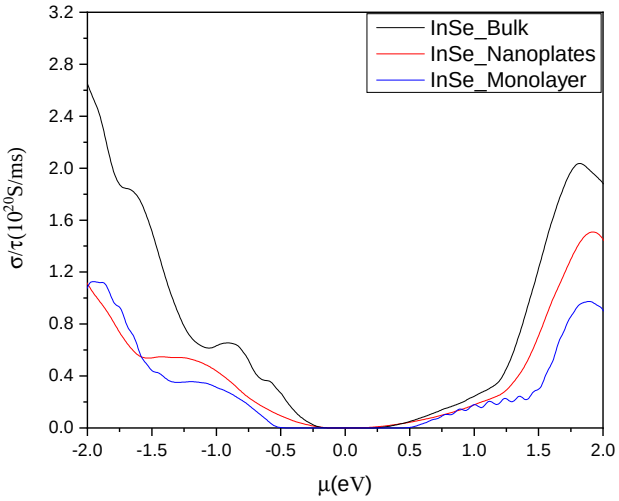

FIGURE 4.6: σ/τ of the bulk, nanoplates and monolayer $\varepsilon-$ InSe at 300K.

In the $n-$type region, σ/τ increase as a function of the chemical potential increase till it reaches to the maximum value and then starts to decrease again. In this region, the maximum value of σ/τ for bulk is 2.04×10^{20} $1/\Omega ms$ followed by 1.51×10^{20} $1/\Omega ms$ the nanoplates and then 0.97×10^{20} $1/\Omega ms$ for monolayer.

In the $p-$type region, σ/τ increases as a function of the chemical potential until it reaches a maximum value but at the same time there was a fluctuation in the curve as there was some points at which σ/τ decreases. In this region, the maximum of σ/τ for bulk is 2.65×10^{20} $1/\Omega ms$ followed by 1.13×10^{20} $1/\Omega ms$ for the monolayer and 1.1×10^{20} $1/\Omega ms$ for the nanoplates case. Therefore, it can be concluded that the values of σ/τ is larger in the bulk case.

The better values of σ/τ was found at high chemical potential and hence in a highly doped region which isn't very favorable experimentally so we will be more interested in the values obtain in a small interval around the zero value of the chemical potential where the values bulk case exhibits the better values of σ/τ than nanoplates and monolayer case.

4.4 Power factors

The power factor of the bulk, nanoplates, and monolayer InSe has been calculated using the obtained results of the Seebeck oefficient (S) and the electrical conductivity relative to the relaxation time (σ/τ) and represented in Fig. 4.7 as a function of chemical potential between ∓ 2 eV at 300 K. PF/τ has been taken in units $10^{14}\mu W/cmK^2s$.

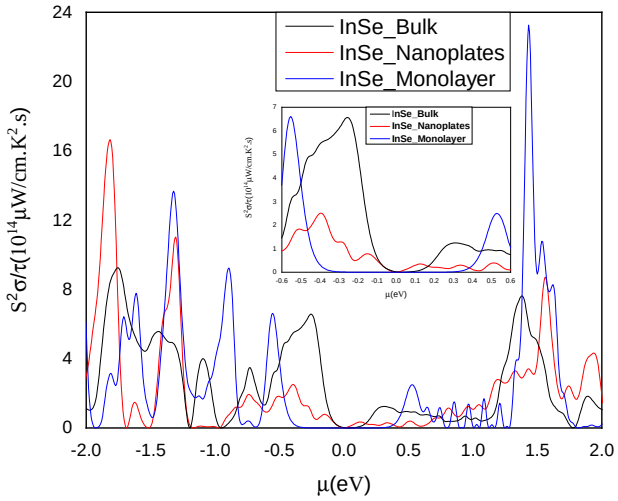

FIGURE 4.7: PF/τ of the bulk, nanoplates and monolayer $\varepsilon-$ InSe at 300 K.

The power factor exhibits the minimum values around the Fermi level that was expected from the small values of the conductivity at the Fermi level. Beyond this region the PF/τ started to increase. It is clear that the behavior of PF/τ was similar in all the studied cases as it consists of several peaks over a continues curves. In the $n-$type region, the case that have shown the maximum value PF/τ, 23.25×10^{14} $\mu W/cmk^2s$ at 1.43 eV, was the monolayer case followed by the value 8.7×10^{14} $\mu W/cmK^2s$ at 1.56 eV in the nanoplates and then 7.62×10^{14} $\mu W/cmK^2s$ at 1.37 eV in the bulk case. In the $p-$type region the maximum value of PF/τ 16.64×10^{14} $\mu W/cmK^2s$ at -1.81 eV has been attained in the nanoplates. Next it comes the value 13.66×10^{14} $\mu W/cmK^2s$ at -1.32 eV in the monolayer and then 9.25×10^{14} $\mu W/cmK^2s$ at -1.75 eV. From all that values and the plot 4.7, it is obvious that the best value of the power factor has been found in the 2 dimension structures but these values are attainable at higher values of the chemical potential; i.e high doping. Inside the interval $[-0.6, 0.6]$ eV of the chemical potential, at lower doping concentration that could be attainable experimentally, the better values of PF/τ can be found in the $p-$type region of the bulk and monolayer as displayed in the inset shown in the figure 4.7.

4.5 Electronic thermal conductivity

For designing efficient thermoelectric devices, materials with low thermal conductivity are required in order to maintain the temperature gradient. The electronic thermal conductivity per relaxation time (k/τ) of bulk, nanoplates, and monolayer InSe versus the chemical potential at the temperature of 300 K is depicted in Figure 4.8. When the value of the chemical potential is zero, the thermal conductivity shows its minimum value and then increases as the chemical potential increases.

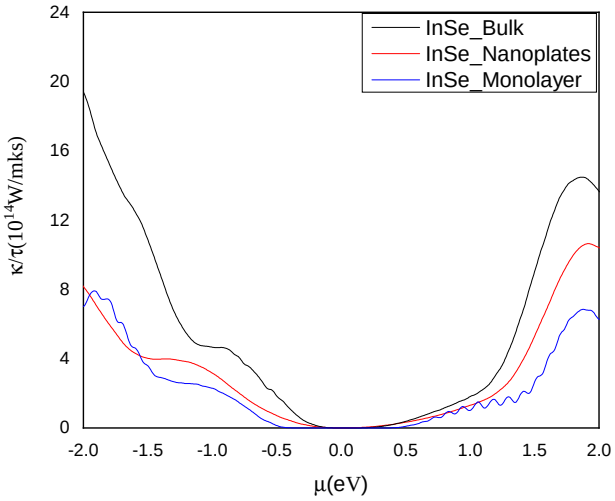

FIGURE 4.8: (k/τ) of the bulk, nanoplates, and monolayer $\varepsilon-$ InSe at 300 K

In the $p-$type region, the values of k/τ for all the investigated cases increases as the chemical potential increases while there was a fluctuation in the curves as there were some points where k/τ decreased. Its peak value in each case was 19.425 $\times 10^{14} W/mKs$ at -2 eV, 8.224 $\times 10^{14} W/mKs$ at -2 eV, and 7.886 $\times 10^{14} W/mKs$ at -1.92 eV in bulk and nanoplates, and monolayer, respectively.

In the $n-$type region the increase of k/τ as a function of the chemical potential was more pronounced than in the $p-$type region. In this region the fluctuation has been noticed only in the case of monolayer. The overall behaviour of k/τ in all the cases was similar as its value increases with the increase of the of the chemical potential till it reaches a maximum value and then starts to decrease. The peak values of k/τ in the $n-$type was 14.48 $\times 10^{14} W/mKs$ at 1.86 eV, 10.64 $\times 10^{14} W/mKs$ at 1.91 eV and 6.84 $\times 10^{14} W/mKs$ at 1.87 eV has been found in bulk, nanoplates, and monolayer, respectively. In the chemical potential between ∓ 0.6 (eV), the investigated materials exhibit minimum value of the thermal conductivity and in both the $n-$type and $p-$type region, the lower values for thermal conductivity can be attained in the monolayer case.

We applied the same strategies that we used in the previous chapter to calculate ZT of the three structure of InSe as a function of the chemical potential. The maximum value obtained for the figure of merit was approximately 0.52 (0.47), 0.49 (0.48) and 0.38 (0.34) in the $p-$type ($n-$type) region of the bulk, monolayer and nanoplates, respectively.

Chapter 5

The electronic, and thermoelectric properties of $\mathrm{InGaSe_2}$

5.1 Crystal structure

The $\mathrm{InGaSe_2}$ heterostructure is constructed by simultaneously stacking one layer of GaSe and one layer of InSe. The layers stacking that have been considered in this work corresponds to the hexagonal $\varepsilon-$ polytype with space group $P\bar{6}m2$. In this polytype, the unit cell consists of two layers, one layer of GaSe and one layer of InSe. In a layer we have the same stacking, independently if we have InSe or GaSe, although the bond distances are different. Each layer has a hexagonal symmetry and is composed of two planes of metal atoms sandwiched between two chalcogen planes. Hence there is one layer where there are two planes of In atoms sandwiched between two planes of Se atoms and the next layer constitutes of two planes of Ga atoms sandwiched between two planes of Se atoms as shown in figure 5.1 where four unit cell of $\mathrm{InGaSe_2}$ in the xy plane and half layer out of the unit cell in the $z-$ direction are drawn.

The unit cell shown in this figure allows us to observe the inter-atomic bonds. The cations are tetrahedrally coordinated to three anions and one cation while the anions are bounded to three cations. Cation-cation bonds are oriented perpendicular to the layer structure. The two planes of Se atoms in two adjacent layers are bound through van der Waals forces and thus, the Se-Se inter-layer distances are larger than the other bond distances. This distance between the layers is called the van der Waals gap. This crystal structure that we proposed [131] differs from the supperlattice proposed by Gashimzade et al. [132], where the stackings of InSe and GaSe are in their bulk-like crystal structure ($\gamma - \mathrm{InSe}/\varepsilon - \mathrm{GaSe}$). The particular configuration that we chose depends on the fact that the symmetries of individual monolayers of InSe and GaSe are similar (D_{3h} point group) and such similarity breaks in the bulk compounds[100].

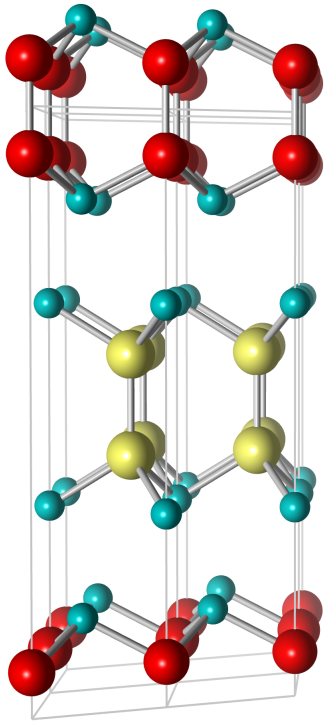

FIGURE 5.1: $InGaSe_2$ supercell with space group $P\bar{6}m2$ showing the stacking of GaSe/InSe. The yellow, red, and turquoise balls represent indium, gallium, and selenium atoms, respectively.

5.2 Computational details

To calculate the electronic band structure, we followed the same procedure as for InSe and GaSe cases. The convergence of the total energy in terms of the variational cutoff-parameters has been guaranteed by using an appropriate set of parameters. The value of RK_{max} used was 13 Ry while the value of the atomic sphere radius R_{MT} has selected to be 2.2 a.u. for both In and Ga atoms while for Se atom it was 2.3 a.u. The value of G_{max} was 13 Ry. A set of 60 $k-$points which is equivalent to a $16\times16\times3$ Monkhorst-Pack grid in the unit cell has been used while for the caluclation of the transport coefficients a dense mesh of $k-$points is needed so we used 364 $k-$points in the irreducible wedge of the Brillouin zone that is equivalent to a $30 \times 30 \times 6$ Monkhorst-Pack grid.

To optimize the lattice parameters, the initial lattice parameters have been chosen to be the average value of the lattice parameters of GaSe and InSe unit cell; $a = 3.8795$ and $c = 16.334$ Å. Also the positions of the atoms inside the unit cell have been optimized by doing a minimization of the forces in the unit cell. The electronic band structure has been calculated using the optimized lattice constants, like GaSe and InSe, for the bulk case $\varepsilon - InGaSe_2$ the modified Becke-Johnson correction, that corrects the systematic underestimation of the electronic band gap showed in DFT

calculations, has been included in part of the calculations while for the nanoplates and monolayer cases it was not included, this is because of the recommendation of authors of the Wien2k not to use this correction for the 2D systems.

5.3 Electronic properties

5.3.1 Electronic band structure

After the optimization of the structural parameters of $InGaSe_2$ we found that the layers of GaSe will be tensioned in the plane and thus there will be a compression in the Z direction, while in the case of InSe layers there will be a compression in the plane and a tension in the z direction which comes from the fact that the In atom has a larger radius than Ga, thus the unit cell of GaSe is smaller than that of InSe as already shown in the last two chapters. The optimized lattice parameters for the $InGaSe_2$ has found to be $a = 3.945$Å and $c = 16.61$Å. In the previous chapters, we have seen that the PBE functional overestimate the lattice parameters with respect to experimental measurements as it doesn't include the van der Waals (vdW) corrections so it could be assumed that if this compound can be synthesized, the experimental value of this superlattice should be larger than the values obtained in this calculations. The van der Waals forces should not affect much the electronic properties so we have calculated the electronic structure using these optimized parameters and the results was presented in the figure 5.2.

The upper panel displays the band structure of the bulk $\varepsilon - InGaSe_2$ the black solid line represents the calculation with the GGA approximation while the blue dotted line represents the calculations by including the mBJ correction. Like the pristine materials, ε−InSe and GaSe, the bulk $InGaSe_2$ shows a direct semiconductor character Since both the minimum of the conduction band and the maximum of the valence band occurs at the center of the Brillouin zone, Γ, while in the superlattice $InGaSe_2$ the band gap is lower than the one of the pristine. The value of the band gap without using the mBJ is $E_g = 0.38$ eV. A very significant difference has been found in the dispersion of the valence band in this compound has a particular aspect since in the $\Gamma - A$ direction the valence band was more dispersed than in the $\Gamma - K$ direction. As explained in previous study this would affect the thermoelectric properties of the material [133]. In this superlattice, the mBJ correction doesn't only increases the value of the band gap by moving the minimum of the conduction band in the upward direction, modifying the band gap $E_g^{mbj} = 1.27$ eV, but also reduced the slope of the dispersion of the valence band in the $\Gamma - A$ direction. We expect that the experimental value should be closer to the band gap calculated with this correction.

In the central and lower panel of the figure 5.2 the calculated band structure of the nanoplates and monolayer case, respectively, is presented to show the effect of reducing the dimensionality of this compound on its band structure. In the nanoplates

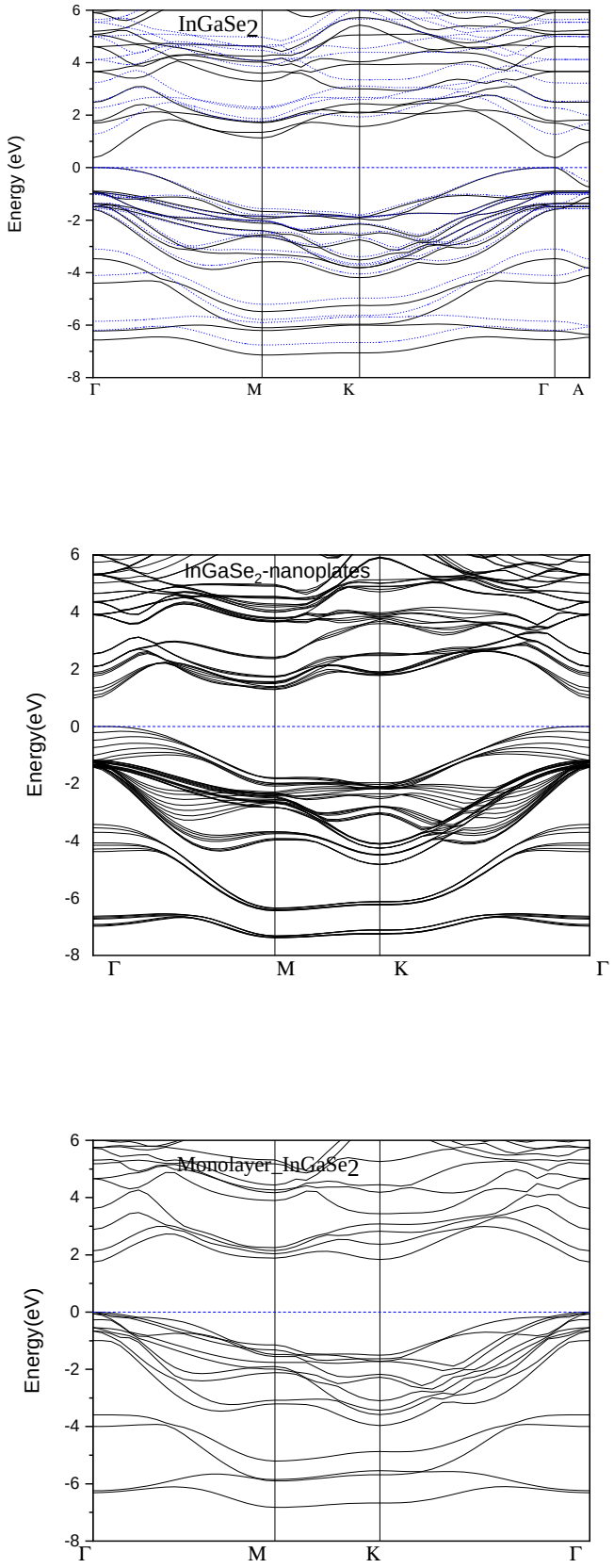

FIGURE 5.2: The calculated band structure for bulk, nanoplates, and monolayer $\varepsilon - InGaSe_2$. The dark solid line represents the calculation with GGA. The blue dotted line represents the calculation with GGA+mBJ.

case the material turned to be indirect semiconductor that coincide with the results obtained in the pristine compounds. Even though the minimum of the conduction band still occurs at Γ, the valence band maximum has moved to be between two symmetry points of the Brillouin zone, K and Γ. The direct band gap, $E_g^{direct} = 0.9898$ eV, was larger than indirect band gap, $E_g^{indirect} = 0.988$ eV, by almost negligible amount, 0.002 eV. Another maximum has been found between Γ and M creating another indirect band gap $E_g^{indirect} = 0.9883$ eV that also less than the direct band gap. The existence of those points reflects how flatten is the valence band of the nanoplates $InGaSe_2$. This results are consistent with the results obtained in the pristine compounds.

In the case of monolayer in comparison with the bulk case no changes have been noticed in the maximum of the valence band and the minimum of the conduction band since both points still occur at Γ. The real change was the increase found in both the band gap value $E_g^{direct} = 1.74965$ eV and the dispersion of the valence band. This indicates that, unlike the indirect band gap nature found in the $InSe$ and $GaSe$ monolayer, the monolayer $InGaSe_2$ is a direct band gap semiconductor. From all the studied cases, the largest band gap value was the one of monolayer followed by the gap of nanoplates and then the bulk.

5.3.2 Total and partial density of states

As the electron states around the Fermi level have an important effect on the thermoelectric transport properties of the material, we calculated the total and partial density of states (TDOS and PDOS) of the bulk, nanoplates, and monolayer $\varepsilon - InGaSe_2$ and draw them in Figure 5.3, 5.4, 5.5 and 5.6, respectively. In the bulk, nanoplates, and monolayer cases the lowest band contribution to the bound is around -7, -7.5, and -6.5 eV, respectively. It means that the width of the valence band in this compound changes depending on the the number of layers. In the three studied cases, the contributions of the orbitals of the atoms to the valence and conduction band is similar. The same that have been illustrates before in the pristine compounds GaSe and InSe. As well as the remarkable difference between the values of the total density of each case has been found. The lower valence band has the $s-$ character since the most important contribution comes from $5s$In and $4s$Ga orbitals and also a small contribution from Se, $4s$, $4p_z$and $4(p_x + p_y)$ states. Meanwhile, the valence band at the Fermi level has the $p-$ character, seeing that the main contribution comes from Se, $4p_z$and $4(p_x + p_y)$ states and a little contributions from $5p, 5s$ In and $4s, 4p$ Ga states reflecting that the bond between the atoms is a covalent bonding. Finally, the conduction band is a mixture of the In and Ga states, mainly $s-$ orbitals, and Se, $4p_z$ and $4(p_x+p_y)$ states. The most important feature of the density of states in the monolayer case, in comparison with the bulk and nanoplates cases, is that in the valence band close to the Fermi level there is a sharp increase in the density of states and another defined peak appears there. These features would contribute to improving the thermoelectric properties of the monolayer case of $InGaSe_2$.

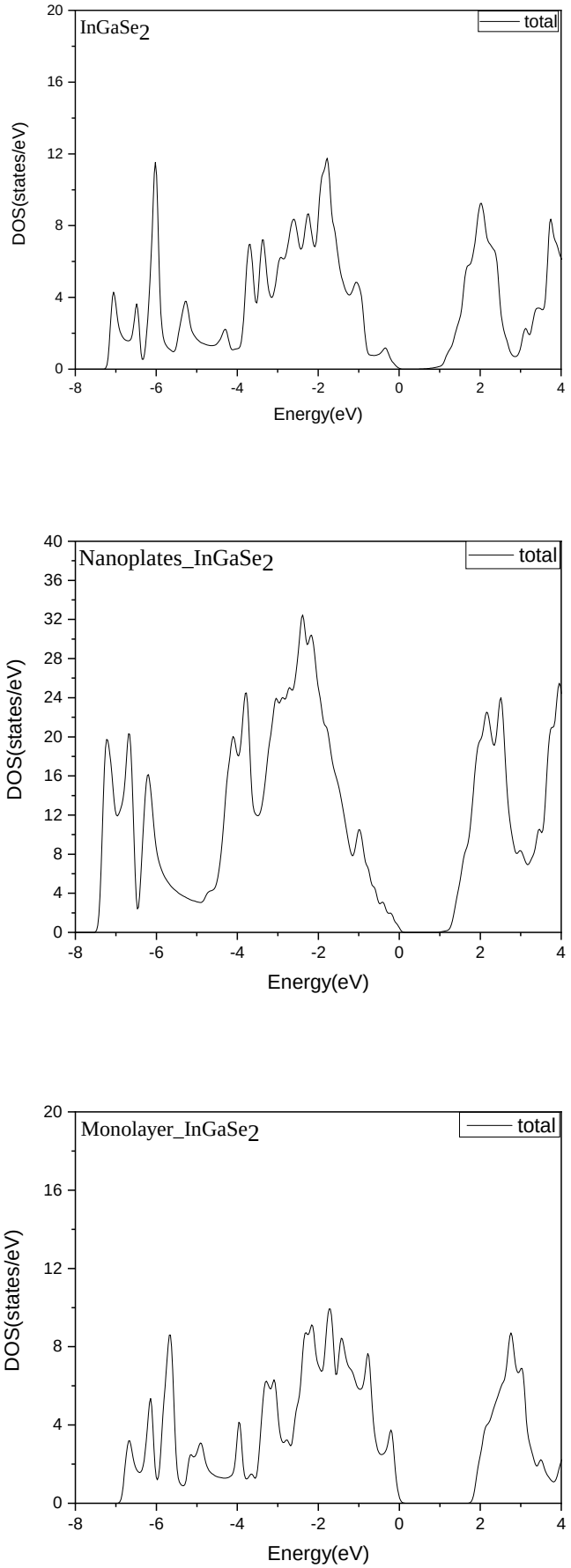

FIGURE 5.3: The calculated total density of states for bulk, nanoplates and monolayer $\varepsilon - InGaSe_2$.

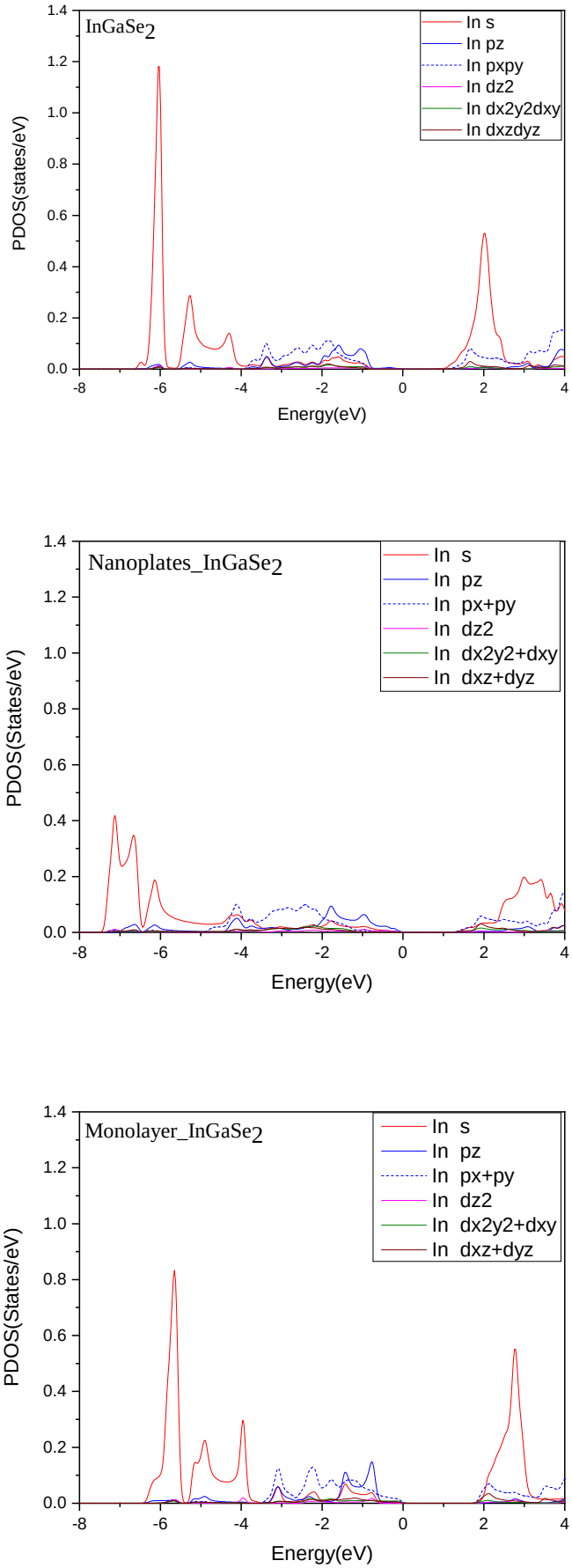

FIGURE 5.4: The partial contribution of In atoms to the total density of states in bulk, plates, and monolayer $\varepsilon - InGaSe_2$.

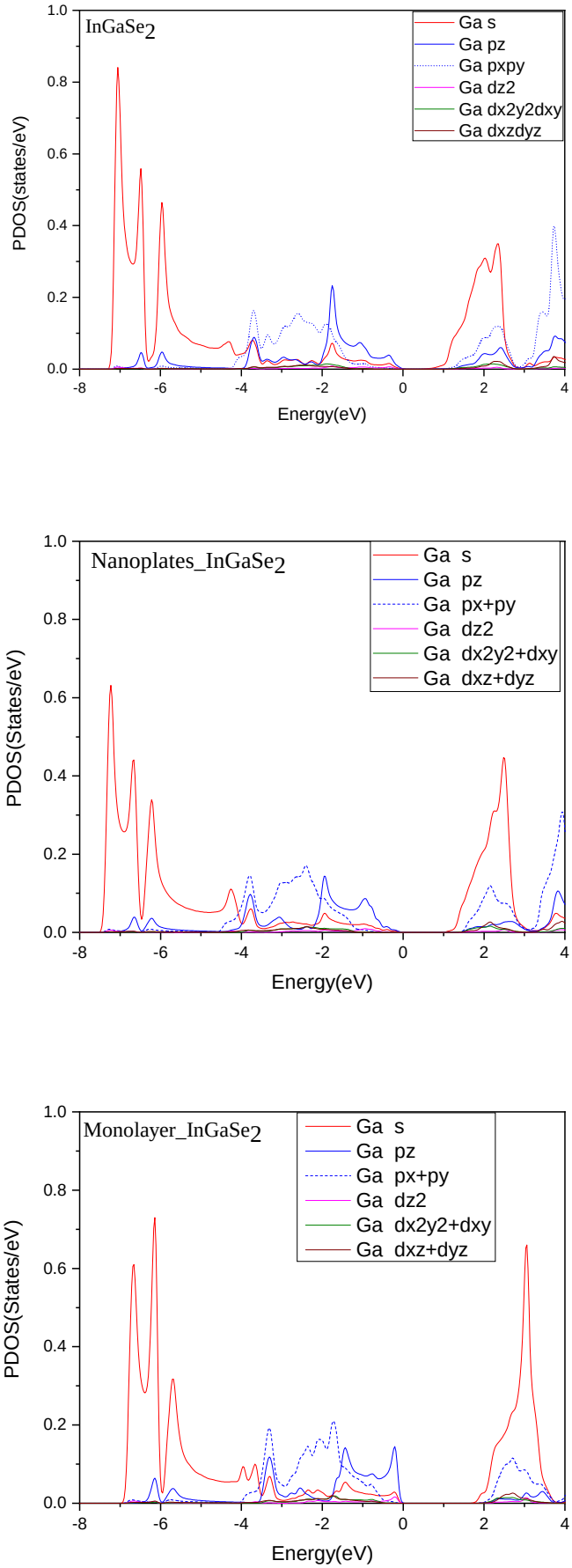

FIGURE 5.5: The partial contribution of IGa atoms to the total density of states in bulk, nanoplates, and monolayer $\varepsilon - InGaSe_2$.

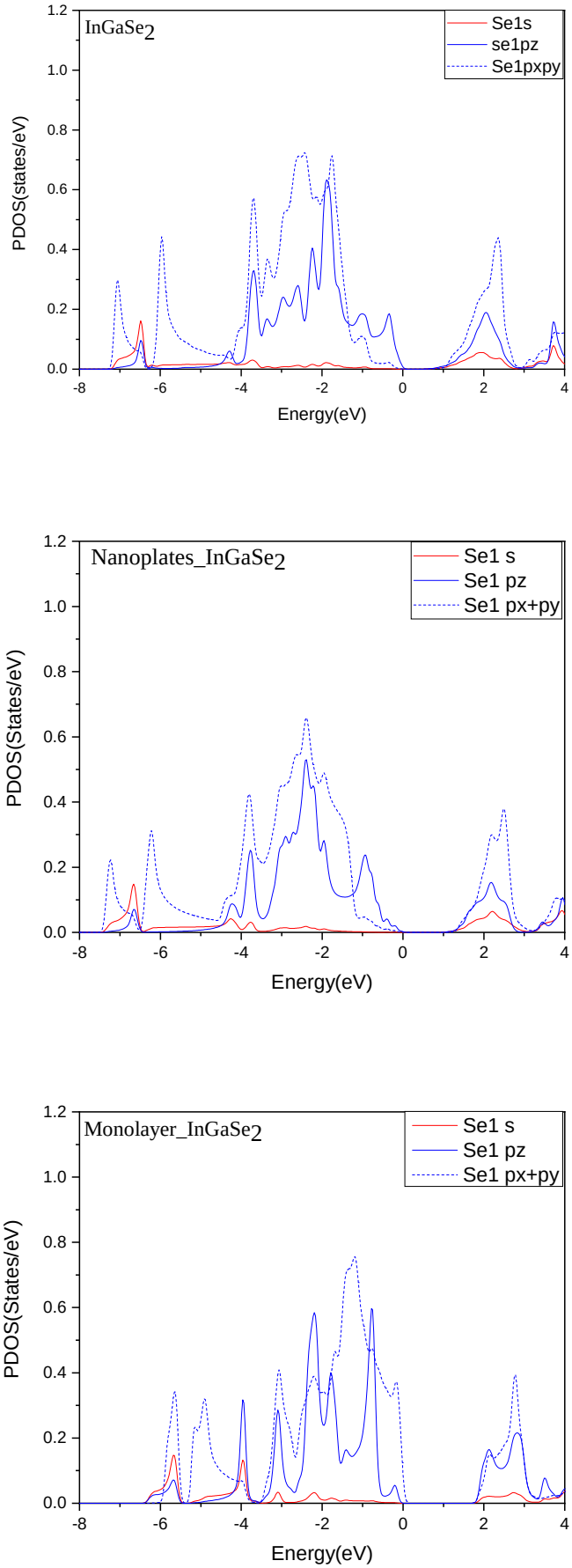

FIGURE 5.6: The partial contribution of Se atoms to the total density of states in bulk, nanoplates and monolayer $\varepsilon - InGaSe_2$.

5.4 Seebeck Coefficient

The Seebeck coefficients of the bulk, nanoplates, and monolayer $\varepsilon-$ polytype of $InGaSe_2$ materials vs chemical potential at 300 K are presented in the figure 5.7.

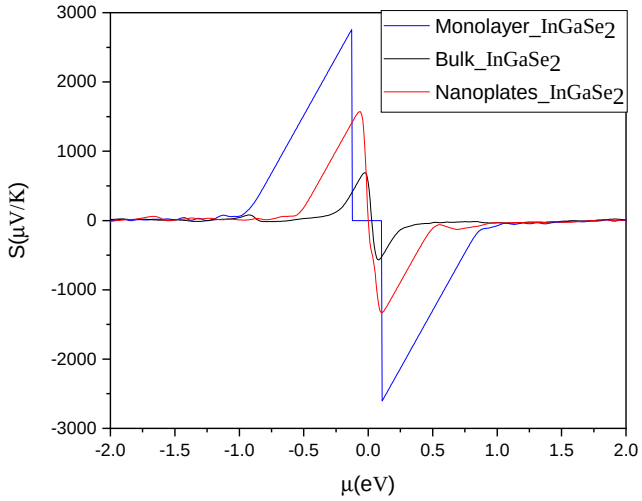

FIGURE 5.7: The Seebeck coefficients of the bulk, nanoplates, and monolayer $\varepsilon - InGaSe_2$ at 300 K

The Seebeck coefficients exhibit two pronounced peak around E_F indicating the existence of $n-$ and $p-$type in all the studied case. The discontinuity in the behavior of the Seebeck coefficient of monolayer $InGaSe_2$, could be attributed to the precision of the calculations as commented before in the case of GaSe. The monolayer case showed a great enhancement in the value of the Seebeck coefficient in comparison with the bulk and nanoplates cases since the maximum value of the Seebeck coefficient at $300K$ for the $p-$type region was $2753\mu V/K$ while it was $2603\mu V/K$ for $n-$type region comes after that the values obtained in the nanoplates case $1571\mu V/K$ in the $p-$type region and $1328\mu V/K$ in the $n-$type region and then the values in the bulk case $691\mu V/K$ in the $p-$type region and $567\mu V/K$ in the $n-$type region. This results assert the proposition [16] mentioned before that the Seebeck coefficient of a material increases with decreasing the thickness of the material as a result of the strong confinement effect. The improvement of the values of the Seebeck coefficient in the monolayer can be also explained based on Mahan-Sofo theory due to the local increase found in the total density of states of the valence band over a narrow energy range around the Fermi level as shown in fig. 5.3(c).

In these materials, better values of the Seebeck coefficient can be obtained in the $p-$type region than the $n-$type region. This could be a result of the conduction band with a low effective mass. No matter $p-$type or $n-$type for all the studied materials, the average of S is larger than the value proposed for a good thermoelectric materials, $200\mu V/K$, within a reasonable value of the carrier concentration

level, which indicates grand values of S and there may be higher values of $S^2\sigma$ and ZT. Our values for the Seebeck coefficient are much better than the results found in previous study on other thermoelectric materials.[134]

5.5 Electrical conductivity

The evolution of the electrical conductivity of the bulk, nanoplates, and monolayer ε polytype of $InGaSe_2$ relative to the relaxation time as a function of the chemical potential at temperature $T = 300$ K is represented in fig.5.8

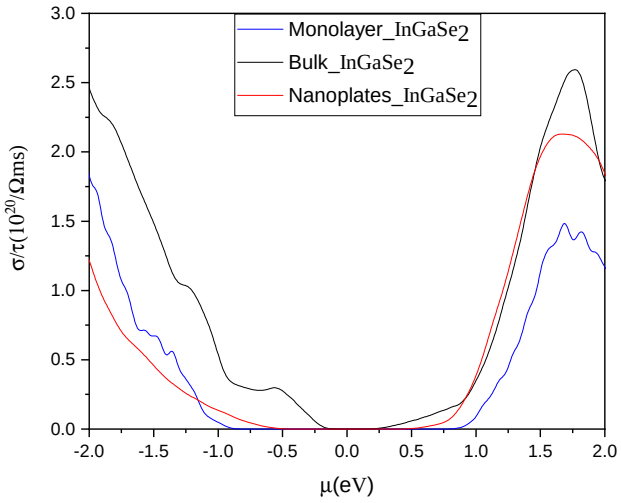

FIGURE 5.8: σ/τ of the bulk, nanoplates and monolayer $\varepsilon - InGaSe_2$ at 300K

The three studied cases of $InGaSe_2$, as in GaSe and InSe, showed an increasing electrical conductivity with rising the chemical potential due to the increase of the carrier concentration. Therefore, σ/τ is high in highly doped region for both $p-$type while in the $n-$type region after a certain value of the chemical potential the electrical conductivity started to decrease with the increase in the chemical potential as a result of the competition between the carrier concentration and electron relaxation as in the Bi_2Se_3 single layer [130]. While in both bulk and nanoplates $InGaSe_2$ the maximum value of σ/τ has been obtained in $n-$type region, the opposite have been found in the case of monolayer, since the maximum value of σ/τ is in the $p-$type region. This could be attributed to the less dispersed valence band in the bulk and nanoplates that leads to a large hole effective mass and hence lower values of the electrical conductivity in the $p-$type region.

The maximum value of σ/τ that can achieved in the $n-$type region is 2.59×10^{20} $1/\Omega ms$ for bulk followed by 2.13×10^{20} $1/\Omega ms$ for nanoplates and 1.48×10^{20} $1/\Omega ms$ for monolayer. In the $p-$type region, the maximum of σ/τ for bulk is 2.47×10^{20}

$1/\Omega ms$ followed by 1.85×10^{20} $1/\Omega ms$ for monolayer and 1.23×10^{20} $1/\Omega ms$ for nanoplates.

5.6 Power factors

Using the existing information on the Seebeck coefficient (S) and the electrical conductivity relative to the relaxation time (σ/τ), we calculated the power factor of bulk, nanoplates, and monolayer $\varepsilon-$ polytype of $InGaSe_2$ relative to the relaxation time ($PF/\tau = S^2\sigma/\tau$) at 300 K as a function of chemical potential between ∓ 2 eV and presented the results in Fig. 5.9.

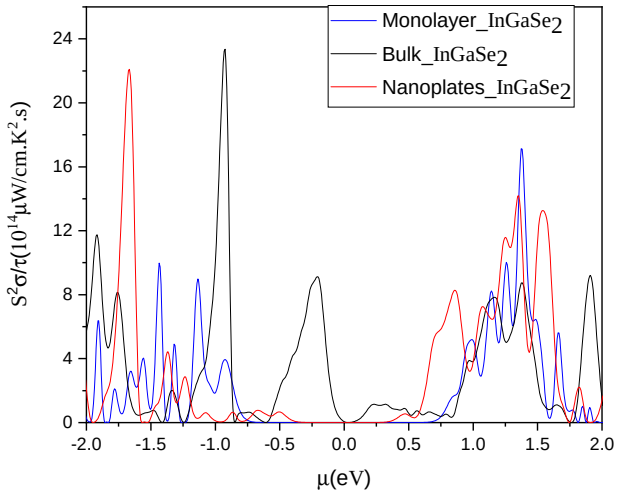

FIGURE 5.9: PF/τ of the bulk, nanoplates and monolayer $\varepsilon - InGaSe_2$ at 300 K

The behaviour of the power factor as a function of the chemical potential in the supper lattice $InGaSe_2$ was similar to the pristine compound, at the vicinity of the Fermi level, the power factor exhibits its minimum values. This is attributed to lower value of carrier concentration and hence the electrical conductivity. In $n-$type region the case that have showed the maximum value of PF/τ was monolayer, since its maximum value was 17.13×10^{14} $\mu W/cmK^2s$ at 1.37 eV followed by the value 14.18×10^{14} $\mu W/cmK^2s$ at 1.35 eV in nanoplates and the lowest value 9.21×10^{14} $\mu W/cmK^2s$ at 1.9 eV obtained in bulk.

In $p-$type region the maximum value of PF/τ 23.354×10^{14} $\mu W/cmK^2s$ at -0.925 eV was obtained in bulk comes next its value 22.09×10^{14} $\mu W/cmK^2s$ at -1.66 eV in nanoplates and then 9.97×10^{14} $\mu W/cmK^2s$ at -1.43 eV in monolayer. It means that the maximum value of PF/τ in each materials hasn't been obtained at the same value of the chemical potential. Consequently, in this material the maximum value of the power factor, in the studied interval of the chemical potential, was found in

the $p-$type region of the bulk case in contrast to what found in the GaSe and InSe materials where the monolayer case exhibit the maximum value of the power factor. As we mentioned before, we are more interested in the values obtained within the smallest range of the chemical potential, i.e. low doping concentration, where the best maximum value of the PF/τ can be achieved in the p-type region of bulk and n-type region of nanoplates.

5.7 Electronic thermal conductivity

The electronic thermal conductivity per relaxation time (k/τ) bulk, nanoplates, and monolayer $\varepsilon-$ polytype of $InGaSe_2$ versus the chemical potential at the temperature of 300 K is depicted in Figure 5.10.

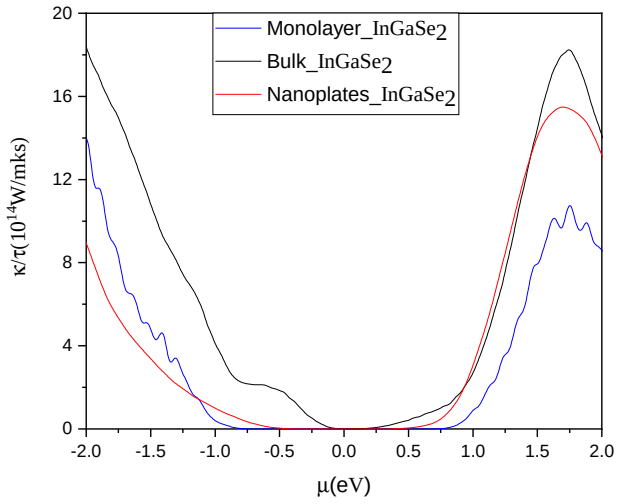

FIGURE 5.10: (k/τ) of the bulk, nanoplates, and monolayer $\varepsilon-InGaSe_2$ at 300 K

As in all pristine atoms, when the value of the chemical potential is zero the thermal conductivity shows its minimum values and increases as the potential increases. The behaviour of the thermal conductivity as a function of the chemical potential was similar to the electrical conductivity as both are affected by the carrier concentration, for example, the bulk showed the maximum values of the electrical conductivity and thermal conductivity as well. In the $p-$type region, the values of k/τ for all the investigated materials increases as the chemical potential increases. Its peak values obtained at -2 eV are 18.46, 14.03 and 9.05 $\times 10^{14} W/mKs$ in bulk, monolayer and nanoplates, respectively so the lowest thermal conductivity was the one of nanoplates. In the $n-$type region, the lowest value of k/τ has found for the monolayer case in contrary to the $p-$type region. As the values 18.23, 15.48 and 10.74 $\times 10^{14} W/mKs$ has been found in bulk, nanoplates and monolayer, respectively. Consequently, the lowest value of the thermal conductivity has been attained for the $p-$type nanoplates.

Calculating ZT of the three structure of $\mathrm{InGaSe_2}$ as a function of the chemical potential. The maximum value obtained for the figure of merit was approximately 0.53 (0.46), 0.49 (0.48) and 0.47 (0.47) in the $p-$type ($n-$type) region of the bulk, monolayer and nanoplates, respectively. Hence to obtain better values of ZT, doping these compounds with an acceptor and creating $p-$type semiconductor is favorable.

Chapter 6

The transport coefficients at high pressure

One of the important branches in the field of material science is the study of the materials properties under high pressure. Applying a pressure on a material can induce a change in the crystal structure of the material and hence its electronic properties and band structure, like the unpredictable new properties that found in sodium chlorides[135] . Due to the strong dependence of the Seebeck coefficient and electrical conductivity of a material on its band structure and the density of states. In such a way, we can infer that the pressure can be used to change the thermoelectric properties of a material. Using the pressure to enhance the thermoelectric properties is better than doping and nanostructuring methodologies since the pressure keep the compound as a perfect, defect-free crystal and enhance its thermoelectric properties intrinsically. In the studies of Ovsyannikov [136, 137], they reported that some thermoelectric materials exhibit dramatic improvements in the thermoelectric power factor under compression. As a result of the different character between intra- and interlayer bonding in the layered compounds, their axial compressibilities are highly anisotropic. It means that the pressure can be used as a way to tune the degree of anisotropy in the bonding, leading to nonlinearities in the pressure dependence of the physical properties. This has motivated us to study the effect of the hydrostatic pressure on the thermoelectric transport coefficients of the bulk $\varepsilon-$ polytype GaSe, InSe and $InGaSe_2$ [138]. The calculations have been performed in this order.

Firstly, the internal structure parameters and the lattice parameters were optimized at different pressures, 10 and 20 GPa, by using as input the optimized lattice parameters of the unit cell of bulk at 0 GPa pressure.

Then, the energy structure of the three compounds has been calculated using the WIEN2k code at three different pressure 0 , 10 and 20 GPa. The calculations have been done by using the same parameters, RK_{max}, G_{max}, and $k-$points, that have been used before for each case and mentioned in the computational details of the previous chapters.

Finally, the obtained information has been inserted in the BoltzTraP program to calculate the transport coefficients of each case. For these calculations finer $k-$mesh is needed. Hence, a set of 364 $k-$ points which is equivalent to $30 \times 30 \times 6$ have been used. All the calculations have been done at the ambient temperature.

6.1 Seebeck coefficient

Figure 6.1 shows the Seebeck coefficient of GaSe, InSe and $InGaSe_2$ as a function of the chemical potential at three different pressures 0, 10 and 20 GPa. In the vicinity of E_f the Seebeck coefficient exhibited two pronounced peaks for $n-$ and $p-$ type materials. From fig. 6.1 it is noticed that the effect of the pressure on the Seebeck coefficient of the studied materials was different. For InSe, the values of the Seebeck coefficient increases with the increase of the pressure and also there is an increase in the range of the chemical potential where the Seebeck coefficient exhibits a good value. It means that the Seebeck coefficient of InSe could be improved by increasing the pressure since its best values have been obtained at 20 GPa followed by its values at 10 GPa while its lowest values have been found at 0 GPa. The behavior was different in GaSe and $InGaSe_2$, for both of them the best values were found at 10 GPa. When the pressure increases to 20 GPa, the values of the Seebeck coefficient starts to decrease again. For $n-/p-$ type $InGaSe_2$ and the $n-$ type region of GaSe the values of S are still better than its values calculated at 0 GPa while in the $p-$ type region of GaSe the values of S are lower than its values obtained at 0 GPa. A comparison between the maximum values of the Seebeck coefficient obtained at three different pressures in the $n-$ and $p-$ type regions of all the studied cases are written down in table 6.1

TABLE 6.1: The highest values of the Seebeck coefficient S obtained in the $n-/p-$ type region of bulk $\varepsilon-$polytype of GaSe, InSe and $InGaSe_2$ at $0, 10, 20$ GPa.

	GaSe		InSe		$InGaSe_2$	
	$p-$type	$n-$type	$p-$type	$n-$type	$p-$type	$n-$type
$S(\mu V/K)$at 0 GPa	1388	-1294	785	-689	691	-567
$S(\mu V/K)$ at 10 GPa	1530	-1650	1001	-863	1331	-1329
$S(\mu V/K)$at 20 GPa	1219	-1330	1395	-1379	1025	-1074

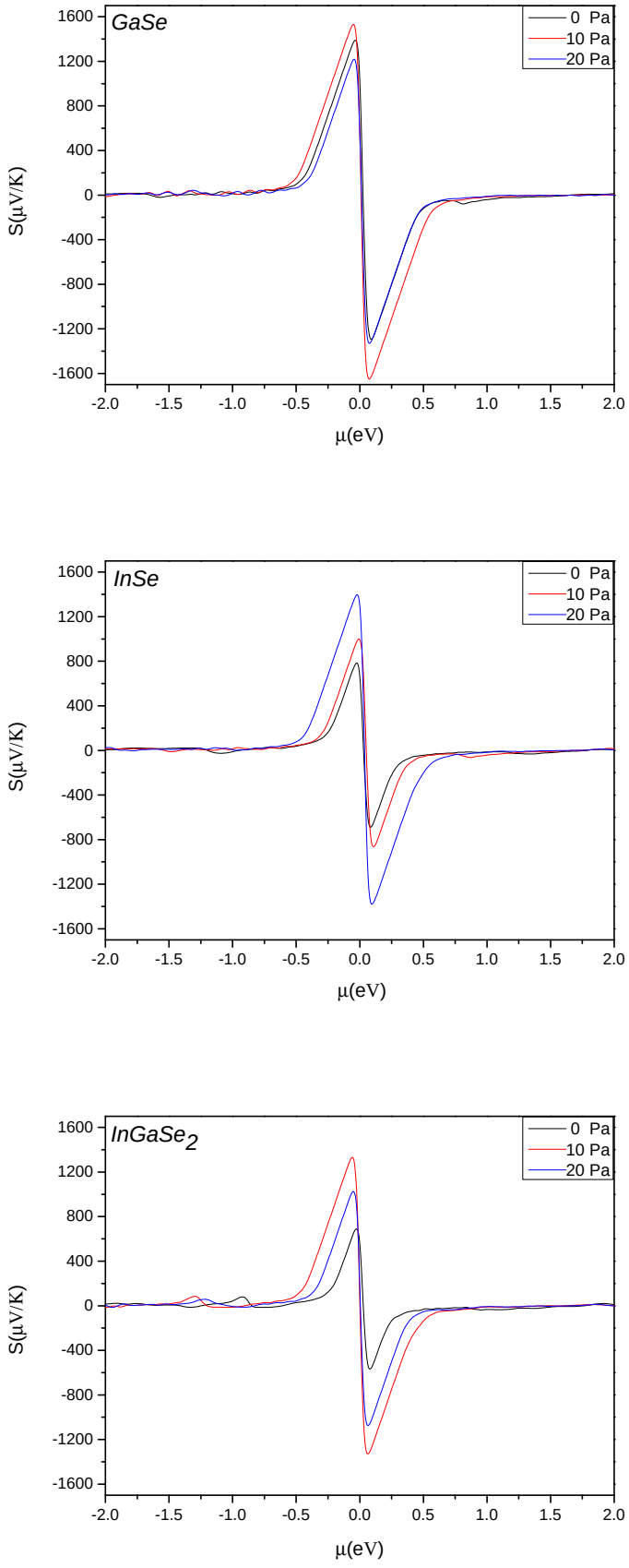

FIGURE 6.1: Calculated Seebeck coefficient as a function of the chemical potential at three different pressures for GaSe, InSe and $InGaSe_2$. The black lines represent the calculated values at 0 GPa, the red lines represent the calculated values at 10 GPa and the blue lines represent the calculated values at 20 GPa.

6.2 Electrical conductivity

It is mentioned before that in the output of the BoltzTraP the electrical conductivity (σ) is expressed in the form of the ratio (σ/τ), thus without the knowledge of the scattering rate τ the value of the electrical conductivity could not be calculated. Hence the electrical conductivity relative to the relaxation time σ/τ has been calculated as a function of the chemical potential for all the studied materials at the three different pressures and the results are displayed in figure 6.2

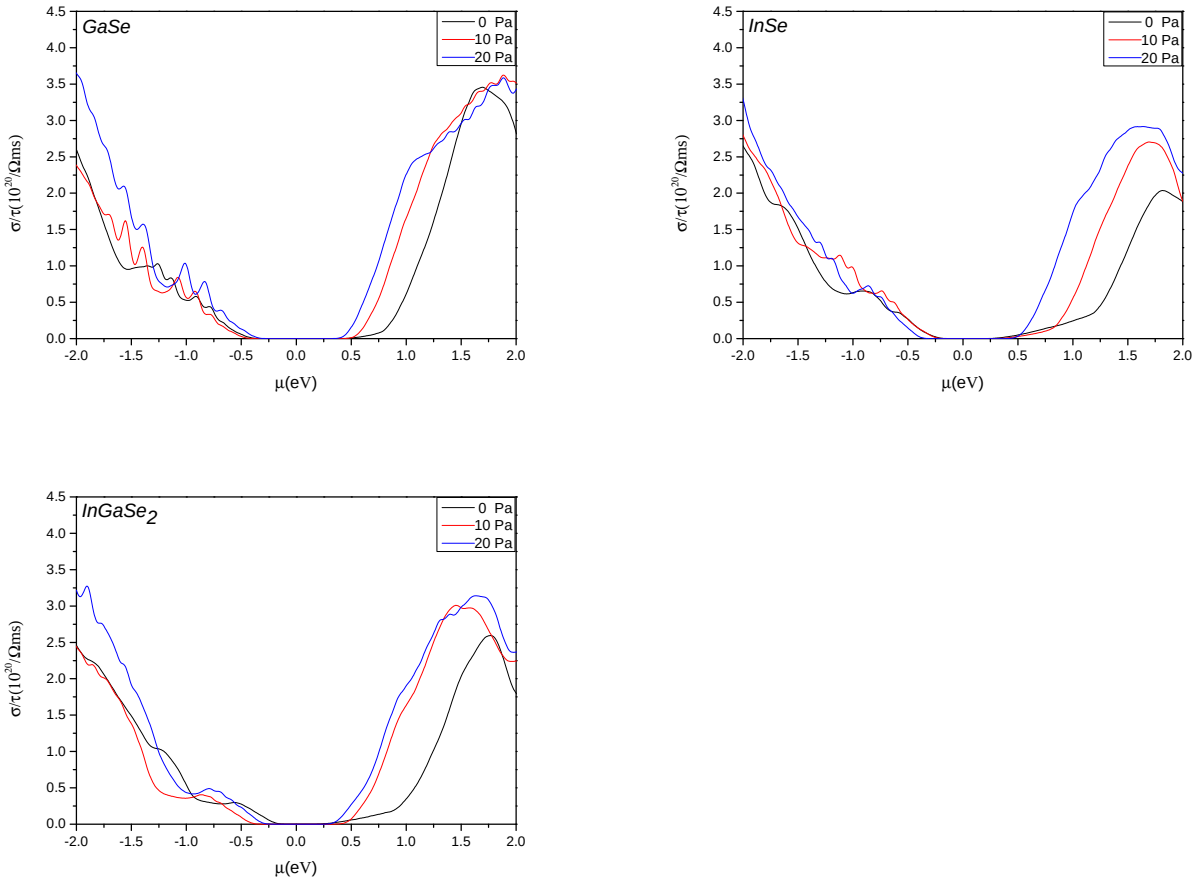

FIGURE 6.2: Calculated σ/τ as a function of the chemical potential at three different pressures for GaSe, InSe and $InGaSe_2$. The black lines represent the calculated values at 0 GPa, the red lines represent the calculated values at 10 GPa and the blue lines represent the calculated values at 20 GPa.

At the zero value of the chemical potential, when the Fermi level is at the middle of the band gap, and close to this value, σ/τ equals zero (a typical semiconductor behavior). When the Fermi level moves up or down, the number of the charge carriers increases and hence the electrical conductivity starts to increases as a function of the chemical potential. In the $n-$ type region σ/τ increases with the chemical potential till it reaches a maximum value and the it starts to decrease again. while in the $p-$

type region σ/τ increases at first and then there is a fluctuation in its value before it reaches its maximum value.

Hence, we can conclude that the overall behavior of the σ/τ in the studied materials under pressure was similar to its behaviour at the ambient conditions. Also it can be noticed that the effect of the pressure on the values of σ/τ was positive since in all the studied cases its values increases as the pressure increases. It is obvious from the result of the electrical conductivity and Seebeck coefficient that the hydrostatic pressure could be a good tool to improve the thermoelectric properties of the studied materials since it improves S and σ/τ simultaneously.

6.3 Power factor

From the results of the Seebeck coefficient (S) and the electrical conductivity relative to the relaxation time (σ/τ) of GaSe, InSe and $\mathrm{InGaSe_2}$ at high pressure, the power factor relative to the relaxation time ($PF/\tau = S^2\sigma/\tau$) has been calculated at high pressure as a function of the chemical potential and the results is displayed in figure 6.3.

As the power factor is directly proportional to the Seebeck coefficient and the electrical conductivity, it means that close to the the Fermi level, when σ/τ experience its lower values, the PF/τ must show its lower values as can be observed in the figure. The general aspect of the effect of the pressure in all the studied materials was increasing the values of the power factor at the small values of the chemical potential; low doping. The improvement of the values of the PF/τ at lower values of the chemical potential was more pronounced in the $n-$type region than in the $p-$type region. For all the studied materials close to the Fermi level ∓ 1 the maximum values were the one calculated at 20 GPa while over all the studied range of the chemical potential,∓ 2, the pressure at which the maximum of PF/τ has obtained in each materials was different.

In spite of the higher values of the Seebeck coefficient obtained under pressure of 10 GPa, it is found that the maximum values of PF/τ in both $p-$ type and $n-$ type in GaSe was at 20 GPa followed by their values at 10 GPa and the lowest ones obtained at 0 GPa. This could be attributed to the large value of the electrical conductivity at 20 GPa . The same results have been found in InSe but in this case due to the largest values obtained for both the Seebeck coefficient and electrical conductivity under pressure 20 GPa. This results reflects how good will be the effect of the pressure on the thermoelectric properties of this material. In contrary, $\mathrm{InGaSe_2}$ showed the best values of PF/τ under 10 GPa, this is due to the reasonable values of the S and σ/τ found under this pressure, comes next its values at 20 GPa and finally the one calculated at 0 GPa.

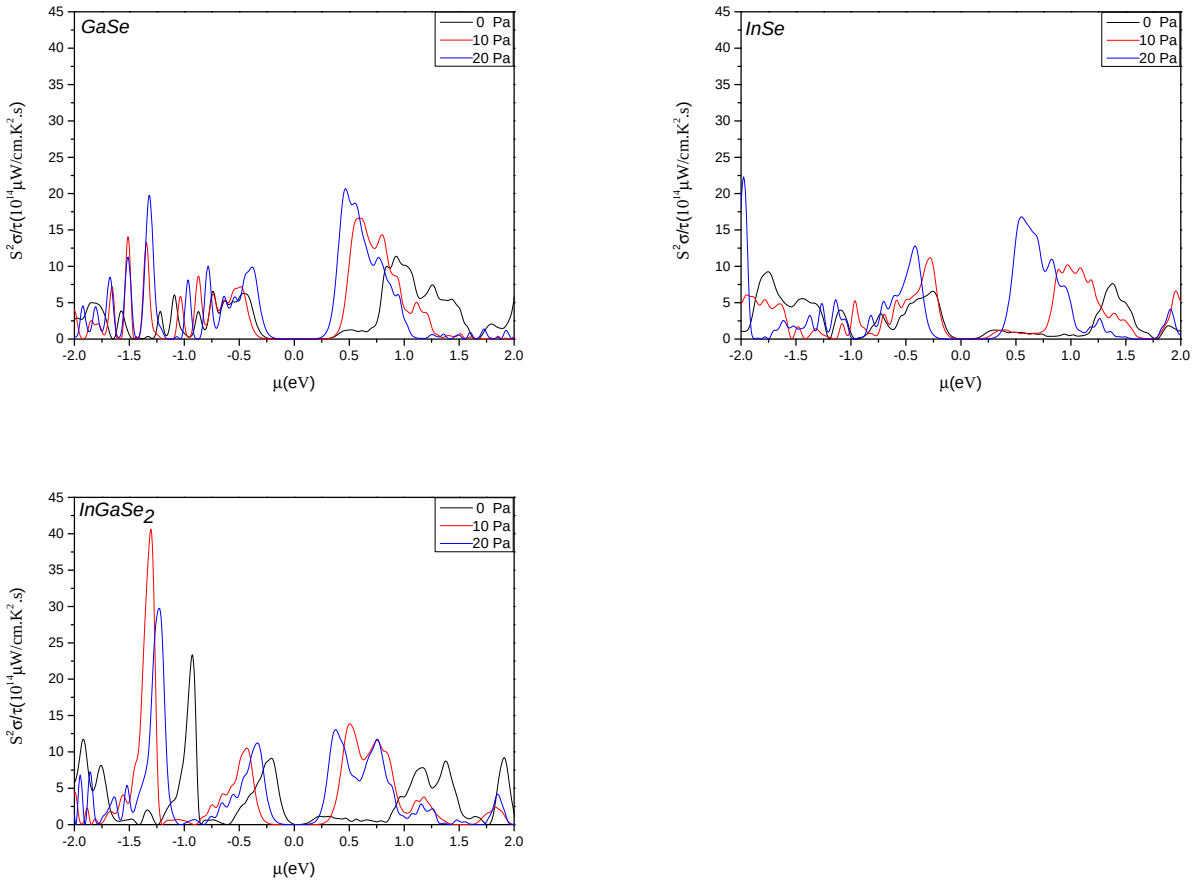

FIGURE 6.3: Calculated PF/τ as a function of the chemical potential at three different pressures for GaSe, InSe and $InGaSe_2$. The black lines represent the calculated values at 0 GPa, the red lines represent the calculated values at 10 GPa and the blue lines represent the calculated values at 20 GPa.

6.4 Electronic thermal conductivity

Figure 6.4 displays the calculated electronic thermal conductivity per relaxation time (k/τ) of bulk $\varepsilon-$ GaSe, InSe and InGaSe versus the chemical potential at three different pressures 0, 10, 20 GPa. From this figure it could be observed that the effect of the pressure on the electronic thermal conductivity is positive, it means that the values of the thermal conductivity for all the studied materials increase as the pressure increase following the same aspect as the electrical conductivity. Hence the lower values of the thermal conductivity are the ones obtained at 0 GPa. Even though the increase that occurred in the other transport coefficients with the pressure is preferable and made from the pressure a good factor to improve the thermoelectric properties of the materials, the increase of the thermal conductivity would lead to a lower value of the figure of merit ($ZT = T\frac{\sigma s^2}{k}$). By assuming that the lattice and ele-

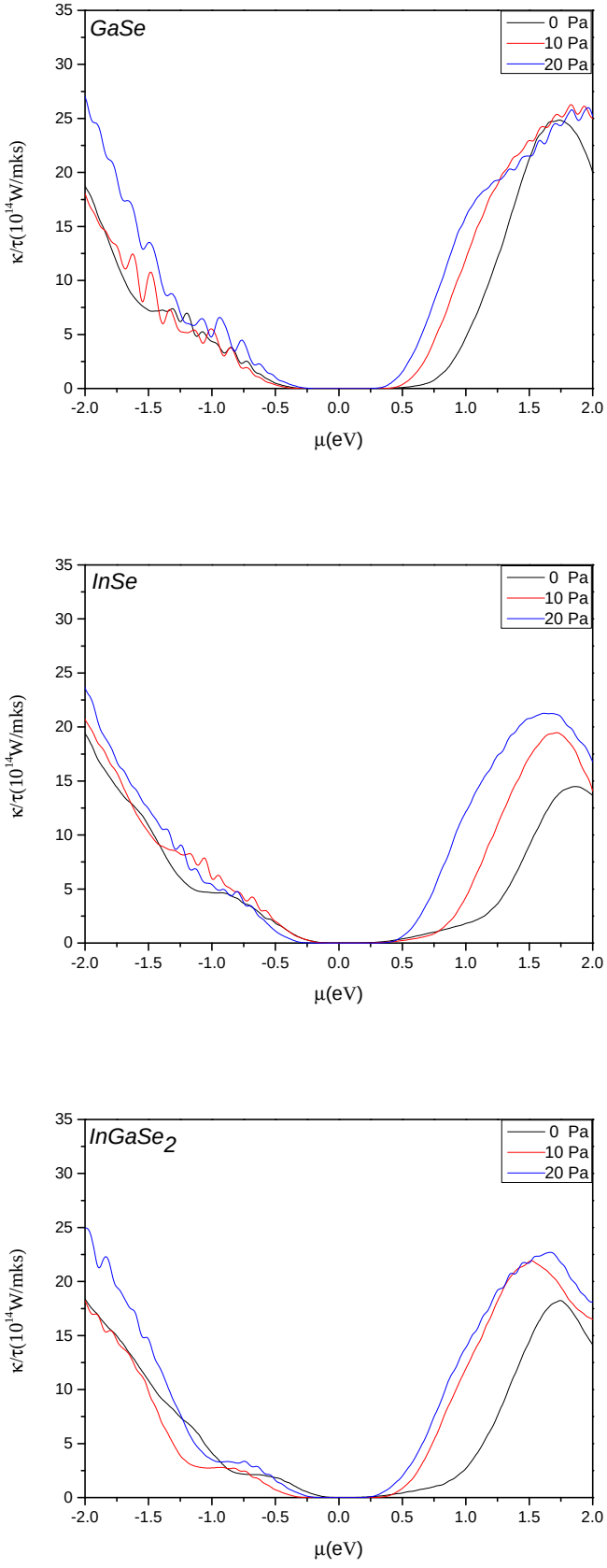

FIGURE 6.4: Calculated k/τas a function of the chemical potential at three different pressures for GaSe, InSe and $InGaSe_2$. The black lines represent the calculated values at 0 GPa, the red lines represent the calculated values at 10 GPa and the blue lines represent the calculated values at 20 GPa.

ctrical contributions of the thermal conductivity are quantitatively equivalent, our calculated value for the figure of merit is approximately 0.5 for the three systems studied in this work. Also it is noticed that ZT values are greater in the $p-$type than the $n-$type.

Chapter 7

Conclusions

From the comprehensive study of the structural, electronic and thermoelectric properties of $\varepsilon-$ polytype of GaSe, InSe, and the new supper lattice $\mathrm{InGaSe_2}$ have been studied at different conditions we extracted the following conclusions.

We encountered that the calculated lattice parameters of the bulk GaSe and InSe have values larger than the value obtained in a previous experimental and theoretical works. The overestimation of the lattice parameters is one of the drawbacks of the generalized gradient approximation in the density functional theory. From this we could deduce that if the heterostructure $\mathrm{InGaSe_2}$ could be synthesized, their experimental lattice parameters should be lower than values obtained in our study.

It is found that effect of the quantum confinement on the electronic band structure of the thickness of few layers of GaSe, InSe, and $\mathrm{InGaSe_2}$ was different in each material. Three cases have been studied to make a comprehensive compression were, the bulk, one layer (monolayer), and 7 layers (nanoplates). Several changes have been noticed in the band structure of all the studied cases since in both GaSe and InSe a cross over from the direct band gap to indirect band gap occurred by moving from the 3 dimensional case, bulk, to the 2 dimensional case; nanoplates and monolayer. The same results have been found in the nanoplates case of $\mathrm{InGaSe_2}$ even though the monolayer case showed a direct band gap semiconductor characteristic.

The effect of the quantum confinement on the dispersion of the valence band was more pronounced in the monolayer case than the nanoplates case of GaSe, InSe since instead of finding the maximum of the valence band at the Γ point as in the bulk case, the maximum of the valence band found between two symmetry points of the Brillouin zone; Γ and K and a valley, Mexican hat dispersion, has been created in the valence band at Γ in accordance with what have found before in the literature. This behaviour didn't occur in the monolayer $\mathrm{InGaSe_2}$ as its valence band showed more dispersion in comparison with both of the bulk and nanoplates case of the same material.

In all the studied cases of all the materials it is found that the largest band gap value was the one of monolayer. Also the partial contributions of the orbitals of the atoms to total density of states in the valence and conduction band wasn't affected

qualitatively by the quantum confinement.

Based on the calculated electronic structure of the studied cases, their transport coefficient have been calculated using the Boltzmann transport equation, to study the effect of the quantum confinement on the thermoelectric transport coefficient. It is found The quantum confinement has a positive effect on the Seebeck coefficient of $InGaSe_2$ since the largest values of S have been found in the monolayer case and then in the nanoplates case. This coincide with the proposition of Hicks et. al. [16] that the Seebeck coefficient of a material increases with decreasing the thickness of the material as a result of the strong confinement effect. Even though in the monolayer GaSe and InSe the same results have been obtained, the opposite has been found in the nanoplates structure of GaSe and InSe as it is found that their Seebeck coefficient values are either comparable to or lower than its values in the bulk, respectively.

In general all the average values of the Seebeck coefficient obtained in this study are much larger than the recommended values for efficient thermoelectric materials [109, 110]. Also, better values for the Seebeck coefficient can be obtained in the $p-$type region than the $n-$type region.

The electrical conductivity in all the studied case showed a typical semiconductor behavior as it is found that σ/τ increased as the chemical potential, doping level, increased and showed its minimum values close to the Fermi level and σ/τ is high in a highly doped region for both $n-$ and $p-$ type region. In contrast with the results for the Seebeck coefficient, the quantum confinement has a negative effect on the electrical conductivity as it found that the values of σ/τ, at the same value of the chemical potential, decreased as the dimension of the material decreased. The same results have been noticed in the overall behaviour of σ/τ in all the studied materials with a small exception in the $p-$type $InGaSe_2$ where the monolayer showed better values of the σ/τ than the nanoplates and also in the $n-$type $InGaSe_2$ at certain values of the chemical potential the bulk and nanoplates showed almost similar values of σ/τ.

The power factor relative to the relaxation time ($PF/\tau = S^2\sigma/\tau$) was calculated From the existing information on the Seebeck coefficient (S) and the electrical conductivity relative to the relaxation time (σ/τ). The behaviour of the PF/τ as a function of the chemical potential in the studied materials was similar since at the vicinity of the Fermi level, the power factor exhibits its minimum values that is attributed to lower value of carrier concentration and hence the electrical conductivity. The better values for PF/τ was found in the 2D cases at higher values of the chemical potential, high doping level, that would not be achieved easily in the experiment. So the values obtained at low chemical potential would be more interested and it is found that bulk cases had the best values of PF/τ near the Fermi level.

The conduct of the electronic thermal conductivity k/τ as a function of the chemical potential was similar to the electrical conductivity as both are affected by the carrier concentration.

The effect of the pressure on the Seebeck coefficients values of all the studied materials was different from one case to another. For InSe its values increase as the pressure increase therefore the best values have been obtained at 20 GPa while for GaSe and $\mathrm{InGaSe_2}$ its values have been improved at 10 GPa but when the pressure increases to 20 GPa the values of the Seebeck coefficient start to decrease again. Furthermore, the pressure has increased both the electrical (σ/τ) and electronic thermal conductivity relative to the relaxation time (k/τ). From the values of PF/τ it can be concluded that the pressure could be a good factor to improve the power factor since it has a positive effect on both the Seebeck coefficient and the electrical conductivity. Our results of ZT in all the structures of the material studied in this thesis was within the range of 0.4 and 0.5.

References

[1] Gibran S. Aleman-Nava et al. "Renewable energy research progress in Mexico: A review". In: *Renewable and Sustainable Energy Reviews* 32 (2014), pp. 140–153.

[2] J. Yang and F. R. Stabler. "Automotive Applications of Thermoelectric Materials". In: *J. Electron. Mater.* 38 (2009), 1245–1251.

[3] G. J. Snyder and E. S. Toberer. "Complex thermoelectric materials". In: *Nature Mater.* 7 (2008), 105–114.

[4] T. M. Tritt. "Thermoelectric Phenomena, Materials, and Applications". In: *Ann. Rev. Mater. Res.* 41 (2011), 433–448.

[5] J. H. Yang H. J. Xiang X. G. Gong A. Walsh J. Kang Y.T. Zhai Sh. Chen and S. H. Wei. "Structural diversity and electronic properties of Cu_2SnX_3 ($X =$ S, Se): A first-principles investigation". In: *Phys. Rev. B* 84 (2011), p. 075213.

[6] R. Prasada Rao G. Hema Chandra O. Lakshmana Kumar and S. Uthanna. "Influence of substrate and selenization temperatures on the growth of Cu_2SnSe_3 films". In: *Journal of Materials Science volume* 46 (2011), 6952–6959.

[7] Th. Colpitts R. Venkatasubramanian E. Siivola and B. O'Quinn. "Thin-film thermoelectric devices with high room-temperature figures of merit". In: *Nature* 413 (2001), 597–602.

[8] FRANCIS J. DISALVO. "Thermoelectric Cooling and Power Generation". In: *Science* 285 (1999), pp. 703–706.

[9] A. Steinfeld C. Suter P. Tomes and A. Weidenkaff. "Heat transfer and geometrical analysis of thermoelectric converters driven by concentrated solar radiation". In: *Materials* 3 (2010), p. 1735.

[10] A. Steinfeld C. Suter P. Tomes and A. Weidenkaff. "A solar cavity-receiver packed with an array of thermoelectric converter modules". In: *Solar Energy* 85 (2011), pp. 1511–1518.

[11] B. C. Sales. "THERMOELECTRIC MATERIALS: Smaller Is Cooler". In: *Science* 295 (2002), pp. 1248–1249.

[12] M. Jonson and G. D. Mahan. "Mott's formula for the thermopower and the Wiedemann-Franz law". In: *Phys. Rev. B* 21 (1980), pp. 4223–4229.

[13] J. M. Berg N. Stojanovic D. H. S. Maithripala and M. Holtz. "Thermal conductivity in metallic nanostructures at high temperature: Electrons, phonons, and the Wiedemann-Franz law". In: *Phys. Rev. B* 82 (2010), p. 075418.

[14] G. J. Snyder Y. Pei H. Wang. "Band Engineering of Thermoelectric Materials". In: *Adv. Mater.* 24 (2012), pp. 6125–6135.

[15] P. Lu X. Shi F. Xu Y. He Y. Tang S. Bai W. Zhang L. Chen Y. Lin L. Shi H. Lin X. Gao X. Zhang H. Chi H. Liu X. Yuan and C. Uher. "Ultrahigh Thermoelectric Performance by Electron and Phonon Critical Scattering in $Cu2Se_{1-x}I_x$". In: *Adv. Mater.* 25 (2013), pp. 6607–6612.

[16] L. D. Hicks and M. S. Dresselhaus. "Effect of quantum-well structures on the thermoelectric figure of merit". In: *Phys. Rev. B* 47 (1993), pp. 12727–12731.

[17] M.H. Du H. Shi D. Parker and D. J. Singh. "Connecting Thermoelectric Performance and Topological-Insulator Behavior: $\mathrm{Bi_2Te_3}$ and $\mathrm{Bi_2Te_2Se}$ from First Principles". In: *Phys. Rev. Applied* 3 (2015), p. 014004.

[18] X. Chen D. Parker and D. J. Singh. "High Three-Dimensional Thermoelectric Performance from Low-Dimensional Bands". In: *Phys. Rev. Lett.* 110 (2013), p. 146601.

[19] J. R. Salvador M. Chi J. Y. Cho H. Wang Sh. Bai J. Yang W. Zhang X. Shi J. Yang and L. Chen. "Multiple-Filled Skutterudites: High Thermoelectric Figure of Merit through Separately Optimizing Electrical and Thermal Transports". In: *J. Am. Chem. Soc.* 133 (2011), 7837–7846.

[20] G. A. Slack. *CRC Handbook of Thermoelectrics*. Ed. by D.M. Rowe. CRC Press, 1995, 407–440.

[21] K. Marty A. F. May M. A. McGuire M. H. Du D. J. Singh A. Podlesnyak G. Ehlers M. D. Lumsden O. Delaire J. Ma and B. C. Sales. "Giant anharmonic phonon scattering in PbTe". In: *Nat. Mater.* 10 (2011), pp. 614–619.

[22] Y. Ma Y. Lan A. Minnich B. Yu X. Yan D. Wang A. Muto D. Vashaee X. Chen J. Liu M. S. Dresselhaus G. Chen B. Poudel Q. Hao and Z. Ren. "High-Thermoelectric Performance of Nanostructured Bismuth Antimony Telluride Bulk Alloys". In: *Science* 30 (2008), pp. 634–638.

[23] R. D. Delgado W. Liang E. C. Garnett M. Najarian A. Majumdar A. I. Hochbaum R. Chen and P. Yang. "Enhanced thermoelectric performance of rough silicon nanowires". In: *Nature* 451 (2008), 163–167.

[24] G. Chen. "Thermal conductivity and ballistic-phonon transport in the cross-plane direction of superlattices". In: *Phys. Rev. B* 57 (1998), p. 14958.

[25] J. Kang2 W. Fan Ch. Ko A. V. Luce K. X. Wang J. Suh K. D. Patel V. M. Pathak J. Li S. Tongay D. S. Narang and J. Wu. "Two-dimensional semiconductor alloys: Monolayer $Mo_{1x}W_xSe_2$". In: *Appl. Phys. Lett.* 104 (2014), p. 012101.

[26] G. Ding G. Li and G. Gao. "Thermoelectric properties of SnSe2 monolayer". In: *Journal of Physics: Condensed Matter* 29 (2017), p. 015001.

[27] H. L. Zhuang and R. G. Hennig. "Single-Layer Group-III Monochalcogenide Photocatalysts for Water Splitting". In: *Chem. Mater.* 25 (2013), pp. 3232–3238.

[28] N. D. Drummond V. Zólyomi and V. I. Falko. "Band structure and optical transitions in atomic layers of hexagonal gallium chalcogenides". In: *Phys. Rev.B* 87 (2013), p. 195403.

[29] M. Yoon X. F. Qiao X. Zhang W. Feng P. Tan W. Zheng J. Liu X. Wang J. C. Idrobo D. B. Geohegan K. Xiao P. Hu J. Zhang. "Highly sensitive phototransistors based on two-dimensional GaTe nanosheets with direct bandgap". In: *Nano Res.* 7 (2014), pp. 694–703.

[30] A. A. Puretzky J. C. Idrobo Ch. Ma M. Chi M. Yoon Ch. M. Rouleau I. I. Kravchenko D. B. Geohegan K. Xiao X. Li M. W. Lin. "Controlled Vapor Phase Growth of Single Crystalline, Two-Dimensional GaSe Crystals with High Photoresponse". In: *Sci. Rep.* 4 (2014), p. 5497.

[31] Y. Liu K. Yan J. Hong C. Jin Y. Zhou J.Yin Z. Liu Y. Zhou Y. Nie and H. Peng. "Epitaxy and photoresponse of two-dimensional GaSe crystals on flexible transparent mica sheets". In: *ACS Nano* 8 (2014), pp. 1485–1490.

[32] Kin Fai Mak et al. "Atomically Thin MoS_2: A New Direct-Gap Semiconductor". In: *Phys. Rev. Lett.* 105 (2010), p. 136805.

[33] A.Brukl and G. Ortner. "Die Sulfide des Galliums". In: *Naturwiss.* 18 (1930), p. 393.

[34] W.C. Johnson and B. Warren. In: *Naturwiss.* 18 (1930), p. 666.

[35] W.Klemm and H. U. v. Vogel. In: *Z. Anorg. Allg. Chem.* 219 (1934), p. 45.

[36] H.Hahn. In: *Angew. Chem.* 65 (1953), p. 538.

[37] E. Dörre K.Schubert. In: *Naturwiss.* 40 (1953), p. 604.

[38] E. Dörre K.Schubert. In: *Naturwiss.* 41 (1954), p. 448.

[39] M. Kluge K.Schubert E. Dörre. In: *Z. Metallkunde* 46 (1955), p. 216.

[40] S. A. Semiletov. In: *Sov. Phys. Cryst.* 3 (1958), p. 288.

[41] V.M. Salmanov Y. P. Sharonov I. D. Yaroshetskii G.A.Akhundov A. A. Agaeva. In: *Sov. Phys. Semicond.* 7 (1973), p. 826.

[42] V. K. Sobashiev V. I. Sokolov Y. F. Solomonov. In: *Sov. Phys.Solid State* 17 (1976), p. 1256.

[43] A. Minafra C. Paorici I. M. Catalano A. Cingolani. In: *Opt. Commun.* 24 (1978), p. 105.

[44] V. K. Sobashiev Y. F. Solomonov. In: *Phys. Status Solidi A* 74 (1982), p. 75.

[45] M. E. Karaseev V. I.Konov L. A. Kulewskii N. B. Mustafaev P. P. Pashinin A. M. Prokhorov Y. M. Starodunov G. B. Abdullaev K. R. Allakverdiev and N. I. Chapliev. In: *Sov. J. Quantum Electron.* 19 (1989), p. 494.

[46] A. Chevy M.S. Martin A. Segura J.N. Besson. In: *Nuovo Cimento Soc. Ital. Fis. B* 38 (1977), p. 345.

[47] A.R. Goñi A. Cantarero U.Schwarz V.Muñoz K. Syassen C. Ulrich M.A. Mroginski. In: *Phys. Status Solidi B* 198 (1996), p. 121.

[48] A. Cantarero M. Hanfland K.Syassen U. Schwarz D. Olguín. In: *Phys. Status Solidi B* 244 (2007), p. 244.

[49] Ho Won Jang Myong-Jae Yoo Dong-Su Paik SeungHyub Baek Jin-Sang Kim u Hyuk Yim Hyung-Ho Park. "Thermoelectric Properties of Indium-Selenium Nanocomposites Prepared by Mechanical Alloying and Spark Plasma Sintering". In: *Journal of Electronic Materials* 41 (2012), 1354–1359.

[50] Yu Li Yan Hai Gang Si Yuan Xu Wang and Guang Biao Zhang. "Structural, Electronic, and Thermoelectric Properties of InSe Nanotubes: First-Principles Calculations". In: *J. Phys. Chem. C* 116 (2012), 3956–3961.

[51] K. Sunouchi A. Koma and T. Miyajima. "Fabrication of ultrathin heterostructures with van der Waals epitaxy". In: *Journal of Vacuum Science Technology B: Microelectronics Processing and Phenomena* 3 (1985), p. 724.

[52] K. Saiki et al. "Application of Van der Waals epitaxy to highly heterogeneous systems". In: *Journal of Crystal Growth* 95 (1989), pp. 603–606.

[53] T. Hayashi et al. "Investigation of the growth mechanism of an InSe epitaxial layer on a MoS2 substrate". In: *Journal of Crystal Growth* 219 (2000), pp. 115–122.

[54] A. Koma. "Van der Waals epitaxy—a new epitaxial growth method for a highly lattice-mismatched system". In: *Thin Solid Films* 216 (1992), pp. 72–76.

[55] T. Shimada K. Ueno K. Saiki and A. Koma. "Epitaxial growth of transition metal dichalcogenides on cleaved faces of mica". In: *Journal of Vacuum Science Technology A* 8 (1990), p. 68.

[56] Le Thanh Vinh. "The van der Waals epitaxial growth of GaSe on Si(111)". In: *Journal of Applied Physics* 81 (1997), p. 7289.

[57] O. Lang C. Pettenkofer W. Jaegermann K. W. Nebesny P. A. Lee B. A. Parkinson N. R. Armstrong R. Schlaf D. R. Louder. "MBE Growth of Thin Films of SnS2 and SnSe2 on Cleaved Mica and Basal Planes of Single Crystal Layered Semiconductors". In: *Journal of Vacuum Science Technology A* 13 (1995), p. 1761.

[58] D. Fargues et al. "Study of the heterointerfaces InSe on GaSe and GaSe on InSe". In: *Applied Surface Science* 65-66 (1993), pp. 661–666.

[59] F.S. Ohuchi et al. "Growth of MoSe2 thin films with Van der Waals epitaxy". In: *Journal of Crystal Growth* 111 (1991), pp. 1033–1037.

[60] A. Conan J. C. Bernède S. Marsillac and A. Godoy. In: *Journal of Physics: Condensed Matter* 8 (1996), pp. 3439–3451.

[61] R.S. Mane C.D. Lokhande H.M. Pathan S.S. Kulkarni. In: *Materials Chemistry and Physics* 93 (2005), 16–20.

[62] M. Konagai T. Okamoto A. Yamada. In: *J. Cryst. Growth* 175 (1997), p. 1045.

[63] K.M. Yu E.D. Bourret J. Cheon J. Arnold. In: *Chem. Mater.* 7 (1995), 2273–2276.

[64] R. Le Ny M. Emziane. "Crystallization of In_2Se_3 semiconductor thin films by post-deposition heat treatment. Thickness and substrate effects". In: *J. Phys. D: Appl. Phys.* 32 (1999), pp. 1319–1328.

[65] L. E. Bell. "Cooling, Heating, Generating Power, and Recovering Waste Heat with Thermoelectric Systems". In: *Science* 321 (2008), pp. 1457–1461.

[66] H. Alam and S. Ramakrishna. "A review on the enhancement of figure of merit from bulk to nano-thermoelectric materials". In: *Nano Energy* 2 (2013), pp. 190–212.

[67] H. Lee. "The Thomson effect and the ideal equation on thermoelectric coolers". In: *Energy* 56 (2013), pp. 61–69.

[68] P. Hohenberg and W. Kohn. "Inhomogeneous electron gas". In: *Phys. Rev.* 136 (1964), B864–B871.

[69] W. Kohn and L. J. Sham. "Self-Consistent Equations Including Exchange and Correlation Effects". In: *Phys. Rev.* 140 (1965), A1133–A1138.

[70] J. C. Slater. "A Simplification of the Hartree-Fock Method". In: *Phys. Rev.* 81 (1951), p. 385.

[71] M. BORN and R. OPPENHEIMER. "ON THE QUANTUM THEORY OF MOLECULES". In: *Ann. Phys.* 84 (1927), p. 457.

[72] C. B. Vining. In: *J. Appl. Phys.* 69 (1991), p. 331.

[73] G. D. Mahan J. O. Sofo and J. Baars. In: *J. Appl. Phys.* 76 (1994), p. 2249.

[74] R. K. Willardson and A. C. Beer. *Transport Phenomena, in Semiconductors and Semi-metals*. Ed. by D. L. Rode. Vol. 10. Academic, New York, 1975.

[75] Georg K.H. Madsen and David J. Singh. In: *Computer Physics Communications* 175.1 (2006), pp. 67 –71.

[76] B. R. Nag. *Electron transport in compound semiconductors*. Springer-Verlag in Berlin, . New York., 1980.

[77] P. B. Allen. *boltzmann theory and resistivity of metals,in quantum theory of real materials*. Ed. by J. R. Chelikowsky and. S. G. Loule. Kluwer, Boston, 1996, pp. 219–250.

[78] J. M. Ziman. *Electrons and Phonons, The Theory of Transport Phenomena in Solids*. OUP Oxford, 2001.

[79] C. M. Hurd. *The Hall Effect in Metals and Alloys*. New York, Plenum Press, 1972.

[80] A. Chevy A. Khun and R. Chevalier. In: *Phys. Status Solidi A* 31 (1975), p. 469.

[81] J. Etienne A. Likforman D. Carre and B. Bachet. In: *Acta Crystallogr., Sect. B: Struct. Crystallogr. Cryst. Chem.B* 31 (1975), p. 1252.

[82] G. Madsen D. Kvasnicka P.Blaha K. Schwarz and J. Luitz. In: *Wien2k: An augmented plane wave plus local orbitals program for calculating crystal properties users guide* (2014).

[83] John P. Perdew, Kieron Burke, and Matthias Ernzerhof. In: *Phys. Rev. Lett.* 77 (18 1996), pp. 3865–3868.

[84] Fabien Tran and Peter Blaha. In: *Phys. Rev. B* 83 (23 2011), p. 235118.

[85] K.-H. Hellwege and O. von Madelung; M. Schulz; H.Weiss; W. Freyland. *Crystal and solid state physics. Semiconductors. Physics of non-tetrahedrally bonded binary compounds.* Vol. 17, Subvolume F. Springer Verlag, 1983.

[86] FD Murnaghan. In: *Proc. Natl. Acad. Sci. U S A* 30 (1944), pp. 244–247.

[87] Axel D Becke and Erin R Johnson. In: 221101 (2013).

[88] Lars Hedin. In: *Phys. Rev.* 139 (3A 1965), A796–A823.

[89] Mark S. Hybertsen and Steven G. Louie. In: *Phys. Rev. Lett.* 55 (1985), pp. 1418–1421.

[90] J.C. Zheng Z.Y. Fan H.Q. Wang. "Searching for the best thermoelectrics optimization of transport distribution function". In: *J. Appl. Phys.* 109 (2011), p. 073713.

[91] J. O. Sofo G. D. Mahan. "The best thermoelectric". In: *Proc. Natl. Acad. Sci. (USA)* 93 (1996), pp. 7436–7439.

[92] L.M. Gelato M. Penzo K. Cenzual and E. Parthe. "Inorganic structure types with revised space groups.I". In: *Acta Cryst. B* 47 (1992), pp. 13244–13249.

[93] M. Kaminskii Z.D. Kovalyuk M.N.Pyrlya S.V. Gavrilyuk and V.V. Netyaga. "Properties of Hydrogenated GaSe Crystals". In: *Inorg. Mater.* 41 (2005), pp. 793–795.

[94] Daniel Olguín, Alberto Rubio-Ponce, and Andrés Cantarero. "Ab initio electronic band structure study of III–VI layered semiconductors". In: *The European Physical Journal B* 86.8 (2013), p. 350.

[95] M. S. Hybertsen and S. G. Louie. "Electron correlation in semiconductors and insulators: Bandgaps and quasiparticle energies". In: *Phyd. Rev.B* 34 (1986), p. 5390.

[96] O.Gunnarson and K. Schonhammer. "Density functional treatment of an exactly treatment of an exactly solvable semiconductors model". In: *Phyd. Rev.lett.* 56 (1986), p. 1968.

[97] R. W. Godby M. Schluter and L. J. Sham. "Accurate exchange correlation potential for silicon and its Discontinuity on addition of an electron". In: *Phyd. Rev.Lett.* 56 (1986), p. 2415.

[98] R. K. Lake D. Wickramaratne F. Zahid. "Electronic and thermoelectric properties of van der Waals materials with ring-shaped valence bands". In: *Journal of Applied Physics* 118 (2015), p. 075101.

[99] Yandong Ma et al. In: *Phys. Chem. Chem. Phys.* 15 (19 2013), pp. 7098–7105.

[100] D. Errandonea et al. "Crystal symmetry and pressure effects on the valence band structure of gamma-InSe and epsilon-GaSe: Transport measurements and electronic structure calculations." In: *Physical Review B : Condensed matter and materials physics* 71 (2005), p. 125206.

[101] T. Seebeck. "Magnetische Polarisation der Metalle und Erze durch Temperatur-Differenz". In: *Abhandlungen der Deutschen Akademie der Wissenschaften zu Berlin* (1823), pp. 265–373.

[102] Giovanni Onida, Lucia Reining, and Angel Rubio. In: *Rev. Mod. Phys.* 74 (2002), pp. 601–659.

[103] Sergey N. Rashkeev and Walter R. L. Lambrecht. In: *Phys. Rev. B* 63 (2001), p. 165212.

[104] Mal-Soon Lee and S. D. Mahanti. In: *Phys. Rev. B* 85 (2012), p. 165149.

[105] G. Pomrehn Y. Takagiwa Y. Pei and G. J. Snyder. In: *APL Mater.* 1 (2013), p. 011101.

[106] L. Jodin et al. In: *Phys. Rev. B* 70 (2004), p. 184207.

[107] D. J. Singh and I. I. Mazin. In: *Phys. Rev. B* 56 (1997), R1650–R1653.

[108] A. H. Reshak. In: *Journal of Applied Physics* 117 (2015), p. 225104.

[109] H. Y. Lv et al. In: *J. Mater. Chem. C* 4 (20 2016), pp. 4538–4545.

[110] J. Sun and D. J. Singh. In: *Phys. Rev. Applied* 5 (2 2016), p. 024006.

[111] N. V. Chandra Shekar J. Sharp D. A. Polvani J. F. Meng and J. V. Badding. "Large Improvement in Thermoelectric Properties in Pressure-Tuned p-Type Sb1.5Bi0.5Te3". In: *Chemistry of Materials* 13 (2001), pp. 2068–2071.

[112] J. Tan et al. "Thermoelectric properties of bismuth telluride thin films deposited by radio frequency magnetron sputtering". In: (2005).

[113] S. Ying Quek X. Luo M. B. Sullivan. "First-principles investigations of the atomic, electronic, and thermoelectric properties of equilibrium and strained Bi2Se3and Bi2Te3including van der Waals interactions". In: *Physical Review B* 86 (2012).

[114] L. D. Hicks and M. S. Dresselhaus. "Thermoelectric figure of merit of a one-dimensional conductor". In: *Phys. Rev. B* 47 (1993), pp. 16631–16634.

[115] D. T. Morelli J. P. Heremans Ch. M. Thrush and M. Ch. Wu. "Thermoelectric Power of Bismuth Nanocomposites". In: *Phys. Rev. Lett.* 88 (2002), p. 216801.

[116] N. F. Mott and H. Jones. *The theory of the properties of metals and alloys*. Courier Dover Publications, 1958.

[117] J. F. Leavy M. Cutler and R. L. Fitzpatrick. "Electronic Transport in Semimetallic Cerium Sulfide". In: *Phys. Rev.* 133 (1964), A1143–A1152.

[118] T. J. Scheidemantel et al. In: *Phys. Rev. B* 68 (2003), p. 125210.

[119] Scheidemantel T.J. Sof J.O. Thonhauser T. In: *Appl. Phys. Lett.* 85 (2004), pp. 588–590.

[120] C. Bertini L.; Gatti. In: *J. Chem. Phys.* 121 (2004), pp. 8983–8989.

[121] W.E. Krakauer H. Allen P.B. Picket. In: *Phys. Reb. B* 37 (1988), pp. 7482–7490.

[122] Zhang Q Liu WS Yu B Wang H Wang DZ Ni G Chen G Ren ZF Zhang QY Wang HZ. In: *Nano Lett.* 12 (2012), 2324–2330.

[123] Dang F Itoh T Wang YF Sasaki H Kondo M Koga K Yabuki K Snyder GJ Yang RG Koumoto K. Wang CL Gu XK. In: *Nat Mater.* 14 (2015), 622–627.

[124] Jie Q Ren Z Liu W Kim HS. In: *Scripta Mater* 111 (2016), 3–9.

[125] C. Kittel. *Introduction to Solid State Physics*. nifth. New York City: John Wiley & Sons, Hoboken, 2004.

[126] S.J. Asadabadi R. Ahmad M. Maqbool M. Bilal I. Ahmad. In: *Electron. Mater. Lett.* 11 (2015), 466–480.

[127] N. Kuroda, I. Munakata, and Y. Nishina. "Exciton transitions from spin-orbit split off valence bands in layer compound InSe". In: *Solid State Communications* 33 (1980), pp. 687–691.

[128] A. Polian M. Gauthier, J. M. Besson, and A. Chevy. "Optical properties of gallium selenide under high pressure". In: *Phys. Rev. B* 40 (6 1989), pp. 3837–3854.

[129] F. J. Manjón et al. "Experimental and theoretical study of band structure of InSe and $\mathrm{In}_{1-x}\mathrm{Ga}_x\mathrm{Se}$ $(x < 0.2)$ under high pressure: Direct to indirect crossovers". In: *Phys. Rev. B* 63 (2001), p. 125330.

[130] Ch. Hu D. Guo. "Ultrahigh thermoelectricity of atomically thick $\mathrm{Bi}_2\mathrm{Se}_3$ single layers: A computational study". In: *Applied Surface Science* 321 (2014), pp. 525–530.

[131] Wilfredo Ibarra-Hernández et al. "Electronic structure, lattice dynamics, and optical properties of a novel van der Waals semiconductor heterostructure: InGaSe_2". In: *Phys. Rev. B* 96 (2017), p. 035201.

[132] N. B. Mustafaev F. M. Gashimzade. "Energy spectrum and effective mass of carriers in the InSe/GaSe superlattice". In: *Zeitschrift für Physik B Condensed Matter* 99 (1995), 219–222.

[133] T. Cui Y. Niu Y. Wang M. Wang Y. Ma Y. Wang X. Chen and G. Zou. "Enhanced thermoelectric performance of PbTe within the orthorhombic Pnma phase". In: *PHYSICAL REVIEW B* 76 (2007), p. 155127.

[134] M. Rizwan Y. Takagiwa H. Khachai M. Jibran R. Khenata S. Bin Omran G. Murtaza A. Sajid. "First principles study of Mg_2X $(X = Si, Ge, Sn, Pb)$: Elastic, optoelectronic and thermoelectric propertiess". In: *Materials Science in Semiconductor Processing* 40 (2015), pp. 429–435.

[135] A. F. Goncharov Q. Zhu S. E. Boulfelfel A. O. Lyakhov E. Stavrou M. Somayazulu V. B. Prakapenka W. Zhang A. R. Oganov and E. Konopkova. "Unexpected Stable Stoichiometries of Sodium Chlorides". In: *Science* 342 (2008), 1502–1505.

[136] Sergey V. Ovsyannikov and Vladimir V. Shchennikov. "Pressure-tuned colossal improvement of thermoelectric efficiency of PbTe". In: *Appl. Phys. Lett.* 90 (2007), p. 122103.

[137] Grigoriy V. Vorontsov Andrey Y. Manakov Anna Y. Likhacheva Vladimir A. Kulbachinskii Sergey V. Ovsyannikov Vladimir V. Shchennikov. "Giant improvement of thermoelectric power factor of Bi2Te3 under pressure". In: *Journal of Applied Physics* 104 (2008), p. 053713.

[138] Hannan Elsayed, Daniel Olguín, and Andrés Cantarero. "Effects of hydrostatic pressure on the thermoelectric properties of the epsilon-polytype of InSe, GaSe, and InGaSe_2 semiconductor compounds: an ab initio study." In: *Mater. Res. Express* 4 (2017), p. 125901.